Development of Insulating Coating on Vanadium Alloys for Liquid Lithium Blanket of Fusion Reactors

YAO, Zhenyu

Doctor of Philosophy

Department of Fusion Science

School of Physical Sciences

The Graduate University for Advanced Studies

2005

CONTENTS

ABSTRACT

Among the concepts for breeding blanket of fusion reactors, self-cooled Li/V blanket, in which vanadium alloy acts as structural material and liquid lithium as both tritium breeder and coolant, is thought to be particularly attractive. Lithium has high tritium breeding capability, good heat transfer and negligible neutron damage. In addition vanadium alloys have low induced radioactivity, good compatibility with lithium, good resistance to neutron damage and high strength at high temperature. These advantages lead to a simple structural design, no use of neutron multiplier beryllium with enough tritium breeding rate, and continuous handling of chemistry for the breeder.

One of the critical issues for liquid Li/V-alloy blanket concept is large magneto-hydrodynamic (MHD) pressure drop against pumping system while liquid lithium flows in blanket ducts in a strong magnetic field. A promising way to mitigate the pressure drop is to apply electrically insulating coating (oxide or nitride ceramics) onto inner wall of the structural ducts.

In-situ formation of oxide coating onto vanadium alloys in liquid lithium is quite attractive because the process will make it possible to deposit coatings onto complex surfaces after fabrication of the components, and it offers the possibility to heal cracks of coatings without disassembling the components. In this method, the vanadium alloy substrate pre-charged with oxygen is exposed in liquid lithium doped with metal, where the oxygen reacts with the metal to form an insulating oxide coating on the vanadium alloys.

Among candidate coating materials, Er_2O_3 ceramics showed good compatibility with liquid Li, a high electrical resistivity, and a high stability in air with moisture, and thus is regarded as a promising candidate material for the insulating coating.

The purpose of this study is to develop an in-situ Er_2O_3 insulating coating method to V-4Cr-4Ti (NIFS-HEAT-2) that is one of the reference vanadium alloys.

For this purpose, the first step is to pre-charge oxygen with proper level and to distribute in the limited depth of V-4Cr-4Ti, without degrading mechanical property of the substrate. In the present study, the oxygen behavior in V-4Cr-4Ti during oxidation and subsequent annealing were investigated first at all. V-4Cr-4Ti alloy was oxidized in flowing Ar with impurity of oxygen, nitrogen and moisture for 0.5-8h and subsequently annealed in vacuum for 16h at

700°C. By oxidation for supplying enough oxygen, the oxygen of 1000-9000ppm was introduced into V-4Cr-4Ti with little nitrogen, where oxygen was concentrated in a region near the surface. The weight gain obeyed a parabolic law indicating that the oxidation process was controlled by thermo-diffusion rate of oxygen in V-4Cr-4Ti. During the annealing for keeping the oxygen in the substrate, oxygen was homogeneously diffused into depth of 150μm. The diffusion depth of oxygen in V-4Cr-4Ti is limited because of Ti-O net precipitates formed as oxygen trap. Ti-O is expected to dissolve supplying free oxygen for forming the coating during the subsequent exposure to liquid Li. The study indicated feasibility to control the level and distribution of oxygen in the surface region of V-4Cr-4Ti. The optimized parameters of pre-charging oxygen into V-4Cr-4Ti for forming in-situ oxide coating are oxidation in Ar (700°C, 6h) followed by annealing in vacuum (700°C, 16h).

The second step is chemical formation of Er_2O_3 coating on V-4Cr-4Ti during exposure in liquid Li doped with Er. In the present study, V-4Cr-4Ti were oxidized at 700°C for 1-8h, annealed at 700°C for 16h, and finally exposed for 100 h at 600°C. By the exposure, the Er_2O_3 layer was formed on V-4Cr-4Ti oxidized plus annealed, but was not formed on those either as-received or oxidized only. The resistivity of V-4Cr-4Ti with Er_2O_3 coating is $\sim 10^6 \Omega m^2$ which is much larger than the minimum requirement ($\sim 10^{-2} \Omega m^2$). The results indicate that the in-situ formation of Er_2O_3 coating is viable, the oxygen source to form coating is the pre-charged oxygen in V-4Cr-4Ti, and that the annealing after oxidation to homogenize oxygen distribution in substrate is necessary for the formation of the coating.

The third step is to characterize and investigate the potential long-term stability of the Er_2O_3 coating. V-4Cr-4Ti substrate was oxidized in flowing Ar at 700°C, annealed in vacuum at 700°C, and finally exposed to liquid Li doped with Er from 500°C to 700°C. The oxygen charged and homogenized in limited depth of the substrate was stored as Ti-O net precipitates. It was verified that Ti-O dissolved to release oxygen at high temperature acting as an oxygen source. The surface layer formed on V-4Cr-4Ti consists of double sub-layers, namely an insulating coating of Er_2O_3 and an intermediate layer of mixed ErN and V-compounds. The Er_2O_3 coating was found to be stable up to 750h of exposure time in liquid lithium doped with erbium at 600°C with its saturated thickness of ~0.1μm, stable up to 300h at 650°C with saturated thickness of ~0.6μm, and stable up to 300h at 700°C with saturated thickness of ~1.3μm. Cracking of coating

can be avoided during the Li cleanout process after exposure by using weak lotion (liquid NH_3) at low temperature (-33.5^oC). Thus it is inferred that no cracks were formed during the exposure in liquid Li. By re-exposure of intentionally cracked coating in liquid Li doped with erbium, the potentiality of self-healing to cracks was shown. The coating once formed in Li doped with erbium at 700^oC was stable in pure Li at 700^oC, thus demonstrating the stability of Er_2O_3 coating in liquid Li. The lower limits of the Er doping level to form Er_2O_3 coating were experimentally gotten to be in the range of 1–2.5wt%(0.04–1at%) and at exposure temperature higher than 500^oC. The limit is expected to be much lower with reduced level of the dissolving oxygen in liquid Li. The in-situ measurement of resistivity during heating in vacuum showed that the coating had resistivity over minimum requirement ($10^{-2}\Omega m^2$) up to 550^oC. The resistivity satisfying the requirement to higher temperature is expected to show with improved measurement apparatus.

Finally, the mechanisms for nucleation and growth of the coating were investigated. By oxidation and annealing, the oxygen was charged into substrate to form Ti-O net phase as oxygen source to the coating. The surface layer formed on V-4Cr-4Ti consists of two sub-layers, insulating Er_2O_3 coating and intermediate layer of mixed ErN and Er-V-O. The durations of nucleation at 600, 650 and 700^oC are experimentally proved to be quite short. The measured growth rate showed the kinetics of logarithmic law with high exponent ($n\approx3$ or 4) at 600^oC and 650^oC, suggesting that the rate of growth to Er_2O_3 coating should be very low. The growth was expedited suddenly at 700^oC resulting in low exponent ($n\approx2$) that almost obeys parabolic law. A phenomenological model was proposed for mechanism of the coating kinetics, which showed growth of Er_2O_3 coating is controlled by diffusion of oxygen and delivery of erbium to interface between the vanadium alloy substrate and the liquid lithium. The model also showed impurity transport across the interface and formation mechanism of the resulting intermediate layer.

In summary, this study has demonstrated that in-situ Er_2O_3 coating on V-4Cr-4Ti in liquid Li doped with erbium is a viable technology. Coating was stable at 600^oC to 750h and at 700^oC to 300h. Coating showed satisfactory resistivity to minimum requirement for reducing MHD pressure drop. Coating showed self-healing potentiality. The kinetics of the coating showed quick nucleation followed by growth with logarithmic law. The phenomenological modeling showed formation mechanism of the observed intermediate layer.

CHAPTER 1

Introduction

Today, scientists and engineers have achieved the first scientific demonstrations of a process for releasing fusion energy for the generation of electrical power. A much more efficient variant of hydrogen fusion which can be used for energy production by mankind, is the fusion of deuterium (D) and tritium (T). The fusion of about a thousand tons of deuterium and tritium would satisfy the annual energy demand for all mankind.

1.1 Fusion reactor and blanket system

(1) Requirements of fusion energy

The world's population and civilization increase substantially. The requirement to energy becomes larger and larger. The world electricity consumption is expected to increase substantially by the middle of the 21st century. The growth of energy demand, the limited reserves of oil and natural gas and the concern about greenhouse effect, require developing a new energy sources. As one of renewable energies, the controlled fusion seems to be a promising development line, although not all is yet understood of the physics and engineering of a power station based on controlled fusion.

(2) Fusion reaction

A scheme to describe D-T fusion reaction to produce fusion energy is shown in Fig. 1.1-1.

$$D + T \rightarrow {}^{4}He\ (3.5MeV) + {}^{1}n(14.1MeV) + Energy$$

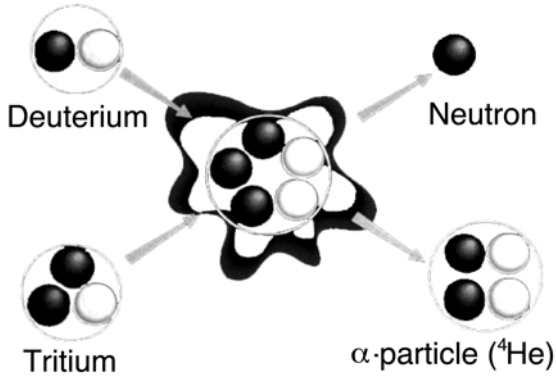

Fig. 1.1-1 Scheme of D-T fusion reaction [1]

The approaches to achieving controlled fusion reactions to produce electric power on earth mainly have two ways, namely Magnetic Confinement Fusion (MCF) and Inertial Confinement Fusion (ICF).

MCF involves that charged particles are deflected by a magnetic field. If the field is strong enough, particles will orbit round a field line. Gradually progressing along it if they have some longitudinal velocity. This feature forms the basis of MCF, which is along a way of long–time burning at low-density.

ICF involves high-energized particle or laser beams from all directions at tiny solid fuel pellets in a reaction chamber. Material sputtered off the pellet by the high-energy beams drives a shock wave towards the pellet center, raising its temperature and density to sufficient conditions of a fusion reaction. ICF is along a way of ultra-short-time burning at ultra-high-density.

These two methods have large difference, no matter in the standpoint of physics or engineering. Here only the introduction and study concerning MCF are mentioned.

(3) Fusion reactor

To realize a MCF to produce fusion power, some devices based on various plasma confinement methods were tested, like Tokamak, Stellarator and Magnetic Mirror etc. In a Tokamak, two superimposed magnetic fields enclose the plasma - the toroidal field generated by external coils on the one hand and the field of a flow in the plasma on the other hand. In the combined field, the field lines run helicoidally around the torus center to get confinement to plasma.

The research on tokamak principle have been performed widely and got many positive results. Thus research on a reactor based on tokamak principle is thought to be the most efficient way, to understand production of fusion power. Now a tokamak type International Thermonuclear Experimental Reactor (ITER) [1] is under design. A DEMO type fusion reactor (e.g. ARIES-RS) is also under design to demonstrate power plant. An example of the conceptual design to DEMO reactor is shown at Fig. 1.1-2.

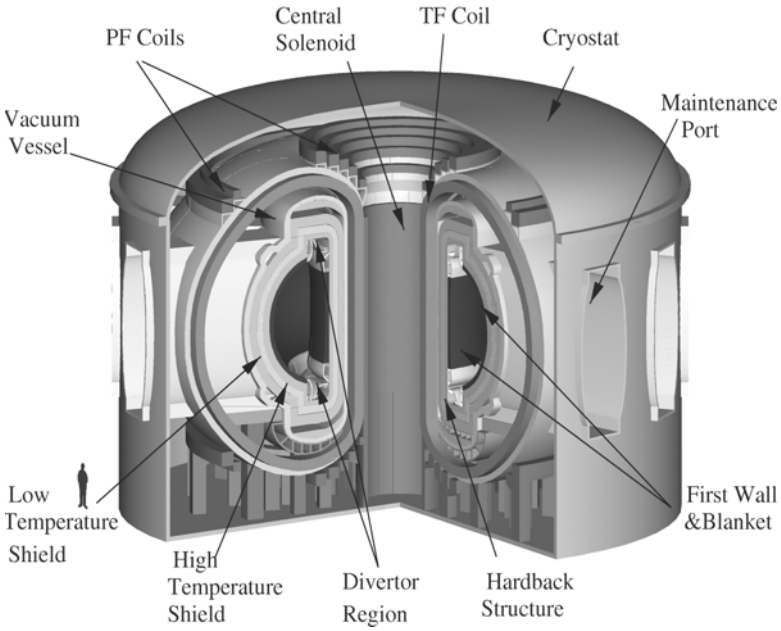

Fig. 1.1-2 Example of conceptual design of DEMO fusion reactor (ARIES-RS) [2]

A power reactor has many systems or parts with various functions:

a) First wall and Blanket absorb heat radiating from plasma, provide neutron shielding and produce tritium from lithium for fuel recycle.
b) Divertor exhausts the flow of energy from charged particles produced in fusion reactions and removes helium and other impurities.
c) Vacuum Vessel provides high vacuum boundary for the plasma and the first line of confinement against radioactive releases within the vessel.
d) Superconducting Magnet systems consist of Toroidal Field (TF) Coils, Poloidal Field (PF) Coils and Central Solenoid (CS) to produce a strong magnetic field to confine plasma.
e) Cryostat keeps ultra-low temperature to Superconducting Magnet.
f) Maintenance Port supplies a route to servicing.
g) Temperature Shielding supplies to shield reaction heat.
h) Hardback Structure supplies a support to parts.

(4) Blanket system

The basic function of the blanket system is to provide the main thermal and nuclear shielding to the vessel and external machine components. For a breeding blanket, another important function is to transfer lithium to tritium for a fuel recycle. An example of the conceptual design to the part of DEMO blanket is shown at Fig. 1.1-3.

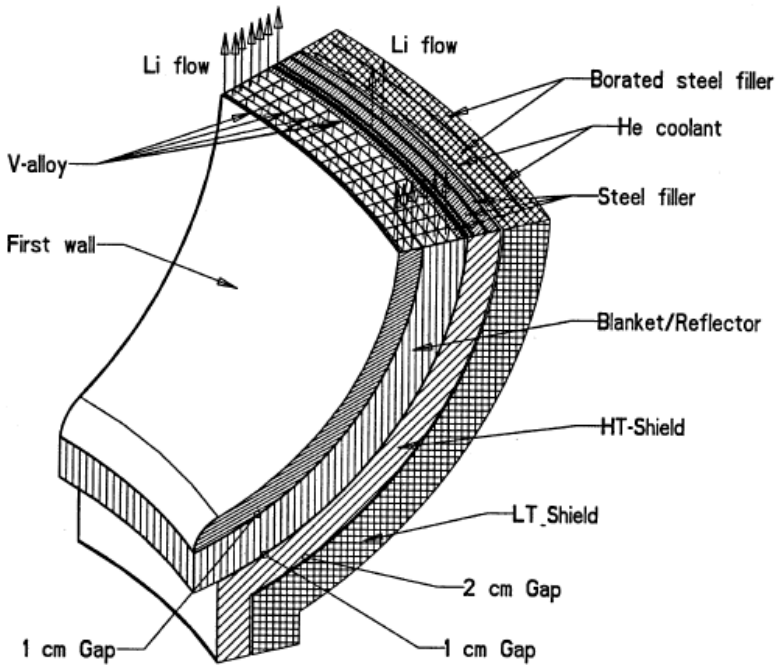

Fig. 1.1-3 Example of conceptual design of DEMO blanket (ARIES-RS)

For the conceptual design of breeding blanket, it is necessary to consider some basic parameters such as neutron flux, shielding capability, heat transfer and tritium breeding ratio etc, which decide capability of the reactor. Based on these parameters, the materials selection and structure design can be performed. Contrarily, the materials selection and structure design can influence the basic parameters.

1.2 Candidate structural materials for blanket

The type of the breeding blanket needs to be selected from the standpoint of the combination of the breeder, coolant and structural materials. The candidate materials for the blanket are listed in Table 1.2-1.

Table 1.2-1 Candidate materials for blanket [3]

Breeder	Coolant	Structure	Neutron Multiplier
Liquid metal (Li, Li_{17}-Pb_{83})	H_2O	Austenitic steel	Be
Ceramic (Li_2O, $LiAlO_2$, etc.)	Li	Ferritic/Martenstic steel	Pb
Molten Salt (Flibe)	Li_{17}-Pb_{83}	Vanadium alloy	
	He	SiC/SiC composite	

Some concepts of blanket were submitted combining various breeder, coolant and structure materials. After selection study, some types of modules have been proposed for testing their performance in a fusion experimental reactor. Several promising concepts named test blanket module (TBM) are planed to test in ITER [1]:

1) H_2O-cooled solid breeder (pebble-bed Li-ceramic/Be blankets with Ferritic/martensitic steel structure).
2) He-cooled solid breeder (pebble-bed Li-ceramic/Be blankets with Ferritic/martensitic steel structure).
3) Self-cooled liquid Li breeder with Vanadium alloy structure.
4) He-cooled or self/He-cooled Li-Pb with Ferritic/martensitic steel structure.
5) Self-cooled or He/self-cooled Molten Salt blankets with Ferritic/martensitic steel structure.

More advanced blankets, using for instance SiC/SiC structures, could be envisaged at a later stage if the on-going long-term R&D is successful.

For blanket concepts grouped by coolant type - liquid metal, helium, pressurized water and molten salt, main critical issues are summarized below [3]:

- Self-cooled liquid metal concepts – 1) liquid-metal magneto-hydrodynamic (MHD) pressure drop, 2) corrosion, 3) lithium reactivity, 4) tritium control and recovery.
- He-cooled concepts – 1) irradiation-induced swelling of ceramic breeder, 2) tritium recovery, 3) helium leakage into plasma, 4) problem on multiplier Be.
- H_2O-cooled concepts – 1) tritium recovery, 2) safety related to pressurized water, 3) limited power variation capability, 4) problem on multiplier Be.
- Molten Salt-cooled concepts – 1) salt stability, 2) tritium recovery, 3) compatibility of coolant with structural materials, 4) activation product control, 5) thermo-fluid control.

Here, just the properties of some structural materials are summarized.

Austenitic stainless steel of the 316L type is the main structural materials for the ITER vacuum vessel and for in-vessel components (shielding blanket, divertor cassette body). This steel type is qualified in many national design codes and has adequate mechanical properties, good resistance to corrosion, weldability, forging and casting potential. It is industrially available in different forms, and can be manufactured by well-established techniques. The modified one for ITER is named 316L(N)-IG [4]. However, 316ss has a working limit of maximum irradiation dose to be up to ~5-7 dpa (for neutron wall loading ~1MW/m^2) within a temperature ranges of 20-300^{o}C corresponding to ITER design parameters for blanket materials [5]. For DEMO reactor, the irradiation dose is ~200dpa (for neutron wall loading is ~3 MW/m^2) within temperature ranges of 300-550 ^{o}C [6]. Void swelling is a concern for 316ss in such rigorous conditions. The low thermal conductivity of 316ss makes it difficult to design advanced high power density blanket.

In addition, the 316ss is not a reduced activation material. For reduced activation ferritic/martensitic (RAFM) steels, F82H (Fe-8Cr-2W), JLF-1 (Fe-9Cr-2W) and EUROFER-97 (Fe-9Cr-1W) were developed as references. They showed reasonable good thermo-physical and mechanical properties, good compatibility with coolant and breeder and low swelling. One of the key issues of these steels is the radiation induced hardening and embrittlement at low temperature, i.e. radiation induced increase in yield stress and increase in DBTT [7].

SiC/SiC composites have been developed for aerospace applications and fossil power generation plants because of their high temperature strength, strength to weight ratio and high corrosion resistance. By using SiC/SiC composites as materials for blanket structural component, significant increase in upper operation temperature will be possible for fusion reactors with the advantage of high thermodynamic efficiency. However, SiC/SiC composites are still the least developed of the three candidate materials and several critical issues are remaining, such as fabrication of massive components, hermetic joining, radiation induced swelling and creep, and radiation induced degradation of thermal conductivity [7, 8].

Vanadium alloys are recognized as attractive candidate materials for neutron interactive structural components of fusion energy systems, because of their high temperature strength, high thermal stress factor, low activation property and so on. High compatibility of vanadium alloys with liquid Li makes it possible to design concepts of liquid Li blanket using vanadium alloys [9]. Based on past results, a V-4Cr-4Ti ternary alloy is considered to be a leading candidate material. Fig. 1.2-1 shows the roadmap of vanadium alloy development [10]. This is arranged for showing exclusively for vanadium alloys. The critical issues for vanadium alloys possibly limiting the operation window will be the irradiation effects, with helium production, on fracture at lower temperature and creep deformation at middle to high temperature, thermal creep and creep fatigue at high temperature, and the influence of environmental impurities [7, 9]. The materials development is planned to proceed with International Fusion Materials Irradiation Facility (IFMIF) and ITER in a coordinated way. For vanadium alloys, small scale testing will be carried out in initial operation period of IFMIF and ITER-TBM followed by full size testing, in contrast to the full size testing planned for the reference materials (RAFM) from the initial period of IFMIF and ITER-TBM. Recent efforts on vanadium alloy development have been focused on characterizing the existing V-4Cr-4Ti heats to establish performance limit and operation window. The efforts include the evaluation of low and high temperature mechanical properties with and without irradiation, improvement of the alloy properties by compositional and microstructural optimization, and exploration of new alloys by changing composition or applying new fabrication processes.

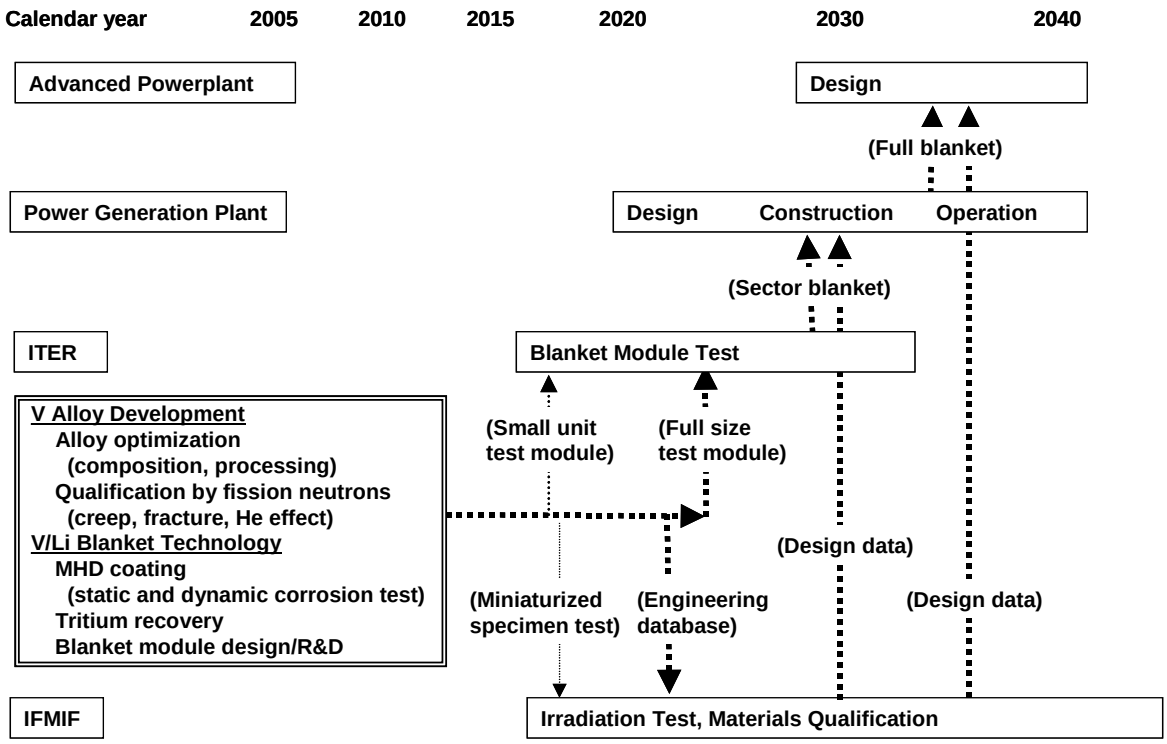

Fig. 1.2-1 Roadmap of vanadium alloy development [10]

1.3 Li/V-alloy blanket and its magneto-hydrodynamic (MHD) issue

There are issues either common or specific to the blanket concepts [3]:

1) materials data base assessment (structural materials, corrosion limits, breeder materials and special materials)
2) tritium containment
3) structural and electromagnetic analyses
4) neutronics analyses (tritium breeding, shielding and activation)
5) reliability, resource and high-power density blanket considerations
6) auxiliary components (limiter/divertor, energy conversion system, etc.)

Among the blanket concepts, a self-cooled liquid-metal blanket was thought to be quite attractive. Use of the same liquid metal for both tritium breeder and coolant greatly simplifies both design and materials consideration, since the blanket requires only a structure material and a coolant. In this case, the compatibility between coolant and breeder is not an issue, and thus the considerations can be focused on the compatibility between coolant and structural materials. Heat removal requirement are also less complex because most of the nuclear heating is deposited directly in the coolant. In this system, the effects of radiation on breeder materials are quite minor. In this concept, two main issues need to be considered [3, 11]:

1) Corrosion of structural materials by liquid metal limits maximum interface temperature.
2) Strong magnetic field causes high pressure-drop.

The liquid Li/V-alloy blanket represents an attractive option for advanced performance fusion power systems. Fig. 1.3-1 illustrates a possible design for the Li/V self-cooled system where liquid lithium is both the breeding material and the coolant and a vanadium alloy (e.g. V–4Cr–4Ti), is the structural material. The blanket is composed of Li cooling channels, reflectors and a shielding area, which is in contrast to solid breeder blankets composed of a solid breeder zone, a neutron multiplier beryllium zone, cooling (gas or water) channels and tritium recovery gas flow channels, in addition to reflectors and shielding.

The major features of the Li/V blankets are:

1) High heat load capability due to the favorable physical properties of vanadium alloys and the good heat transfer characteristics of liquid lithium.

2) High operating temperatures, up to 650–700°C for vanadium alloys, which provides high power conversion efficiency.
3) Long lifetime of the structure as a result of low swelling and good retained mechanical property of vanadium alloys by neutron irradiation.
4) Relatively simple design enhancing fabric ability and system reliability.
5) Reduced activation since the V–Cr–Ti alloys and liquid Li have low activation characteristics by neutron irradiation.
6) Small leakage of tritium from liquid Li allows for greater flexibility in selecting and operating the tritium recovery system outside of the fusion vessel.

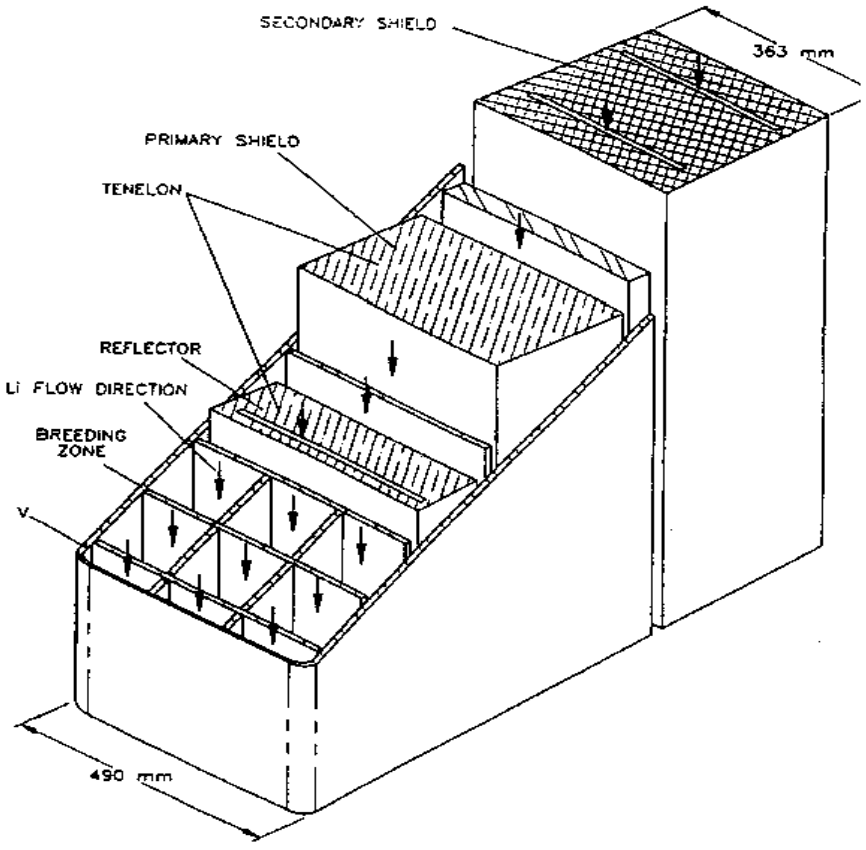

Fig. 1.3-1 Example of self-cooled Li/V blanket design [12]

The self-cooled Li/V blankets have been designed as advanced concepts for DEMO and commercial fusion reactors [2, 13]. One of the attractive features of this blanket system that was confirmed by neutronics calculation [14, 15] is, that the neutron multiplying beryllium is

in most cases not necessary for obtaining the required Tritium Breeding Ratio (TBR). Without beryllium, the system is released from the issues concerning beryllium such as handling safety and natural resource limit. Moreover, the replacements frequency of the blanket will be reduced once long life structural materials are developed, because the blanket system is free from periodic replacement due to the lifetime of beryllium. Without beryllium, the blanket can be designed with much more simple structures.

However, the development of Li/V systems requires solution of several issues [12]:

1) Development of vanadium alloys, which have only a limited database.

   The areas of interest include optimization of vanadium alloys for use in the fusion environment, e.g. neutron irradiation response, and development of industrial procedures for fabrication.

2) Reduction of MHD pressure drop.

   Liquid metals moving through a magnetic field are subjected to magneto-hydrodynamic (MHD) effects that can increase the pressure drop and affect the flow profiles and heat transfer.

3) Other issue.

   Li is reactive with air and water. The tritium recovery method from Li has not been established. The compatibility of Li and structural materials is also an issue.

The present study will be focused on the issue of MHD pressure drop.

The interaction between the circulating liquid metal and the strong toroidal magnetic field results in large electromagnetic body Lorentz forces that determine the flow distribution of liquid metal and produce large magneto-hydrodynamic (MHD) pressure gradients. The resulting MHD pressure drop may cause excessive pumping power loss and large material stress. In addition, MHD flow distribution may drastically affect the heat transfer characteristics of blanket in general and the first-wall coolant channels in particular [16, 17].

For the design of self-cooled liquid-metal blanket, a MHD analysis was shown [18]:

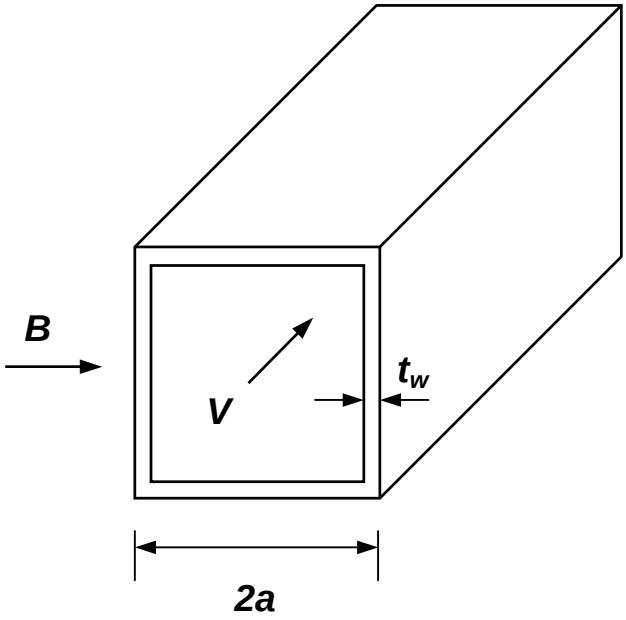

Fig. 1.3-2 Scheme of flow channel of liquid metal in magnetic field [18]

For rough estimation to MHD pressure drop, the scheme of flow channel is shown at Fig. 1.3-2, and an empirical equation is given by:

$$\Delta p = 0.2\sigma V B^2 \sqrt{\phi}$$

where Δp = MHD pressure drop at unit of channel length, σ = coolant electrical conductivity, V = average velocity of coolant in channel, B = magnetic flux density, ϕ = wall conductivity ratio $\sigma_w t_w/\sigma a$ (σ_w-wall electrical conductivity, t_w-wall thickness, a-channel radius).

The total MHD pressure drop with whole-size length of flow channel is estimated as about 3MPa according to an example of design parameters for a Li/V blanket of Tokamak Reference Design Reactor [18]. Other calculations according to various design parameters estimated the MHD pressure drops of about 8-30MPa [19, 20].

Assuming extremely small thickness of 0.1mm contacting with liquid Li, the MHD pressure drop already exceeds 8MPa, which is unacceptable. From the standpoint of pumping power and mechanical property for structure, the acceptable MHD pressure drop is proposed to be 1-2MPa [19, 20]. Thus, efforts are needed to reduce the MHD pressure drop.

1.4 Promising solution – insulating coating

There are three groups of MHD issues involved in design of self-cooled blankets: (1) pressure drop; (2) flow partitioning between parallel channels; (3) velocity distribution in channels.
In this study, only the issue of MHD pressures drop is considered. A method to use insulating coating on inner wall of metallic duct can reduce MHD pressure to an acceptable level. The schemes to describe MHD pressure and insulating coating are shown at Fig. 1.4-1.

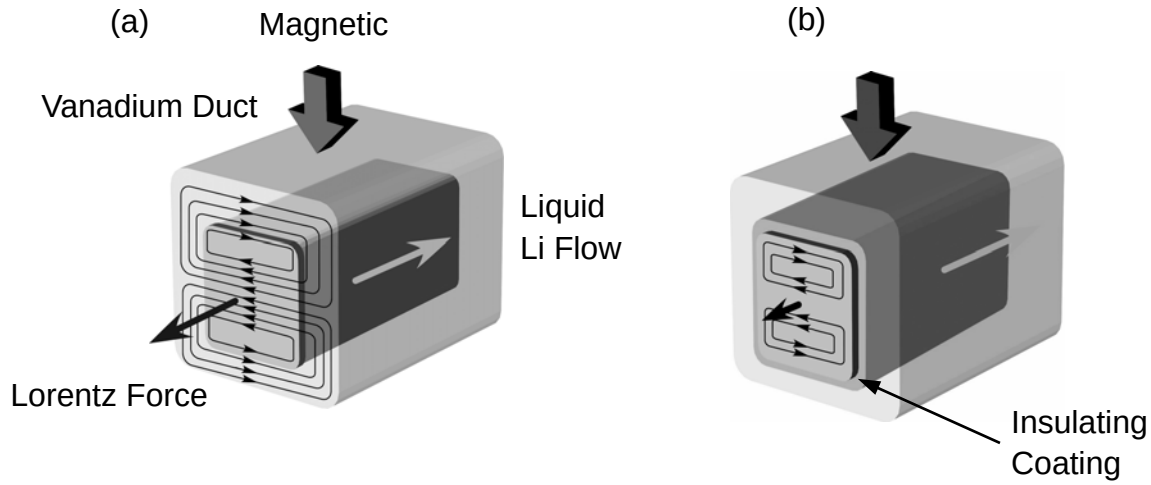

Fig. 1.4-1 Schemes of MHD pressure drop. (a) without coating (b) with coating [10]

To give an example to explain MHD pressure, role of insulating coating and minimum requirement to an insulating coating, an approximated geometry of a poloidal duct was proposed at Fig. 1.4-2.

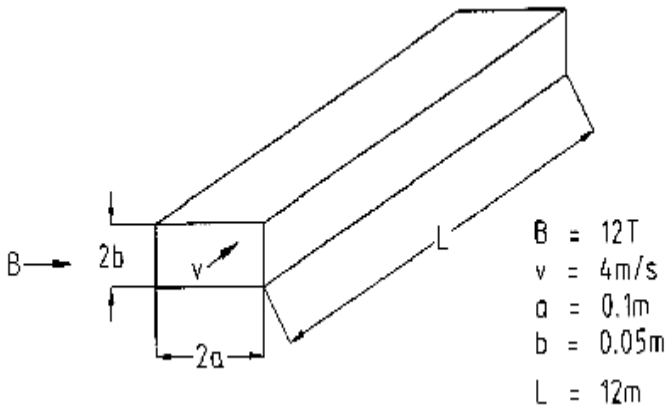

Fig. 1.4-2 Approximated geometry of a poloidal duct [20]

In a magnetic field, the both kinds of current flow (perfectly insulated ; leaked) within the flowing Li are shown in Fig. 1.4-3. The insulating coatings must lead to conditions very close to those in a perfectly insulated duct. The current flow in such a duct is shown in Fig. 1.4-3(a) in which the sidewalls are perfectly insulated. This flow pattern shall be compared with the case where the finite resistance of the insulating coating allows for a certain leakage current from the liquid metal region into the duct walls at Fig. 1.4-3(b). The requirement is that this leakage current I_{leak} assumes only a small fraction of the current I in a perfectly insulated duct.

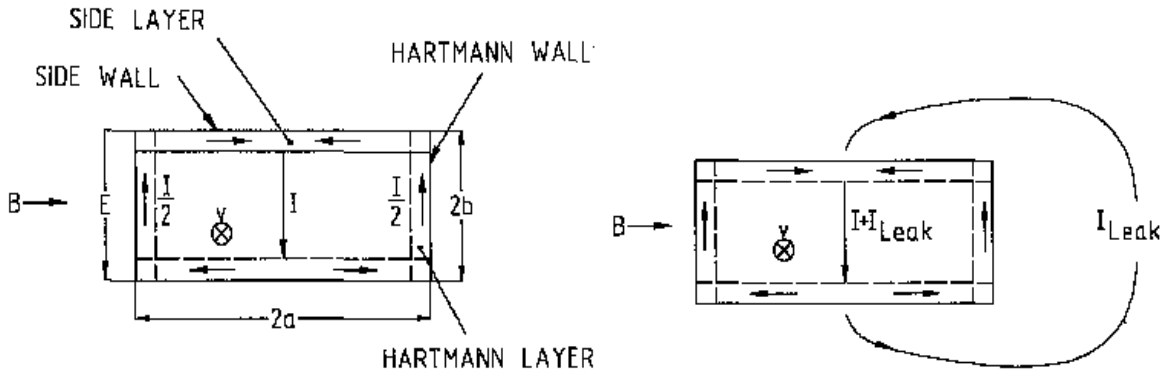

(a) **(b)**

Fig. 1.4-3 Current flow – (a) perfectly insulated duct, (b) current-leaked duct [20]

A lower limit for the pressure drop would be achieved with perfectly insulated walls (Fig. 1.4-3(a)). In this case, the induced voltage E and flowing current I defines an internal resistance in liquid metal as

$$R = \frac{E}{I} = \frac{bM}{aL\sigma} \qquad (1)$$

a, b, L –geometry size of duct, dimensionless Hartmann number $M = Ba(\sigma/\eta)^{1/2} = 10^5$, B- magnetic flux density, σ- liquid Li electrical conductivity=3.3×10^6S.m^{-1}, η-viscosity of liquid Li=4.5×10^{-4}Pa.s.

A finite coating opens an additional current path, leading to an increased pressure drop Δp_{leak} by I_{leak} (Fig. 1.4-3(b)). At a constant magnetic field, a given tolerable factor for additional pressure is defined as $f_{leak} = \Delta p_{leak}/\Delta p = I_{leak}/I = R/R_{leak}$

Once f_{leak} was decided, a minimum required resistance R_{leak} for a leakage current loop is defined as,

$$R_{leak} = \frac{R}{f_{leak}} = \frac{1}{f_{leak}} \frac{bM}{aL\sigma} \qquad (2)$$

1) All inner wall are covered by coating with resistivity ρ and thickness t

The R_{leak} was also defined by fig. 1.4-3 (b) [21],

$$R_{leak} = 2 \frac{\rho \cdot t}{(2a)L} \qquad (3)$$

Combining Equations (2) and (3),

$$\rho \cdot t = \frac{1}{f_{leak}} \frac{bM}{\sigma} \qquad (4)$$

Equation (4) can be used as estimation for a minimum requirement to a given geometry, boundary conditions and tolerable factor. If a tolerable factor f_{leak} of MHD pressure drop is allowed 10%, boundary conditions are shown at Fig. 1.4-2. Therefore the minimum requirement of resistivity to a finite coating is estimated to be $\sim 10^{-2}\ \Omega m^2$ [20].

2) Effects of uniform cracks through insulating coating

The insulating coating will probably be subjected to thermal cycling that may induce cracks through the coating. An un-repaired cracks could adversely affect the pressure drop.

To study the effect on MHD pressure drop, it is assumed that the cracks are uniformly distributed over the duct wall surface, at any given time the cracked coating can be regenerated (self-healed) and the regenerated layer inside the cracks has reached a certain fraction of the original coating thickness. In a calculation [19], the crack fraction is defined as the ratio of total crack area to total wall surface area. The regenerated layer thickness t is treated as a parameter in that analysis. It is seen that the increase in pressure drop is insignificant even for large crack fraction if thin layers with 1/100 of thickness of the original coating thickness are formed inside the cracks.

Thus a uniformed insulating coating with self-healing function is thought important.

1.5 Coating methods and advantages of in-situ coating

In general, the coating method is divided to two types, according to the fabricating process of components. The so-called ex-situ and in-situ coating methods are shown at Fig. 1.5-1.

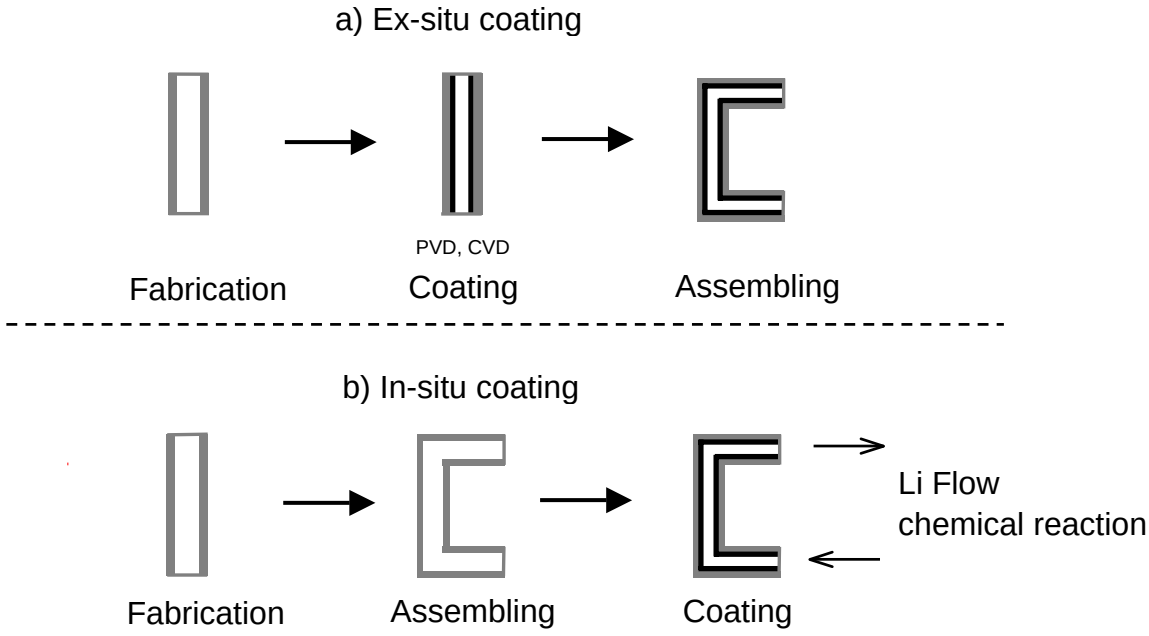

Fig. 1.5-1 General types of coating method

In Ex-situ method, physical vapor deposition (PVD) and chemical vapor deposition (CVD) are common technologies that are widely used for industrial application.

The scheme of filtered vacuum arc deposition, as one of PVD methods, is shown in Fig. 1.5-2 [22]. A vacuum arc discharge on a solid metal cathode produces metal plasma, and together with oxygen added from a gas inlet an oxide ceramic coating is deposited onto the substrate. The arc discharge, however, also produces droplets of molten material, which would significantly reduce the performance of the films if they were incorporated into the coating. A very effective method of avoiding this drawback is to prevent the droplets from reaching the substrate by employing a 90^{o} magnetic toroidal filter system. By this method, an obvious decrease of the droplet contamination of the coatings can be achieved [23].

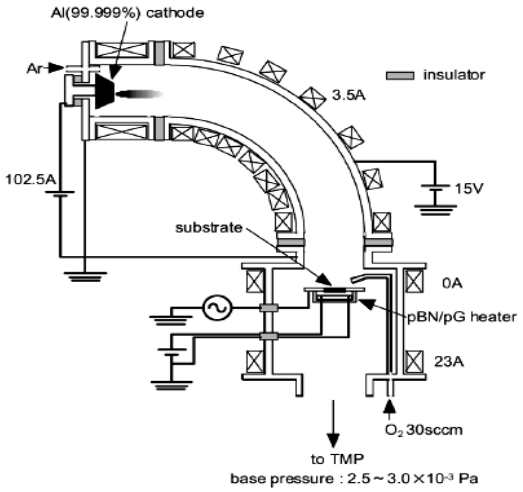

Fig. 1.5-2 Scheme of filtered vacuum arc apparatus [22]

A schematic diagram of catalytic CVD apparatus (for AlN coating) combined with a bias source is shown in Fig. 1.5-3. The catalyzer was made up of a screwed tungsten wire with a diameter of 0.4mm. The substrate was put on a molybdenum substrate holder placed at beneath the catalyzer, and a negative bias versus the chamber walls was applied to the substrate. The catalyzer temperature was measured by an optical pyrometer. The substrate temperature was measured by a thermocouple attached onto the substrate surface. The pressed $AlCl_3$ piece was put in a container, whose temperature was kept at a certain temperature. High purity N_2 and H_2 gases were used as reactant gases. When the pressure in the chamber was reached, the negative bias was applied to the substrate. As the bias was increased to a high value, a glow was observed near the substrate surface, and an increase of electric current accompanied with a small drop of voltage was detected. Then the coating started to grow.

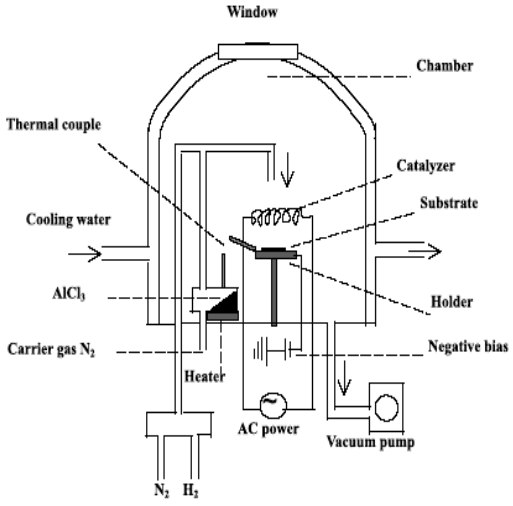

Fig. 1.5-3 Schematic diagram of catalytic CVD apparatus [24]

Radio Frequency (RF) sputtering method was adopted because it is a rather simple and cheap method. The principle of the sputtering method is that atoms are struck out from a target by energetic particles coming from plasma and the sputtered atoms pile up on the substrate to form a thin film. This method has some advantages compared with the vacuum evaporation method: 1) the kinetic energy of the incident atoms onto the substrate is so high that the prepared coating adheres to the substrate very well. 2) many kinds of materials are available for coating. 3) the difference in chemical composition between the target and the prepared coating is relatively small. The vacuum chamber containing a substrate and a sputtering-gun for coating is shown at Fig. 1.5-4, whose distance is adjustable by a driving gear.

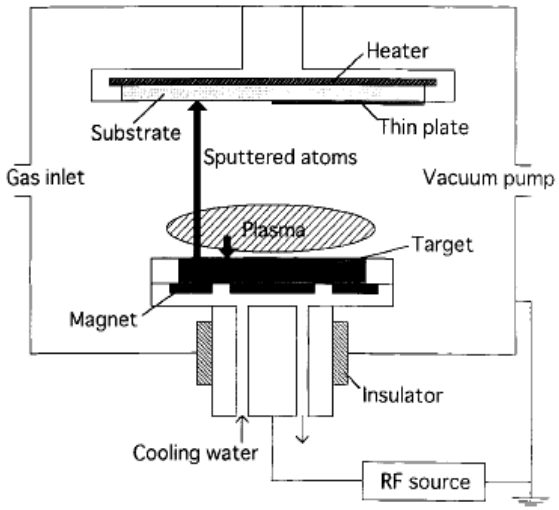

Fig. 1.5-4 Schematic drawing of the apparatus for RF sputtering coating [25]

For the ex-situ method, production of coating on inner wall of part is subsequent to fabrication, the last procedure is the assembling of part to a component. However, for the in-situ method that is interested in this study, the coating is produced on the inner of component by the chemical reaction with liquid lithium, after fabrication and assembling of parts. This method is especially suitable to a system using liquid lithium that acts as both coolant and breeder of a self-cooled Li/V blanket concept. The principle for the in-situ coating method is shown in Fig. 1.5-5.

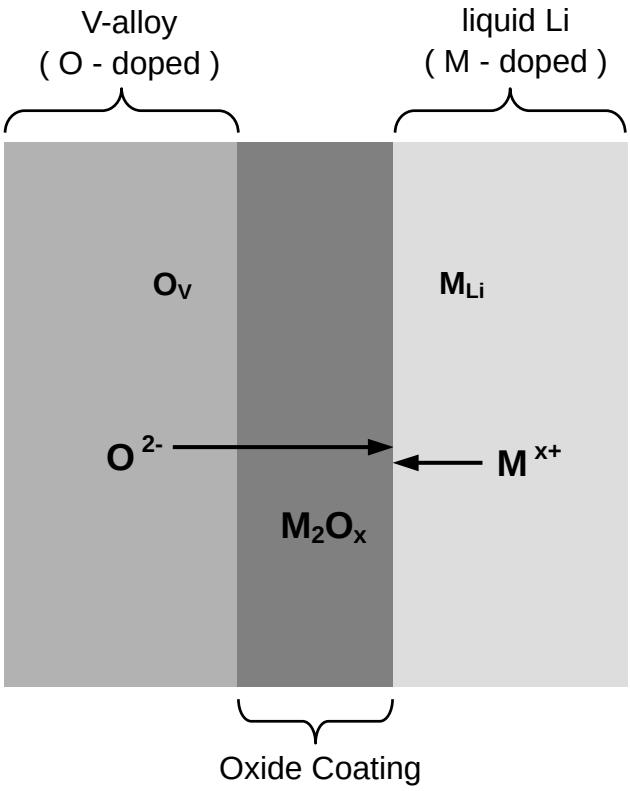

Fig. 1.5-5 Generic model for in-situ coating

The generic process for in-situ coating is that the metallic substrate pre-doped with oxygen is exposed in liquid lithium doped with metal element at high temperature. The pre-charged oxygen diffuses forward the surface of substrate, reacting with metal element dissolved in liquid lithium to produce an oxide coating with high electric insulating property.

The in-situ method has many attractive advantages,

1) Possibility to deposit coatings onto complex inner surfaces (including joints) of components after fabrication.
2) Possibility to heal cracks of coatings without disassembling components during operation or maintenance.
3) Coating process can be controlled by Oxygen-Vanadium-Metal-Lithium chemistry.
4) Coating has compatibility with lithium under controlled chemistry.

1.6 Research status of insulating coating

(1) Materials selection for coating

The requirements for the coating material are extensive. Key considerations for the selection of candidate coating materials include the following [26]:

1) reasonably high electrical resistivity.
2) chemical stability/compatibility with Li at elevated temperatures.
3) potential for coating on complex channel configurations.
4) potential for in situ self-healing of any defects that might occur.
5) mechanical integrity/thermal expansion match with V-alloy.
6) safety/environmental characteristics, e.g. low activation.
7) materials availability/cost.
8) favorable neutronics properties.
9) resistance to irradiation damage.

In this study, the considerations for candidate coating materials were mainly from three aspects, i.e. thermodynamic stability, resistivity and compatibility in liquid Li. Because metals are electrically conductive, the selection should be from ceramics (oxide, nitride or carbide).

The first step is to understand the properties of bulk materials according to the above factors. Only a limited number of materials offer a potential for meeting the most basic requirements for the MHD coatings, viz. electrical resistivity and chemical compatibility with lithium. Most carbides exhibit low electrical resistivity, many nitrides also exhibit low electrical resistivity and only a limited number of oxides are stable in lithium.

The thermodynamic stability (Gibbs free energy of formation) of several ceramics materials is shown at Fig. 1.6-1 (oxide) and 1.6-2 (nitride), from calculations by MALT2 code [27]. In oxides, the compounds that Gibbs free energy of formation is more negative than that of Li_2O are thought to be stable in liquid lithium. Although Al_2O_3 is a common insulating material, it was rejected because it dissolved in molten lithium at 500^{o}C [28]. From thermodynamic standpoint, MgO, BeO, CaO, Y_2O_3 and Er_2O_3 were considered as candidate oxides. Especially, CaO, Y_2O_3 and Er_2O_3 have similar thermodynamics stabilities that are highest in the available oxides up to 800^{o}C.

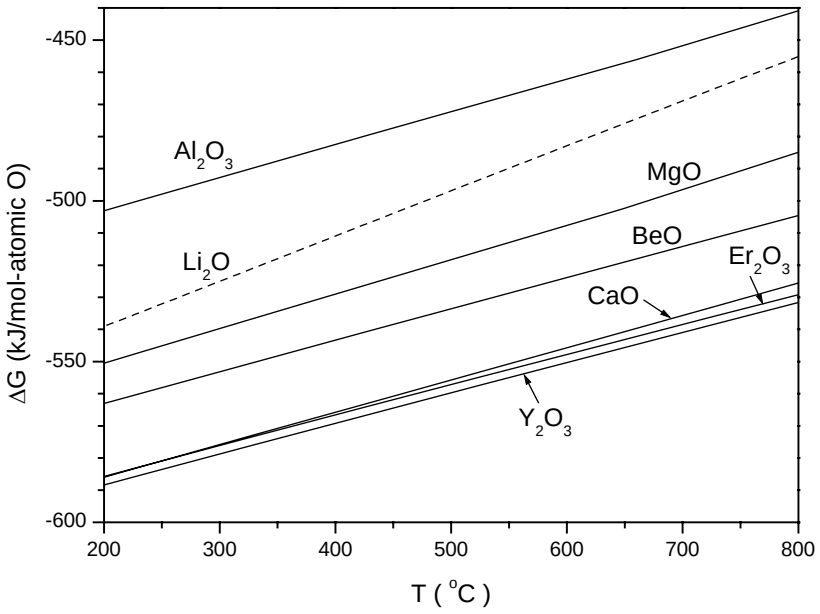

Fig. 1.6-1 Gibbs free energy of formation for several oxides

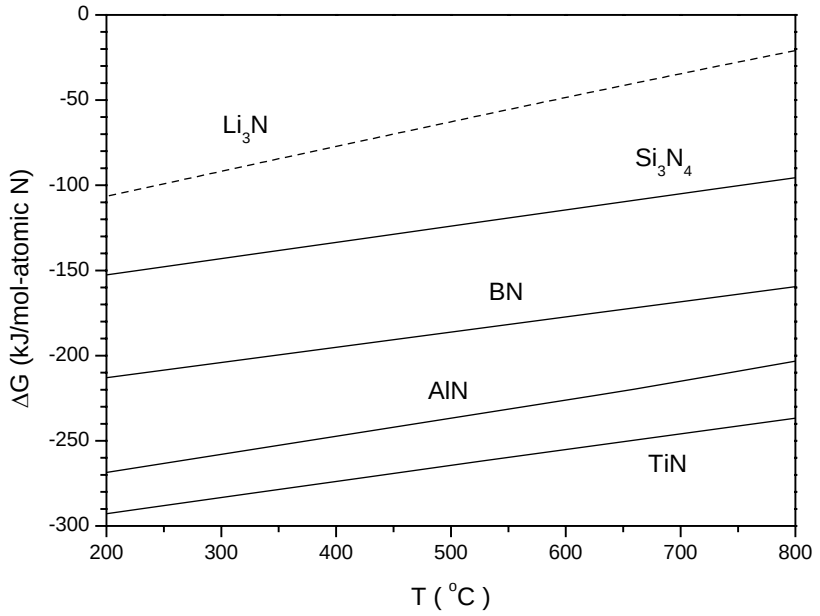

Fig. 1.6-2 Gibbs free energy of formation for several nitrides

In nitrides, the compounds that Gibbs free energy of formation is more negative than that of Li_3N are thought to be stable in liquid lithium. Although TiN was most stable in this respect, it was rejected because it has a relatively low electrical resistivity [29, 30]. The Si_3N_4, BN and AlN were considered as candidate nitrides. Especially, studies have been focused on AlN.

The relative thermodynamic stabilities of several oxides, with respect to Li/Li_2O equilibrium and the oxygen activity in liquid lithium with oxygen concentrations of 1, 10 and 100 wppm, were indicated. CaO and Y_2O_3 should be stable in lithium containing only a few wppm of oxygen over the temperature range of interest. Similar calculations for the thermodynamic stability of several nitrides with respect to Li/Li_3N and lithium with low nitrogen concentrations were shown [29, 31].

The essential factor for insulating materials is whether their resistivity exceeds a minimum requirement for insulating property to reduce MHD pressure drop to an acceptable level. Fig. 1.6-3 and 1.6-4 showed some results of resistivity of some candidate coating materials at high temperature.

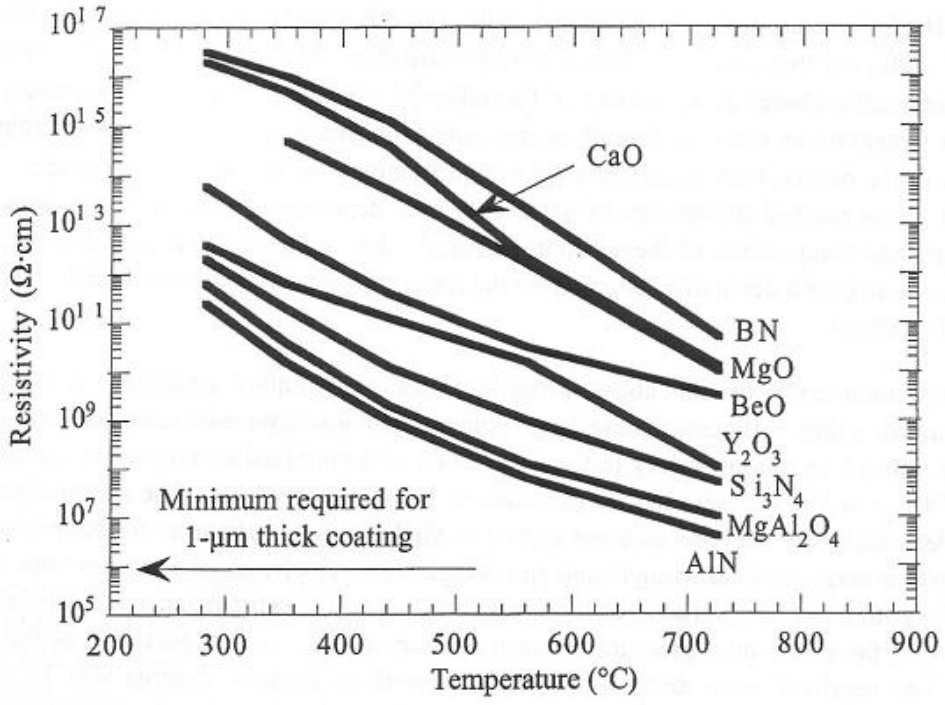

Fig. 1.6-3 Some results of resistivity of some candidate oxides and nitrides in vacuum [29]

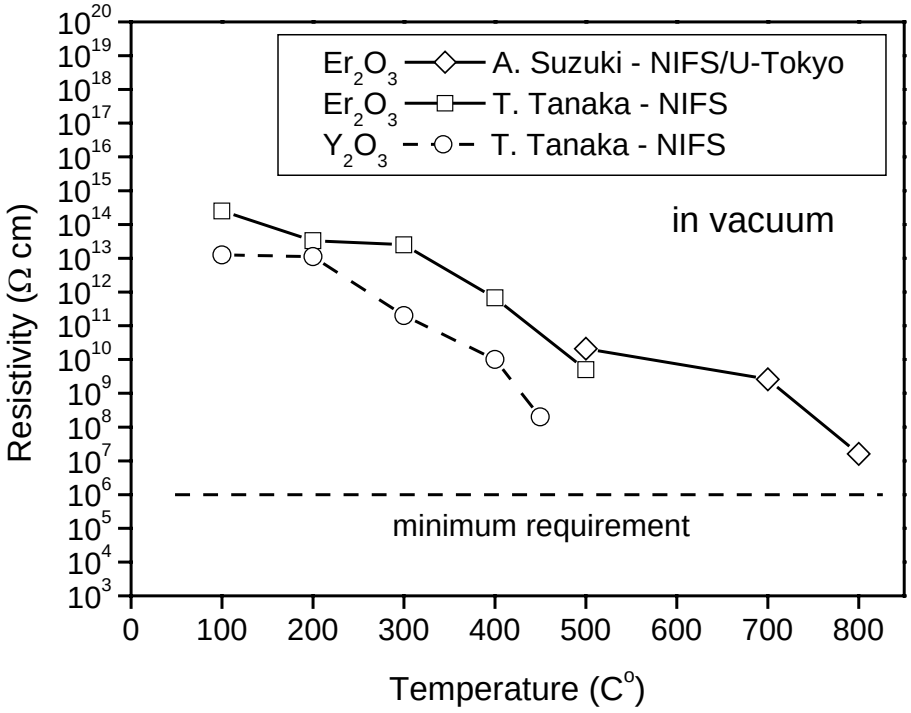

Fig. 1.6-4 Recent results of resistivity of Er_2O_3 and Y_2O_3 bulk in vacuum [32]

From the standpoint on electric insulating property with temperature, CaO exhibits very high resistivity while that of AlN is much lower but still appears to be adequate according to a minimum requirement. Recent results on Er_2O_3 and Y_2O_3 showed their good resistivity [32]. In addition the above oxides and nitrides showed that the degradation of insulating properties under 14MeV neutron irradiation were within allowable levels for application to Li/V blanket system [33].

Once the candidates were fixed from the standpoints of thermodynamic and insulating properties, the remaining issue is their compatibility in liquid lithium at high temperature. The above estimations are just for the pure and stable bulk materials. In practice, however, the both bulk materials and liquid lithium contain some impurities that may influence compatibility of the bulk with lithium largely. An important aspect concerning the thermodynamic stability of the candidate coatings in lithium relates to complex reactions involving other impurities in Li or with Li itself.

A powder sintering AlN was not compatible with liquid lithium in screening tests, because oxygen was enriched at grain boundaries during fabrication. Oxygen may form Al_2O_3 at the grain boundary area, which is not stable in liquid lithium [34].

High purity AlN decreased weights after exposure in liquid Li in contact with vanadium alloy over 700°C, while those in Li not in contact with vanadium alloy survived up to 800°C. Nitrogen dissolution from AlN into the liquid Li and absorption of dissolved nitrogen by vanadium alloy are considered to be a corrosion mechanism. Small decreases of electrical resistance were observed after the exposure tests over 600°C because of the conductive corrosion layer on the surface caused by nitrogen dissolution. In the cases of low purity AlN samples, large weight decreases were explained by fragile grain boundary caused by oxygen dissolution, which also results in the decrease in resistance at low temperatures. Decrease of oxygen impurity in AlN and addition of nitrogen in liquid Li are considered to give a possible solution to the Li/AlN corrosion problem in the Li/AlN/V-alloy blanket system, where Li with N addition should not contact with the V-alloy [35].

Initial characterization of AlN and CaO by 1000h exposure in lithium indicated that bulk, polycrystalline CaO reacts with lithium and loses mass significantly above 400°C. Significant mass losses were also observed for AlN+5%Y_2O_3 above 500 °C. Thus subsequent testing focused on AlN+0.04%Y, which appeared more resistant to reaction with lithium. However, at 600°C, AlN+0.04%Y appeared to form an oxide at the surface that could be deleterious to the performance of a thin AlN coating [36].

The sintered AlN with or without sintering-aid of Y_2O_3 examined in lithium at 500°C for 1390h showed a slight decrease in electrical resistivity because of reduction of Al_2O_3 impurity, though AlN and Y_2O_3 components themselves were not subject to severe corrosion [37].

Fig. 1.6-5 showed a mass loss for AlN+0.04wt%Y after exposure at various temperatures. Specimens of AlN+0.04%Y showed significant mass loss at 700 and 800°C, but a thin reaction layer formed at 600°C. For testing at 700°C, changing from a V-alloy capsule liner to a Mo capsule resulted in a greater reduction in mass loss than adding 1000ppm N to the Li in a V alloy capsule test. The maximum temperature for the use of AlN may be higher than 600°C, but further testing is necessary to confirm sufficient compatibility at higher

temperatures. These results raise concern about the compatibility of AlN with V–4Cr–4Ti, for example, that Ti in the V alloy may getter N from an AlN coating [38]. In higher temperatures capsule tests showed that the behavior of AlN was very sensitive to the capsule material. With a Mo capsule, very little mass change was noted after 1000 h at 800°C. When a vanadium alloy capsule was used, the mass losses were much higher. The effect can be understood based on the dissolution equilibrium equation for AlN = Al (Li) + N (Li). The vanadium alloy capsule got N from the Li during the exposure and prevented the Li from becoming saturated with N and thus stopping the dissolution. With capsules made from Mo, which does not form stable nitride, the Li becomes saturated with N and the dissolution stops. Thus, the use of AlN appears problematic because uncoated vanadium alloy channel walls could getter N from the Li. A further complication is that it is extremely difficult to make AlN without oxygen contamination. Any Al_2O_3 formed during coating fabrication would be readily dissolved by lithium [39].

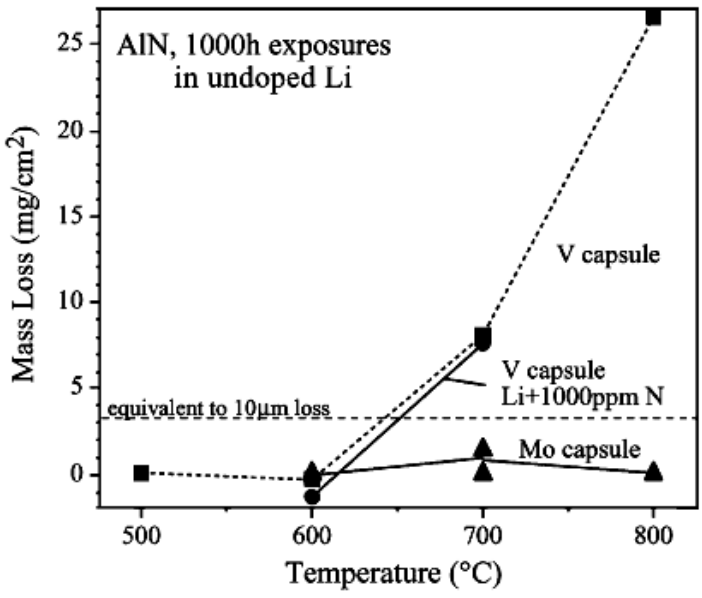

Fig. 1.6-5 Mass loss for AlN+0.04wt%Y after exposure at various temperatures [38]

BN specimens corroded by lithium became fragile because impurities in specimens were dissolved in lithium. It was expected that BN specimens containing no unstable impurities against lithium have good compatibility with lithium [28].

MgO is stable against lithium at 500°C in the case of the Li-Li_2O coexistent system. However, magnesium oxide is unstable against lithium if the oxygen activity is smaller than that of the Li-Li_2O coexistent system [28].

CaO was thought a quite promising candidate material for insulating coating, which has good thermodynamic stability and high resistivity. Thus the study on its compatibility with lithium was performed widely. The mass change data for CaO indicate that there was little interaction with lithium at 400°C. However, at 500-800°C, significant mass losses of CaO were recorded that generally increased with temperature. The polycrystalline CaO did not show its high thermodynamic property [36].

To confirm the compatibility of CaO with liquid lithium further, a single CaO was used to exposure in lithium [38]. The Fig. 1.6-6 showed the mass change for single crystal CaO after 1000h exposure at 600°C (a) and 700 °C (b).

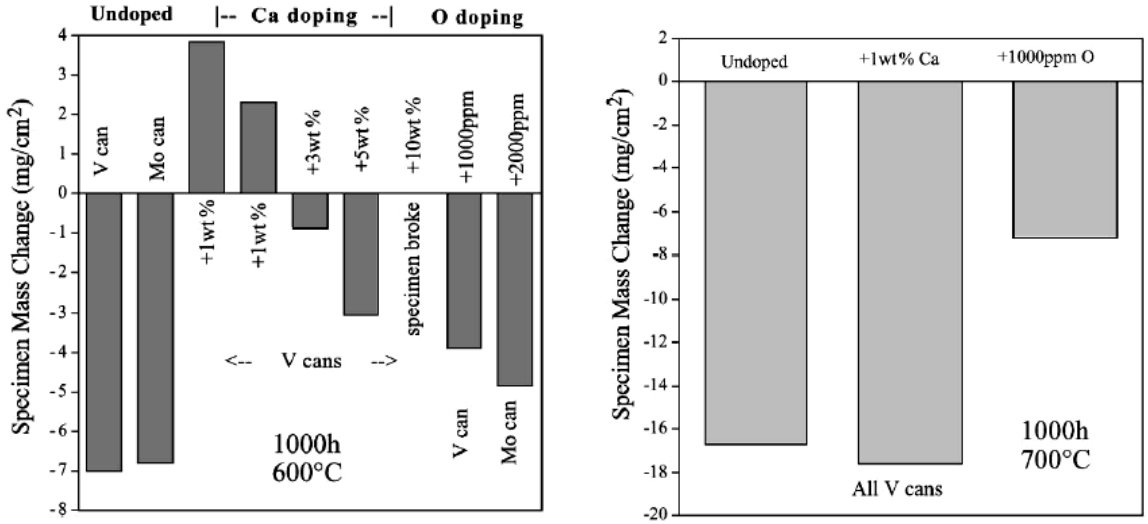

(a) (b)

Fig. 1.6-6 Mass change for single crystal CaO after 1000h exposure in lithium at 600°C (a) and 700 °C (b) with both V and Mo capsules [38]

For single crystal CaO, relatively high mass losses were observed in un-doped Li at 600 and 700^{o}C. In this case, neither V nor Mo would be expected to get O from Li. Therefore, no effect of capsule type was expected. These mass losses for CaO single crystals are contrary to its anticipated compatibility with Li. The 400- 450^{o}C experimental results and thermodynamic calculations indicate CaO should have acceptable compatibility. However, no other experimental results have been reported in un-doped Li for 1000 h at 600-700^{o}C, and several of the previous thermodynamic calculations only considered the Gibbs free energies of formation. It should be noted that rather than comparing the reaction energy for

$CaO + 2Li \leftrightarrow Ca + Li_2O$

the more relevant reactions are the dissolution reactions for the ceramics and the lithium until equilibrium is reached in solution:

CaO = Ca (Li) + O (Li)

With the high levels of Ca and O in solution at equilibrium, the thermodynamic calculations suggest that the high dissolution rates of CaO in un-doped Li are clearly possible [38].

This combination of experimental results and thermodynamic analysis suggests a new strategy for selecting possible MHD coating materials. The elements (e.g. Ca) that are highly soluble in Li may be more susceptible to dissolution at high temperature. Thus, one-selection criteria could be cations that are insoluble in Li. Of course, looking for insoluble cations does not obviate the thermodynamic requirement. There are other oxides such as Y_2O_3 and Er_2O_3, which have similar stabilities as CaO (Fig. 1.6-1), but have low solubility.

Fig. 1.6-7 showed Mass losses for oxide and nitride after 1000 h at various temperatures [39]. Compared to AlN and CaO, the Y_2O_3 specimen lost a small amount of mass while the Er_2O_3 specimen showed a mass gain after exposure. The specimens also changed color from pink for Er_2O_3 and opaque for Y_2O_3 to gray or black after the test, suggesting possible O getting from the specimens. Because the specimen of Er_2O_3 was not fully dense, penetration of Li may have caused the mass gain and color change. Previous work on Y_2O_3 found the formation of $YLiO_2$ surface layer that may degrade a thin Y_2O_3 coating [28].

In addition, Er_2O_3 and Y_2O_3 will not disintegrate in ambient air with moisture, which would eliminate the fabrication issues associated with CaO.

Therefore, Er_2O_3 and Y_2O_3 are thought to be attractive candidates.

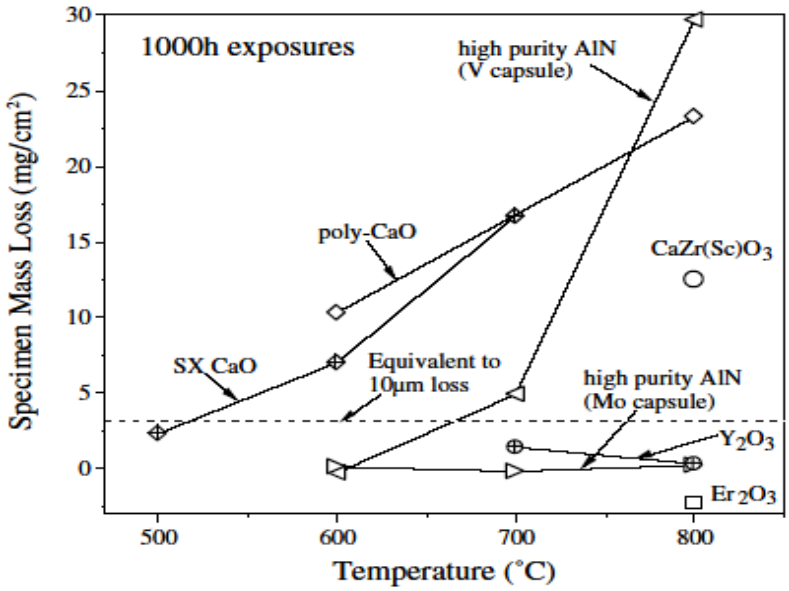

Fig. 1.6-7 Mass losses of oxide and nitride after 1000h exposure in Li at various temperatures [39]

(2) Research progress of insulating coating

The special requirements for insulating coating of Li/V blanket system are as follows [29],

- Resistivity × Thickness > 100 Ωcm^2
- Good compatibility with Li

AlN coating was produced on SUS430 steel substrate by RF sputtering [40]. It showed very low electrical resistivity that perhaps due to non-stoichiometry of the products. The formation of a stoichiometric coating is required by N_2 addition to environmental gas in sputtering.

The resistance of the AlN coating by RF sputtering was dependent on the concentration of N_2 in the working gas. In case of 100% N_2 gas, AlN coating of very high electrical resistance was prepared [25].

AlN coating by RF sputtering showed 3-10at% of oxygen as impurity, and Al : N ratio of 1:1. All the coating had some amount of crystallinity observed by XRD, and orientation that is dependent on fabrication temperature. Crystallinity of coatings increased with annealing. However, the coatings exposed to liquid lithium were mostly lost [41].

AlN coating was made by reactive sputtering, that is, an Al target was sputtered by Ar as the primary sputtering gas with a partial pressure of high-purity N_2. The process proceeds at a relatively low temperature. The exposure of AlN coating produced by PVD method in liquid

lithium for 400h at 300^{o}C and the following resistance measurement at room temperature showed that AlN has some chemical compatibility in lithium and electrical insulating characteristics. However, after Li exposure, the coating surface exhibited reaction product that contained Al and O that may influence insulating property at high temperature and for long exposing time [42]. The AlN coatings on V-alloy substrate by PVD needed a thermal/chemical hardening treatment to improve the adhesion characteristics and probably to reduce the porosity of the coatings. These coatings showed adequate chemical compatibility in normal-purity Li. They also retained their insulating properties after exposure to Li. However, the coating surfaces reacted with Li to form ternary oxides of Li, Al, and O. The effect of increased N content in the Li environment on the coating performance was minimal. Hardness measurements seem to indicate that the absolute values of the hardness of the coating, rather than the difference in hardness between coating and substrate, may play a role in adhesion and spallation [30].

An aluminide layer presented on a V-5Cr -5Ti specimen was nitrided in Li-Li_3N mixture (about 3-5 at% N) in a system that also allowed measurement of the electrical conductivity during formation of the AIN layer. It showed the dependence of in-situ resistance on temperature over the duration of the experiment. However, thermal cycling tends to decrease the resistivity. The reaction between the aluminide layer and N would proceed at a higher rate and thereby show an increase in resistance. This trend, if it had occurred, would indicate that nitriding of spalled regions or defects in the film occur rapidly [34].

Pre-aluminized V-5Cr-5Ti samples were exposed in liquid Li containing 100-150ppmN at 410°C and 500°C for 672 h to examine the formation of nitride layers. During the exposure the electrical resistance was monitored as a function of time. Ti enrichment occurred at the sample surfaces. This trend is consistent with the thermodynamic stability of TiN, which exhibited the highest stability. Although it was predicted that AlN would form in liquid Li containing 150ppm N, Ti enrichment facilitates the formation of a V-Al-Ti-N phase, which is rather conductive [34].

The electrical resistance of insulator coatings produced on as-received (non-aluminided) V-5Cr-5Ti by exposure of the alloy to liquid Li that contained 5 at% N, with and without 5at% dissolved Al, was measured as a function of time at temperatures between 250-500°C.

The solute elements (N and Al) in liquid Li reacted with the alloy substrate at 415°C to produce thin adherent coatings. These results suggest that thin homogeneous coatings can be produced on various shaped surfaces by controlling the exposure time, temperature, and composition of the liquid metal [34].

An optimal method for AlN coating consists: 1) Pre-saturation of V-alloys surface in Li with Al additive within the limits of 5-15wt% at 800°C for the formation of aluminide surface layer; 2) Subsequent exposure of the pre-saturated V-alloys to Li with 1-5wt% of Al and 0.5-5wt% of N under stepwise variations of temperature (ΔT=50°C) from 600 to 800°C, resulting in continuous formation of AlN coating without dependency on alloy composition. Although its resistivity was not high enough for application, it showed the self-healing property in Li [43].

Three kinds of insulating barriers have been made: (1) Two-layered or multi-layered metal-ceramic barriers obtained with deposition/spraying technique; (2) Ceramic and ceramic/metal-clad barriers; (3) Multi-layered metal-ceramic barriers obtained by baking technology. It was shown as well that mechanical integrity and specific electrical resistance of AlN ceramic after Li exposure, depended on the initial composition of ceramic and technology of its fabrication [44].

CaO coatings on vanadium alloy were prepared by metallorganic chemical vapor deposition (MOCVD). The best substrate temperature to grow the coating is 650^{o}C. The CaO layers were formed fairly compact. No crack was noted after five thermal cycles from 25 to 715^{o}C. Although resistance of the coatings dropped 100 times after exposure in liquid Li at 600^{o}C for 100 h, their areal resistance was still high enough for the insulator application [45].

CaO coatings were also made by thermal/chemical vapor-deposition (T/CVD) process and an in-situ approach in a liquid Li-Ca environment. Results showed that thick adherent coatings could be fabricated by T/CVD, especially if a double Ca treatment is applied. Coatings were also developed by the in situ approach, but the coatings were much thinner than the desired. Furthermore, the coating composition was non-uniform, with significant presence of V in several locations on the coated surface. Extensive microstructural analysis of the coatings developed by the T/CVD showed almost 100% CaO over a coating; electrical resistance (measured by the two-probe method) of the coatings was at least 2 orders of magnitude higher

than the minimum requirement for blanket application. Electrical resistance of in situ developed coatings was adequate at temperatures up to 350°C, but decreased substantially at higher temperatures. The results indicate that CaO is a viable coating for V-Li blankets, but needs additional effort, especially from the standpoint of structure/composition relationship to its electrical resistance [46, 47].

The approach for in-situ coating involves an interfacial reaction of calcium dissolved in lithium with oxygen dissolved in the V-alloy to form a CaO coating on the V-alloy substrate. The scheme for in-situ formation of CaO is shown at Fig. 1.6-8.

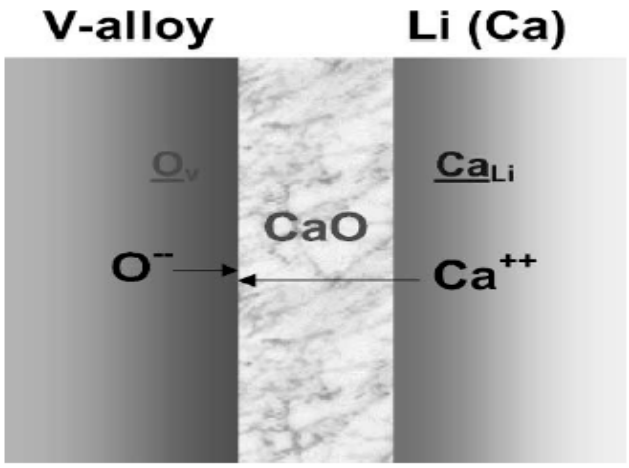

Fig. 1.6-8 The scheme for in-situ formation of CaO in liquid Li [26]

The factors that aid the coating formation include a high solubility of Ca in Li, relatively high solubility and mobility of oxygen in V-alloys, and the stability of CaO in Li with low-oxygen concentration. Calcium oxide coatings have been successfully formed on V-alloy substrates by exposure of oxygen-charged V-alloys to Li doped with Ca. Oxygen charging of V-alloys was varied from 0-2.5 mgO/cm^2. The V-alloys were conditioned at ~750°C to dissolve surface oxide into metal and to avoid formation of complex Ca-V-O compounds that exhibit low-electrical resistivity. V-alloy specimens were exposed to Li-2.8at% Ca at 600°C for 120h and at 700°C for 50h. The coating thickness correlated with oxygen pre-charge and varied with exposure time and temperature. The coatings appear to be adherent and relatively uniform, and exhibit high electrical resistivity (~108 Ωcm at 500°C) [26]. CaO coating was formed after exposure to Li-2.8at% Ca at 600°C. The electrical resistivity of a CaO coating on

V-4Cr-4Ti was shown at Fig. 1.6-9. The resistivity was measured as a function of temperature up to 500°C with liquid Ga contacts after exposure to the lithium. The measured electrical resistivity is approximately 3 orders of magnitude higher than required for the projected application [31].

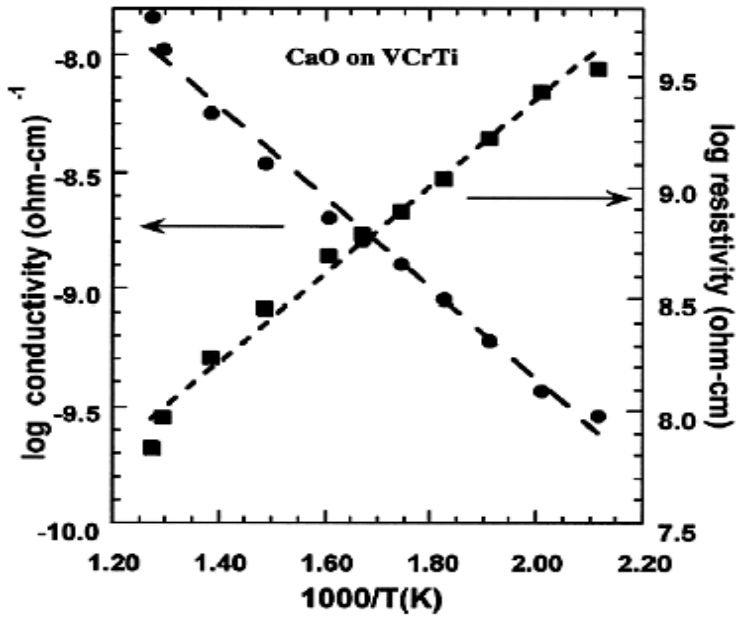

Fig. 1.6-9 Electrical resistivity of CaO coating formed on V-alloy [31]

However, thermodynamic calculations and recent experimental work [38] on bulk CaO specimens have proven that CaO cannot perform adequately at 600-800°C in static Li tests. A mass loss of ~3 mg/cm^2, is equivalent to a 10μm loss of material during exposure in Li. These mass losses at high temperatures are unacceptable for a thin coating. An even higher dissolution rate (0.085μm/h) was observed for single crystal CaO in Li-2.8 at% Ca at 600°C. Results for coatings formed on V-4Cr-4Ti with different oxygen preloading showed a lower dissolution rate when tested under the same conditions at 600°C (Fig. 1.6-10). However, the dissolution rates were sufficient to remove a significant fraction of coating after 1000 h and suggested coating lifetime of <3000h at 600°C (Fig. 1.6-10). Because of its poor compatibility at high temperature, the CaO coating development program in the USA has been concluded.

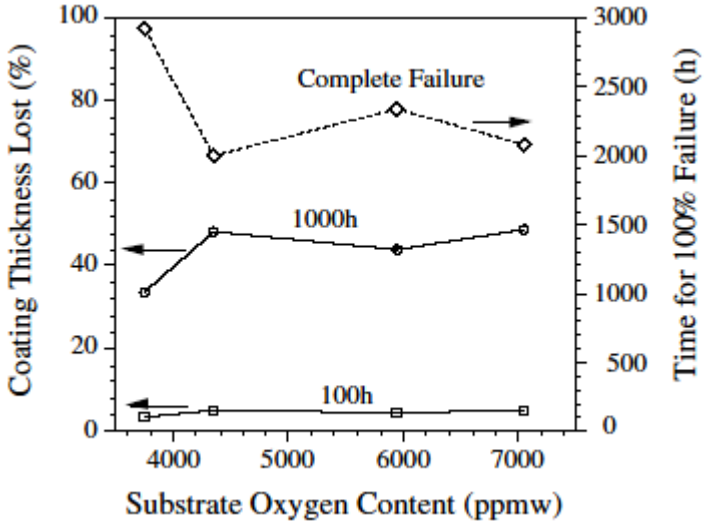

Fig. 1.6-10 Performance of CaO coatings in Li-2.8 at% Ca at 600°C [39]

The process of formation and degradation of CaO on V-alloys is being modeled. The oxygen from the substrate can react with Ca in Li to form a CaO outer layer. However, this requires balanced fluxes of Ca in the Li and O from the substrate, which are in most case difficult to achieve. As oxygen is removed from the substrate, Ti-rich oxide particles dissolve. Eventually, some Ca and Li become incorporated into the metal while V and Ti can become incorporated into the oxide. This process degrades the coating and substrate. To eliminate the mixture of V and oxide, the effect of deposition of CaO layer prior to exposure to Li-Ca was investigated [48, 49]. In this case, similar problems eventually developed as oxygen is removed from the substrate and V and Ti are incorporated into the oxide.

Because of the problems CaO coating met, more emphasis is now being placed on developing Y_2O_3 and Er_2O_3 as coating candidate materials.

Y_2O_3 coatings were deposited on V-4Cr-4Ti substrate, by an electron-beam assisted, physical vapor deposition process (EB-PVD) [39]. The figure of merit for coating evaluations is the change in coating resistivity at 700°C after exposure to Li. The coating must maintain adequate resistivity in order to warrant further testing. In order to avoid oxidation of the vanadium alloy substrate, the electrical resistance was measured in a vacuum. This initial set of coatings showed relatively low resistivity. The coated specimens were exposed to lithium in sealed vanadium alloy capsules for 100-1000 h at 700 and 800°C. After exposure, performance varied from little change in resistivity and microstructure to complete loss of the

coating. The electrical resistance measured after 3, 100h cycles at 800°C (cooling to room temperature between each cycle) was higher than the as-received coatings. However, after 1000 h at 800°C, degradation in the resistivity was observed. At long exposure time and high temperature, $LiYO_2$ were observed. The surface morphology of the coating changed significantly after exposure. Oxide particles containing Ti and Y were observed as well on the coating surface. After a 2000 h exposure at 800°C, the coating was destroyed. Exposures at 700°C on a second set of coatings typically showed a complete loss of the coating. Although Y_2O_3 coatings show a potential compatibility problem, additional work is needed on coating development to further study the phenomenon as well as the role of coating microstructure on the reaction with Li.

Characterization of electron beam physical vapor deposition (EB-PVD) Y_2O_3 coatings after exposure to Li showed significant changes in the microstructure. Single and bi-layer EB-PVD coatings of Er_2O_3 and Er_2O_3/V have been fabricated and initial characterization has started. A new test rig was constructed for measuring coating resistivity during contact with Li at temperatures up to 500°C. Initial performance of the Er_2O_3 coatings in an in-situ test showed loss of insulating behavior after the Li became liquid (180°C) and significant degradation after exposure to Li at 500°C [50].

Er_2O_3 coating were deposited by plasma-assisted physical vapor deposition using a filtered vacuum arc device. Its crystallization of the cubic crystal phase occurs at room temperature, when a bias voltage of -100 V is applied [51]. The coating has a very smooth structure and is almost stoichiometric with polycrystalline phase [52]. However, its property for insulator needs to be tested further.

Er_2O_3 coating was deposited by RF sputtering, which has high resistivity in vacuum. After annealing tests, some coatings have generated many pits and cracks on surface. After sintering in liquid lithium, all of the coatings had damaged. The damage shows peeling, however it also shows the coatings themselves were not dissolved in liquid lithium. The high crystalline coating has succeeded to stand chemical attack of liquid lithium. The peeling off occurred by exposure in liquid lithium is due to the cracks caused by the annealing followed by preferential corrosion of the coating-substrate interface [53,54].

In-situ insulating coating in liquid lithium is quite attractive, because of possibility to self-heal cracks of coatings without disassembling components during operation, and possibility to deposit coatings onto complex inner surfaces of components after fabrication. However, there is no report about the in-situ coating of Er_2O_3 and Y_2O_3 on vanadium alloys for insulator application to Li/V blanket.

1.7 Objectives of present study

The objective of this study is to investigate the feasibility of the author's original idea:
To produce Er_2O_3 (or Y_2O_3) insulating coating on a reference vanadium alloy (V-4Cr-4Ti) by in-situ method of exposure to liquid lithium at high temperature.
For the purpose of reducing MHD pressure drop to an acceptable level to a self-cooled Li/V blanket, the coatings should have high insulating property, self-healing function and good compatibility with liquid Li.

To verify new kinds of coating, this study aims:

- To demonstrate feasibility for formation of Er_2O_3 (or Y_2O_3) coating on V-4Cr-4Ti
- To perform characterization of the microstructure, phase, composition, resistivity of the coating, stability of coating in liquid Li and potentiality of self-healing to cracks in the coating in liquid Li.
- To understand the mechanism of oxygen performance during the pre-charging to V-4Cr-4Ti substrate.
- To understand the nucleation and growth kinetics of the coating in erbium (or yttrium) doped Li.
- To obtain the optimized process for the coating including the condition for oxygen pre-charging to V-4Cr-4Ti, erbium-doping level in liquid Li and various exposure parameters in Li.

For above purposes, the research steps taken in this study are:

- To obtain the optimized method and test conditions for oxygen charging (oxidation, annealing) in V-4Cr-4Ti.
- To examine the performances of in-situ coating by exposure to liquid lithium.
- To perform the modeling for understanding nucleation and growth of the coating in liquid lithium.

CHAPTER 2

Experimental Procedures

The procedures of in-situ coating on vanadium alloys in liquid lithium generally consists of three steps,

1) Oxygen introduction at surface region of vanadium alloy substrate
2) Oxygen homogenization into limited depth of vanadium alloy substrate
3) In-situ formation of insulating coating onto vanadium alloys substrate in liquid Li.

The scheme on the formation procedures of in-situ coating is shown at Fig. 2.1-1.

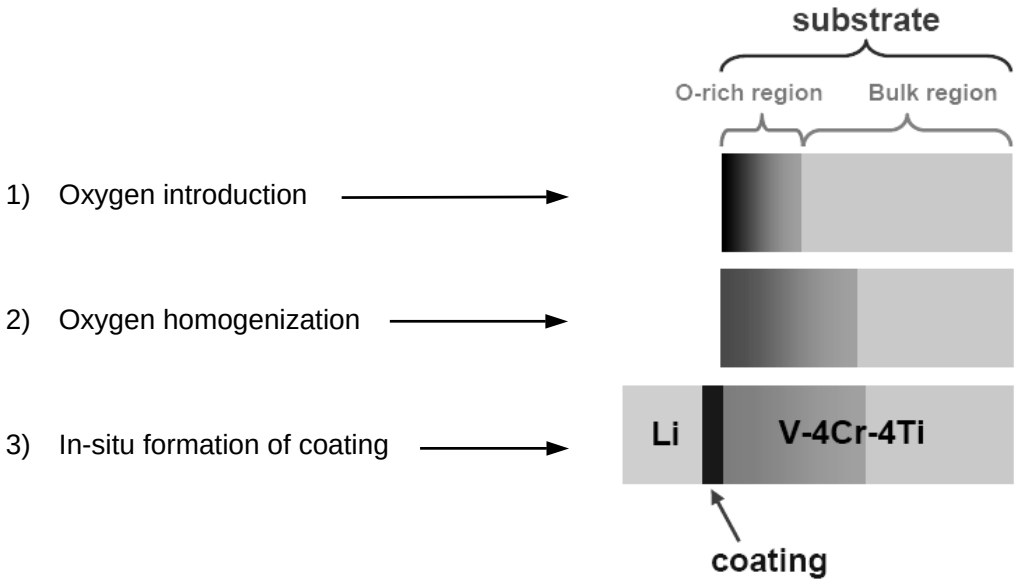

Fig. 2.1-1 Scheme on formation procedures of in-situ coating on V-alloy in lithium

In this study, V-4Cr-4Ti (NIFS-HEAT-2) that was developed by National Institute for Fusion Science (NIFS) for structural materials of advanced blanket, was selected as a substrate for the coating. In the later text, Vi4Cr-4Ti (NIFS-HEAT-2) is expressed shortly as V-4Cr-4Ti. Pure V (reference material) was also used for comparison. The analytical data were reported [55, 56] and reproduced in Table 2.1-1.

Table 2.1-1 Chemical composition of V-4Cr-4Ti and pure V

	O [ppm]	N [ppm]	Ti [wt%]	Cr [wt%]	V [wt%]
V-4Cr-4Ti	148	122	3.98	4.02	balance
Pure V	69	116	—	—	balance

2.1 Oxidation and annealing of V-alloys

(1) Oxidation

The purpose of oxidation is to introduce oxygen at surface region of vanadium alloy substrate. The substrates were cut to ~7×7×0.5mm for V-4Cr-4Ti and ~7×7×1mm for pure V. The surfaces of samples were pre-treated by mechanical and electrical polishing. The weight was measured by analytical balance with accuracy of 10^{-5}g. The samples were set at a alumina holder in a gas flowing chamber and oxidized at 600-1000^{o}C for 0.5-8 hours, by exposing specimens to flowing argon with nominal purity of 99.9999wt% grade (O_2 < 0.1ppm, N_2 < 1ppm, moisture < 0.5ppm) and flow rate of 400ml/min, using a thermo-gravimetric (TG) apparatus (Fig. 2.1-2).

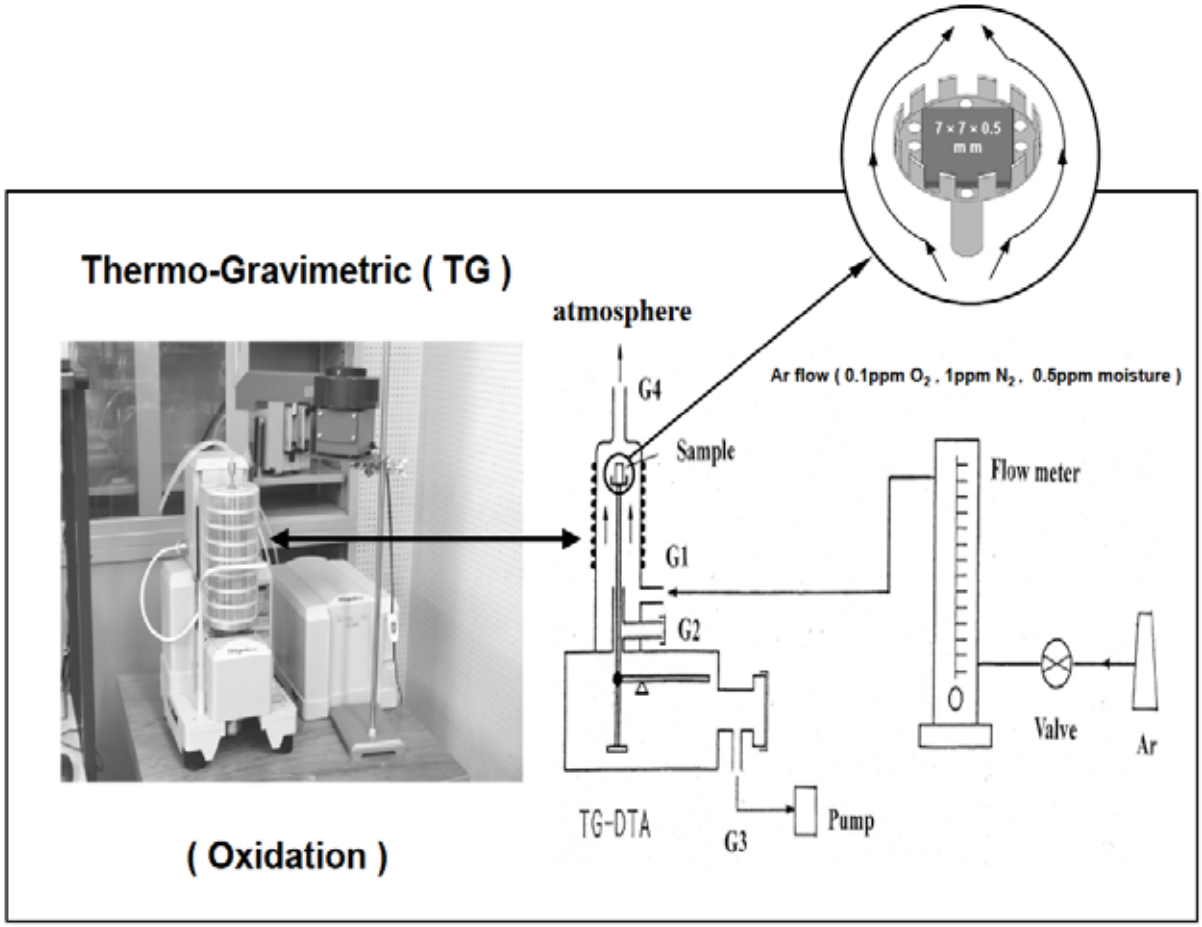

Fig. 2.1-2 Thermo-gravimetric (TG) apparatus for oxidation of vanadium alloys

(2) Annealing

The purpose of annealing is to homogenize oxygen into a limited depth of vanadium alloy substrate. After oxidation, half of each oxidized samples was set in a vacuum quartz tube to be annealed at 700^{o}C for 4-32h. In the tube, the samples were kept in a Ta box (avoiding adherence between sample and Zr foil) wrapped with Zr foil (oxygen getter). The quartz tube was continuously pumped to vacuum of about 10^{-5} Pa during the annealing process, by use of a turbo molecule pump (TMP). Weight change was measured by analytical balance with accuracy of 10^{-5}g. No weight change was measured after annealing, it suggested that no impurity elements were gotten in the pre-oxidized samples during the annealing process. The vacuum furnace for the annealing is shown at Fig. 2.1-3.

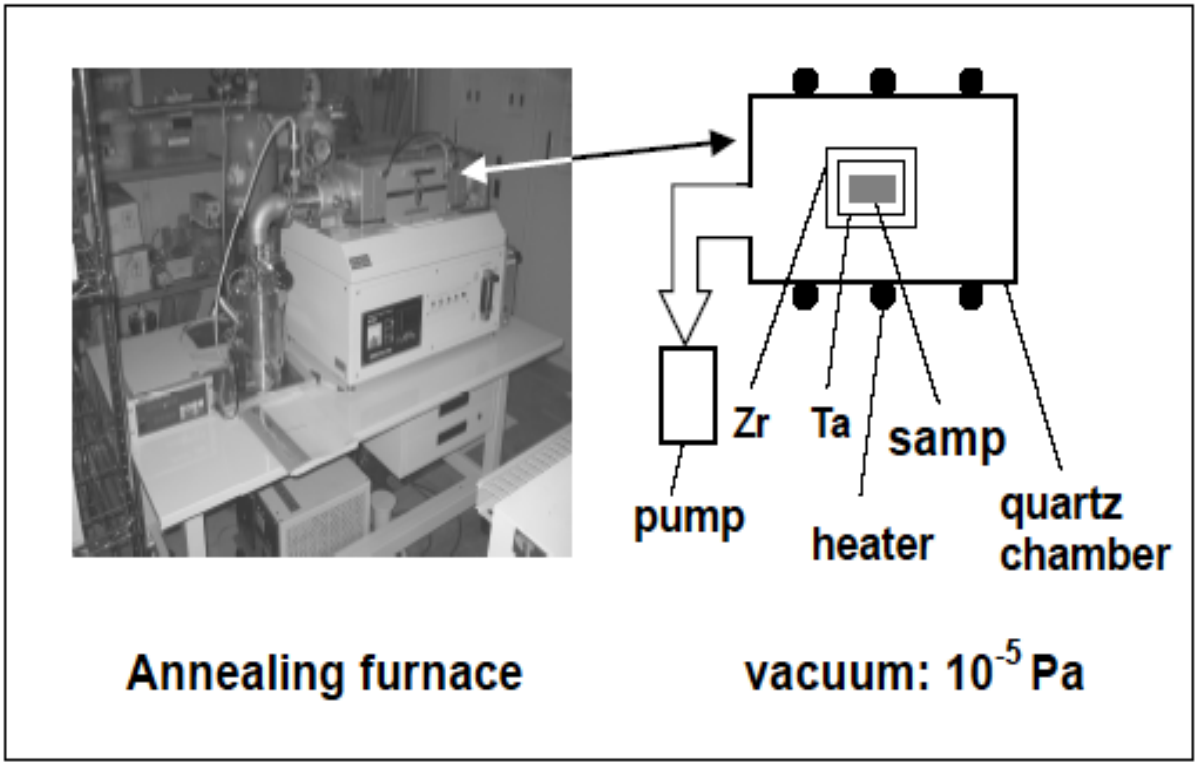

Fig. 2.1-3 Vacuum furnace for annealing process

2.2 Exposure to liquid lithium doped with erbium

The as-received, oxidized only and oxidized plus annealed samples were exposed in static liquid lithium (nominal purity of 99.9%) doped with Er or Y powders (99.9% purity). This process was performed in a glove box filled with inert argon. A cylinder of Li (~25g) was molten in Mo crucible in argon atmosphere and the oxide floater on the surface of liquid lithium was filtered. The Er powder with doping level of 1-16wt% of Er/Li was introduced into liquid lithium, while the erbium solubility in lithium was estimated to 0.15wt% by sampling lithium during exposure at 600^{o}C and analysis with atomic absorption spectrometry. Then the samples were put in the lithium. After freezing, the lithium with Mo crucible (with a Mo cover to stop strong Li vaporization above 600^{o}C) was set into test container (Fig. 2.2-1) of stainless steel. Finally the container was sealed by Cu gasket in glove box with Ar.

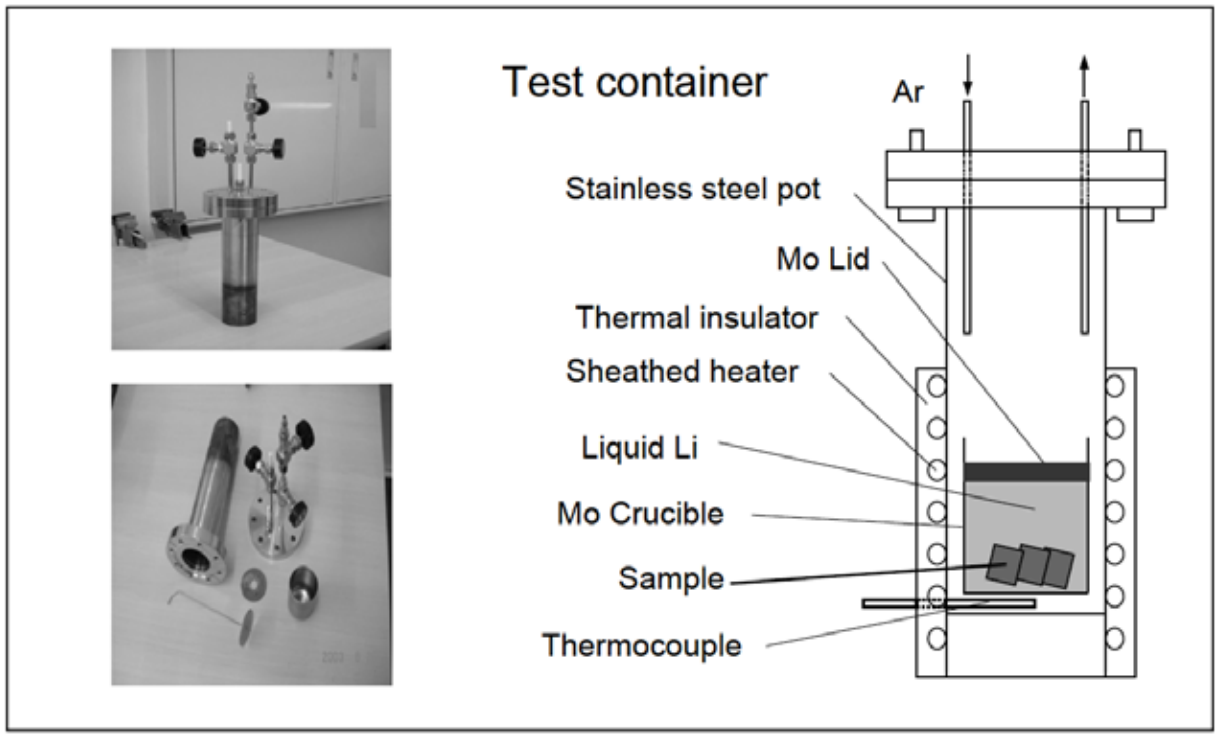

Fig. 2.2-1 Test container with argon atmosphere for Li exposure

The test container was taken out from the glove box to be set in a resistance furnace (Fig. 2.2-2). The upper section of the container was out of the furnace for cooling the sealing flange. The test temperature was controlled by a heating controller with an adjuster. After required test time, the power supply was stopped and test container was cooled with furnace naturally.

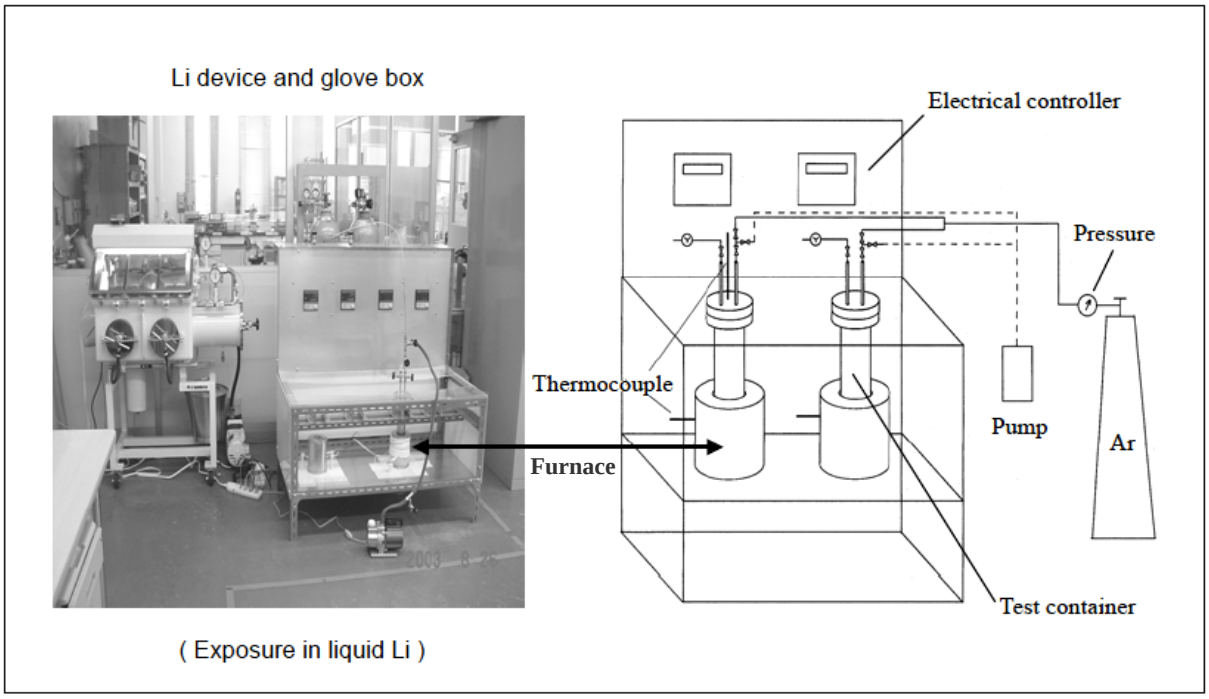

Fig. 2.2-2 Glove box and heating device for Li exposure

After Li exposure, the container was moved to open in glove box with argon atmosphere. Lithium was re-melted and samples were taken out from lithium. After samples were moved from the glove box to air following cooling, the solid lithium adhering on surface of samples was washed by using strong lotion (H_2O) and dehydrated by ethanol at room temperature (20^oC) or weak lotions (liquid NH_3) at low temperature (-33.5^oC) and dehydrated by acetone at room temperature. Then the dry and clean samples were analyzed further.

2.3 Characterizations of coating

Many analytical methods were applied for characterizations of the coatings (also for vanadium alloys before or after oxidation and annealing). Generally, the surface and depth elemental state profile were analyzed by X-ray photoelectron spectroscopy (XPS) under sputtering with Ar ions at a calibrated rate of ~13nm/min. The microstructure and composition were analyzed by transmission electron microscopy (TEM), electron diffraction (ED) and scanning electron microscopy (SEM) with energy dispersive X-ray spectroscopy (EDS). Vickers hardness was measured by hardness meter with a load of 10gf. The content of oxygen and nitrogen in vanadium alloys at various conditions were analyzed by chemical method. The phase of coating was identified by X-ray diffraction (XRD). XRD with 0.2^{o} incidence angle enhanced the contribution from surface layer. The resistivity of as-received, oxidized, annealed and Li exposed samples were measured in air at room temperature or vacuum (10^{-3} Pa) at a range of room temperature to 600^{o}C, by the two-electrode method (Fig. 2.3-1).

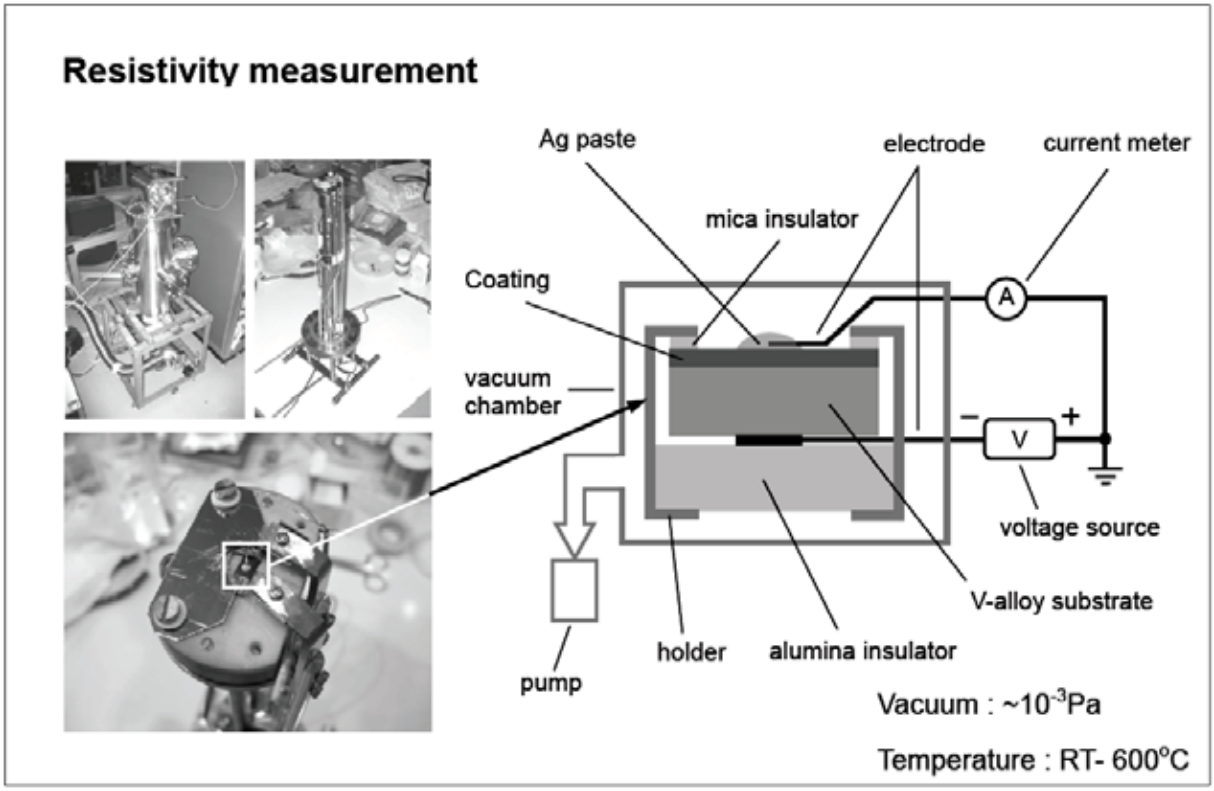

Fig. 2.3-1 Apparatus for resistivity measurement

CHAPTER 3

Optimizations of Oxygen Charging into Vanadium Alloys as Pre-treatment for In-situ Coating

3.1 Distributions and states of oxygen in V-alloys by oxidation and annealing

(1) The choice of parameters for oxidation and annealing of vanadium alloys

To understand the oxygen absorption behaviors, pure V was tested as well as the reference V-4Cr-4Ti alloy.

The effects of impurity level of initial oxygen and nitrogen on the oxidation behavior were investigated. Fig. 3.1-1 shows the weight gain of pure V and V-4Cr-4Ti alloy with various levels of oxygen and nitrogen for 0.5-8h at 700°C.

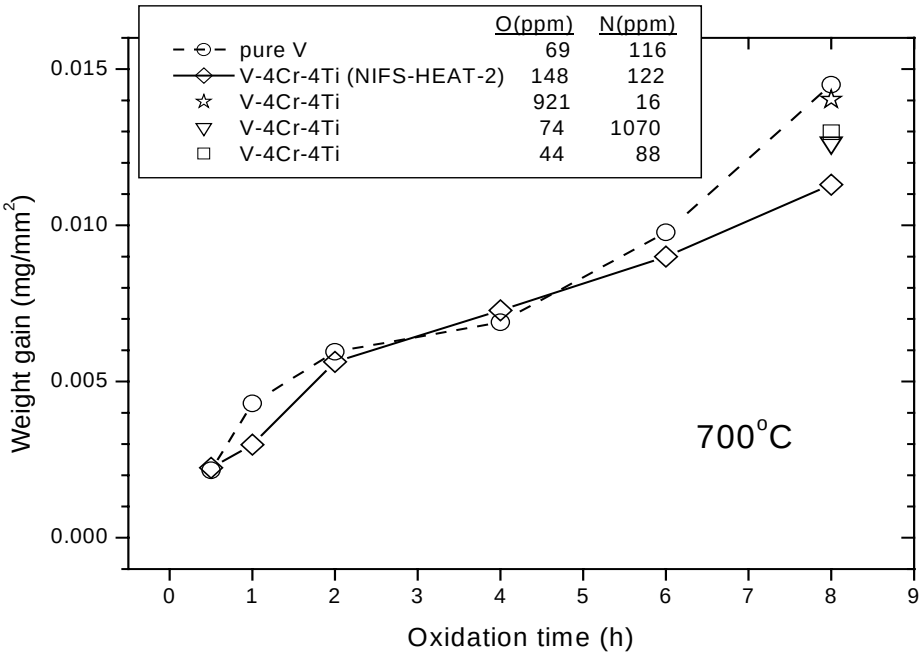

Fig. 3.1-1 Effect of initial levels of oxygen and nitrogen on weight gains of V-alloys

The weight gain corresponds to the amount of oxygen or nitrogen charged into specimens. The above figure indicates that initial level of oxygen or nitrogen has a small effect on the weight gain in the further oxidation process. The differences of weight gain between V-4Cr-4Ti and pure V seem to be due to the effects of alloying elements (Ti or Cr) in V-4Cr-4Ti on absorbing oxygen.

The key parameter was the oxidation temperature. Fig. 3.1-2 showed the surface view of V-4Cr-4Ti and pure V after oxidation for 1h at 600-1000°C.

Pure V

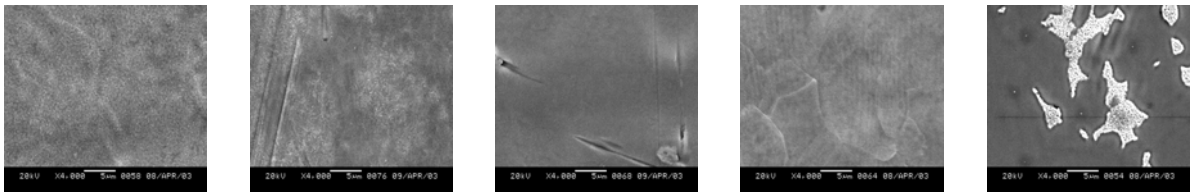

600°C **700°C** **800°C** **900°C** **1000°C**

V-4Cr-4Ti

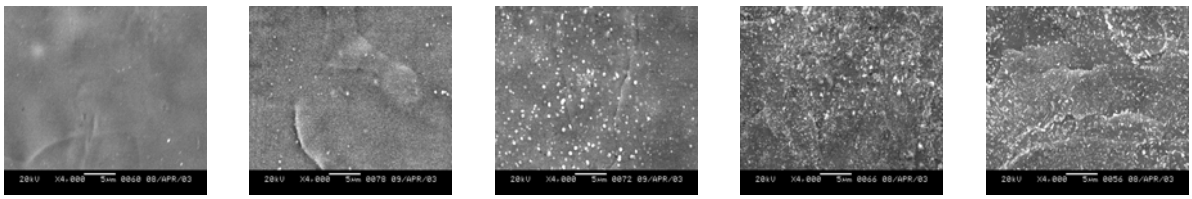

Fig. 3.1-2 Surface view of V-4Cr-4Ti by SEM after oxidation of sample for 1h

At 1000°C, the surface oxidation layer of pure V, which is presumable of the V_2O_5 phase, was melted and partially evaporated, similar to the reported results on oxidation of pure V in air [57]. However this phenomenon was not observed for V-4Cr-4Ti, perhaps due to alloying elements of Ti or Cr that absorb O, inhibiting the formation of V_2O_5, in low oxygen environment in this study.

Fig. 3.1-3 shows the weight gain of pure V and V-4Cr-4Ti as a function of oxidation temperature during oxidation for 1h. The figure clearly shows that weight gain had big drop at 1000°C for pure V, which is likely to be caused by the evaporation of surface oxide layer.

Fig. 3.1-4 showed the Vickers hardness profile of V-4Cr-4Ti oxidized for 1h at various temperatures. It is known that the Vickers hardness is a positive function of the oxygen level for V-4Cr-4Ti and pure V, because of both solid solution and precipitates of oxygen [58, 59]. The size and density of Ti-O precipitates influence hardness as well as solid solution level of oxygen. The figure indicates the charged oxygen was concentrated in the surface layer with large gradient. At 600°C or 700°C, the diffusion depth of oxygen was almost same, although the oxygen concentration gradients were different. At 800°C, the diffusion depth and the oxygen concentration gradients became much larger than that at 600-700°C. Above 800°C, the gradients became lower but the depth became even larger. Especially a plateau of hardness is

observed at 1000°C, perhaps owing to dissolution of Ti-O and deep diffusion of oxygen into the substrate.

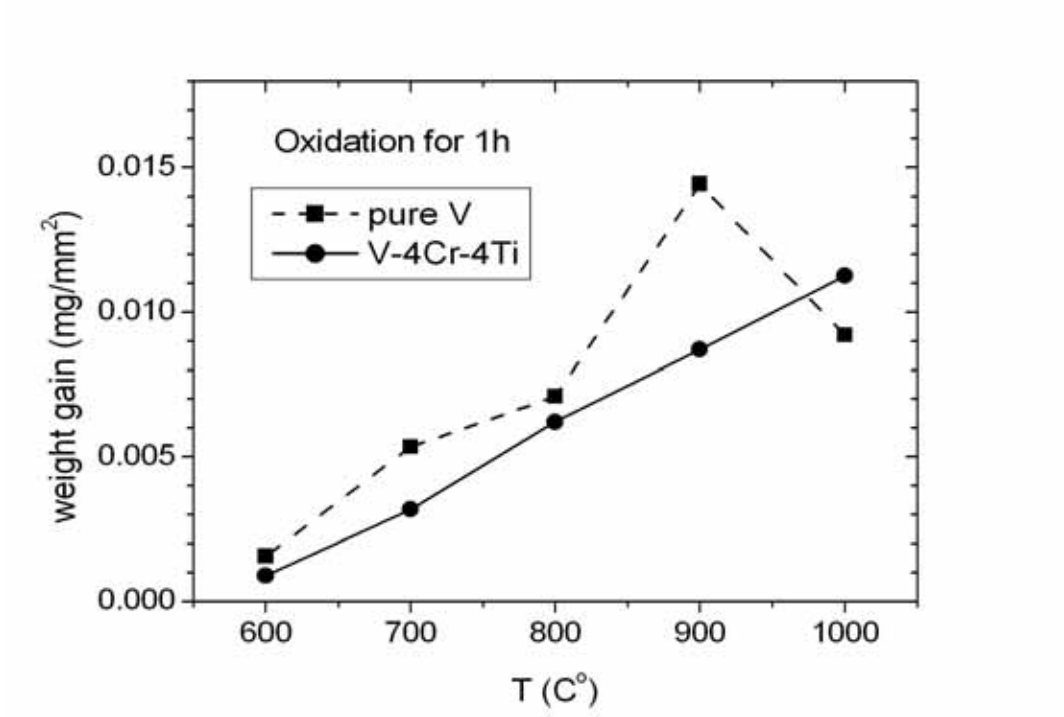

Fig. 3.1-3 Oxidation temperature dependence on weight gain of pure V and V-4Cr-4Ti

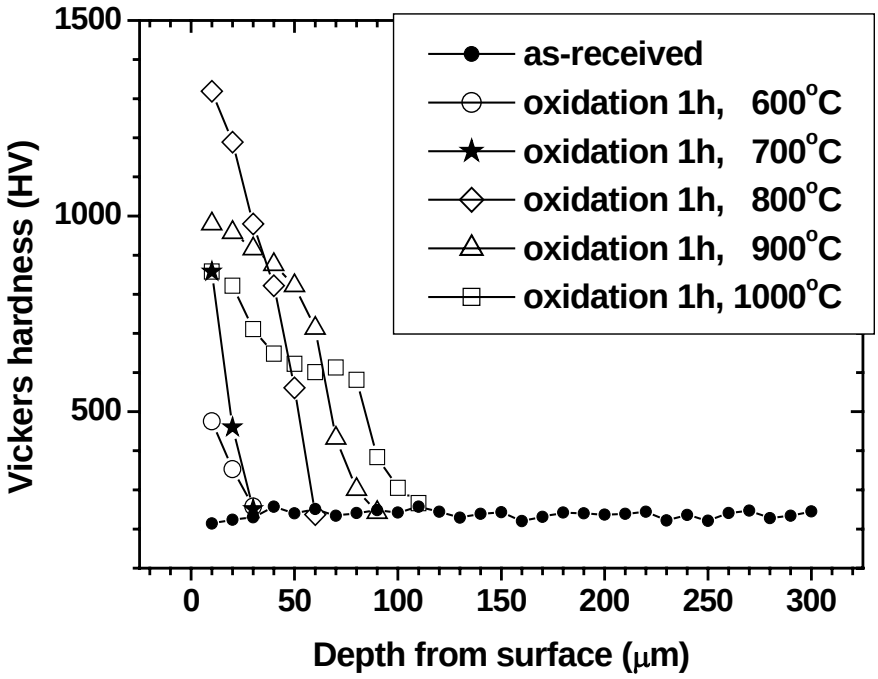

Fig. 3.1-4 Vickers hardness profile of V-4Cr-4Ti oxidized for 1h at various temperatures

Vanadium alloys under investigation for the structure typically contain about 100wppm oxygen; however, the solubility of oxygen in vanadium is over 1wt% at the temperatures of interest. Oxygen is also relatively mobile in vanadium with a diffusivity of about 10^{-9} cm^2/s at 600°C. Therefore, at temperatures of primary interest, 500-700°C, oxygen is sufficiently mobile to diffuse to the surface of the V-alloy [26]. Additional oxygen was pre-charged into the surface of the alloy to provide sufficient oxygen to form the coating.

The amount of oxygen charged into vanadium alloys is increased with oxidation temperature. However, the maximum operating temperature limit for vanadium alloys in design studies is typically assumed to be about 700°C [60]. Alternately, it has been suggested that vanadium alloys might be capable of operation at 750°C [61] from standpoint of mechanical properties. Thus an oxidation temperature of 700°C was selected.

The oxidation and annealing processes charged oxygen and little nitrogen into V-4Cr-4Ti, that was consistent with the results of pure V exposed in air [62]. The literature indicated that the oxygen was charged into pure V above ~250°C and the rate increased strongly above ~450°C, with little nitrogen charged up to ~650°C. Since the hardness increased steeply with nitrogen introduction [59], the oxidation was carried out in this study at 700°C in high purity argon to avoid introducing nitrogen. Because excessively strong and rapid oxidation should result in thick oxide layer on the surface that may act as barrier to the following oxygen introduction into substrate, the slow oxidation at low oxygen partial pressure and annealing in vacuum were carried out at 700°C.

From the both standpoints of keeping mechanical property of vanadium alloys and avoiding harmful nitrogen introduction, a temperature of 700°C was considered to be suitable for the oxidation of vanadium alloys in a low oxygen environment.

After fixing the temperature of 700°C for oxidation and annealing, the subsequent consideration is the time for oxidation and annealing. Fig. 3.1-5 showed the Vickers hardness profiles of V-4Cr-4Ti oxidized for various time at 700°C. The amount of oxygen charged increased with oxidation time. However after oxidation of 4h, the oxygen concentration gradient changed little. After oxidation of 8h, a plateau appeared in the oxygen depth distribution indicated the oxygen re-distributions or phase change.

During oxidation, since the extensive oxygen diffusion or phase changes were not intended, an oxidation time of 6h was chosen at 700°C.

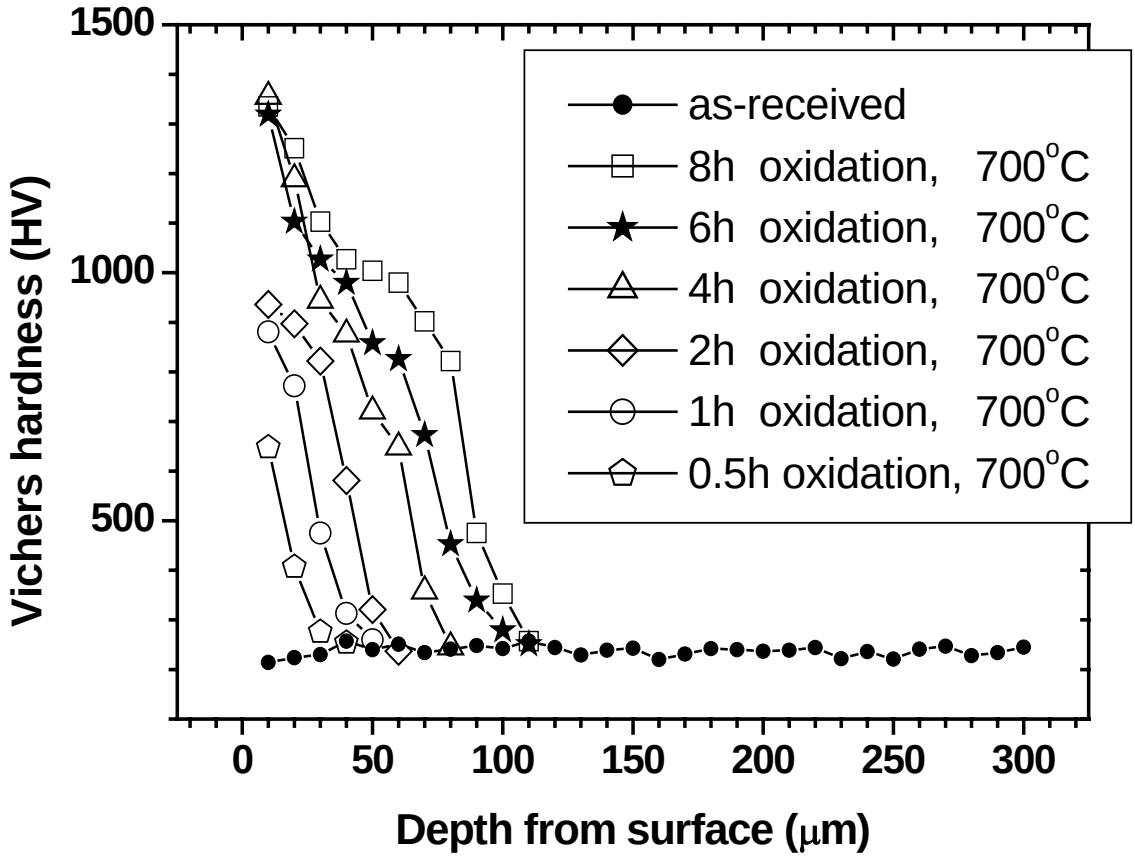

Fig. 3.1-5 Vickers hardness profiles of V-4Cr-4Ti oxidized for various time at 700°C

The remaining parameter is the annealing time. Fig. 3.1-6 showed Vickers hardness profiles of V-4Cr-4Ti oxidized for 6h plus annealed for various time at 700°C. After annealing, the large gradient of hardness disappeared. A plateau to a depth of about 150μm appeared, suggesting that oxygen distribution became uniform owing to the phase formation to trap oxygen in V-4Cr-4Ti. The depth of oxygen rich region into substrate had a small dependence on the annealing time, thus suggesting that the requirement to the annealing time could be lenient.

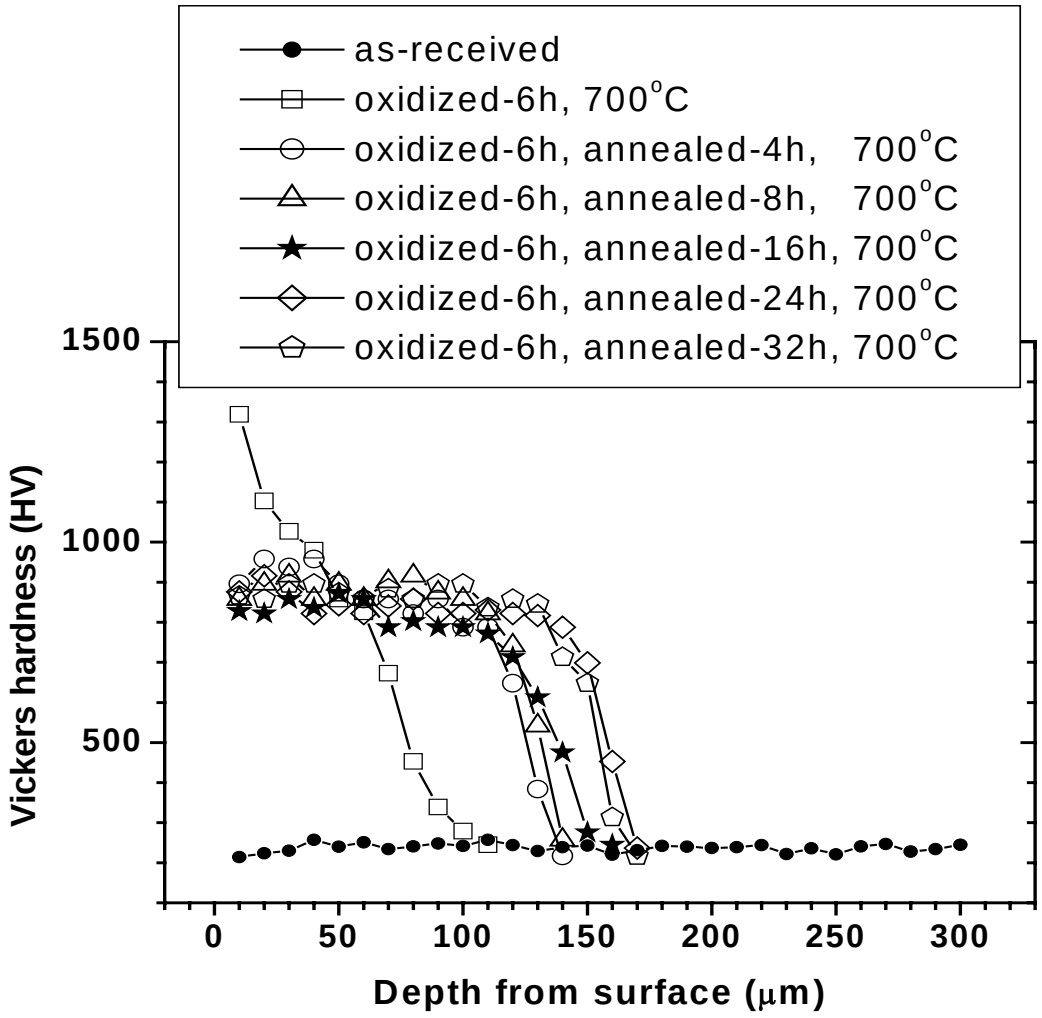

Fig. 3.1-6 Vickers hardness profiles of V-4Cr-4Ti oxidized for 6h plus annealed for various time at 700°C

The parameters used in most of this study were: oxidation in argon flow for 6h at 700°C plus annealing in vacuum for 16h at 700°C.

(2) Characterizations of oxygen behaviors in V-alloys by oxidation and annealing

Fig. 3.1-7 showed the contents of oxygen and nitrogen in V-4Cr-4Ti and pure V by chemical analysis after various pre-treatments (oxidation-6h, 700°C ; annealing-16h, 700°C).

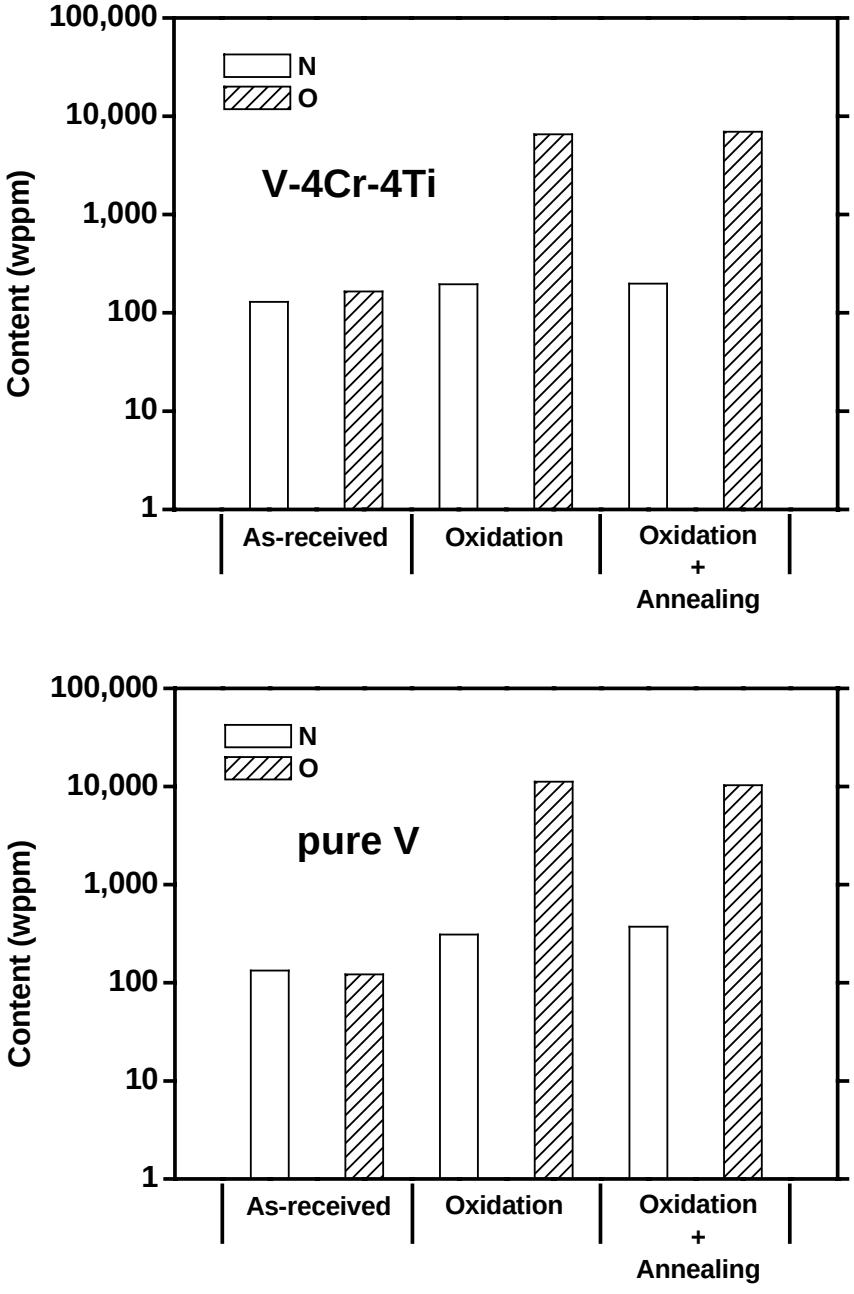

Fig. 3.1-7 Contents of oxygen and nitrogen in V-4Cr-4Ti and pure V by chemical analysis (oxidation-6h, 700°C ; annealing-16h, 700°C)

By choosing a suitable temperature and time for oxidation and annealing, the goal of oxygen charging process was achieved, i.e. the oxygen was charged to an enough high amount with little nitrogen into vanadium alloys. Fig. 3.1-7 showed that the content of oxygen increased from original about 100ppm to 10000ppm, while the contents of nitrogen almost did not increase, by oxidation in high purity argon. Nitrogen is difficult to be introduced at 700^{o}C [62]. No change of contents for both oxygen and nitrogen was shown in oxidized vanadium alloys during subsequent annealing in vacuum, because the source of oxygen or nitrogen was very short in vacuum. No weight change after annealing within the measurement resolution also supported the above interpretation. Relative to V-4Cr-4Ti, more oxygen was charged into pure V. The reason could be presumed that alloying elements (Ti or Cr) in V-4Cr-4Ti could absorb oxygen to form oxide precipitate, and the oxide region at the surface of substrate could be a barrier for farther oxygen diffusion into substrate.

Fig. 3.1-8 shows Vickers hardness depth profile of V-4Cr-4Ti and pure V (as-received, oxidized for 6h at 700^{o}C and oxidized for 6h at 700^{o}C plus annealed for 16h at 700^{o}C). The Vickers hardness is a positive function of the oxygen level for V-4Cr-4Ti and pure V [59, 60], so that a hardness profile could describe the oxygen distribution along depth from the surface into bulk. The figure indicates the charged oxygen was concentrated in the surface layer with large gradient. The thickness of O-rich layer is ~100μm for V-4Cr-4Ti and ~250μm for pure V. The thickness was extended to ~150μm for V-4Cr-4Ti and more than 500μm for pure V by the annealing. The distribution of oxygen in V-4Cr-4Ti became uniform as a result of diffusion of oxygen at high temperature. Considering the necessity of maximizing oxygen storage for supplying to oxide coating and minimizing the harmful effect of oxygen on mechanical property of vanadium alloys, both high amount of oxygen charging and limited depth of oxygen enrichment are required. For pure V, either by oxidation or annealing, the oxygen cannot be concentrated in a region with limited depth of substrate, although the oxygen-charging amount is large. Fortunately, the above two requirements can be achieved in V-4Cr-4Ti. The large amount of oxygen was charged into substrate by oxidation, and the distribution of oxygen was homogenized in a region with depth of about 150μm of V-4Cr-4Ti substrate by the following annealing.

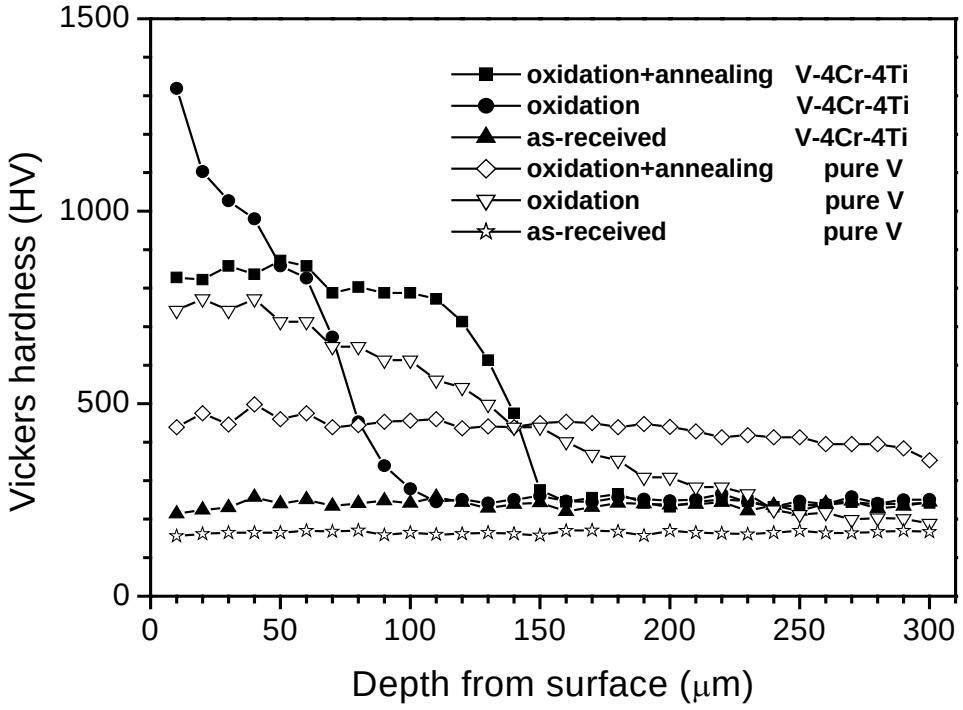

Fig. 3.1-8 Depth profile of Vickers hardness for V-4Cr-4Ti and pure V (as-received, oxidized for 6h at 700°C, oxidized for 6h at 700°C plus annealed for 16h at 700°C)

After oxidation, the oxygen is just rich in surface layer and the surface color turned dark by the observation of naked eye. By the subsequent annealing, the oxygen diffused quickly into depth of bulk and surface color recovered to silvery white similar to that of as-received ones.

Fig. 3.1-9 shows TEM images of microstructure in region near the surface of V-4Cr-4Ti corresponding with Vickers hardness profile at various test conditions. The as-received V-4Cr-4Ti contained blocky precipitates of Ti-N-O-C as already identified in the previous study [9, 58]. The oxidized V-4Cr-4Ti showed complex image of V-O compounds. XPS at the surface showed the binding energy of V2p3 of ~ 516eV as VO_2 in agreement with literature [63-65]. By TEM, the oxidized plus annealed V-4Cr-4Ti showed precipitates oriented to <200>. XPS of the specimen indicated Ti2p3 of ~ 459eV as TiO_2 in agreement with literature [63, 64]. No Cr-O precipitates were found during oxidation and annealing. The reason was thought that Ti is much more active than Cr to react with oxygen . So that Cr acts no role as oxygen storage, for the subsequent formation oxide coating.

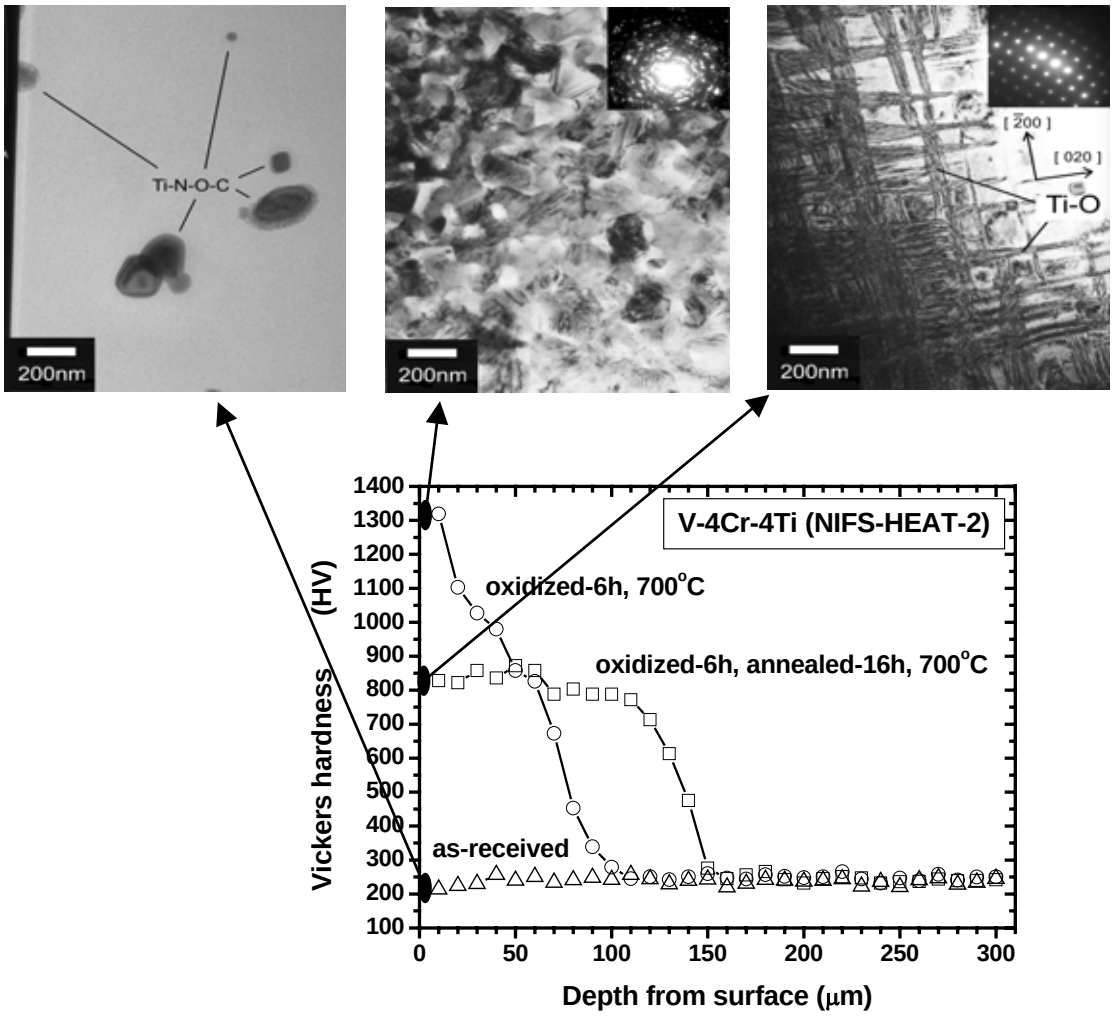

Fig. 3.1-9 TEM images of microstructure in region near surface of V-4Cr-4Ti corresponding with Vickers hardness profile at various test conditions

Fig. 3.1-8 indicates that the diffusion of oxygen in V-4Cr-4Ti is much slower than that in pure V. The reason is that Ti acts as a strong trapping center for oxygen atoms. Ti is more active than V to react with O in V-4Cr-4Ti forming large amount of oriented Ti-O precipitates (see Fig. 3.1-9) that suppress the diffusion of oxygen strongly. This is in agreement with literature [66, 67]. Although the charging amount of oxygen in pure V is larger than that in V-4Cr-4Ti by oxidation and annealing (Fig. 3.1-7), it is expected that charged oxygen in pure V is much easier to be lost than that in V-4Cr-4Ti at high temperature, because pure V is short of Ti as a strong oxygen-trapping agent.

3.2 Effect of oxygen charging conditions on Er_2O_3 in-situ coating

After oxidation and annealing, the oxygen charged V-4Cr-4Ti and pure V were exposed to liquid Li doped with Er. The purpose of this step is to verify the feasibility of coating formation and to obtain the most effective oxygen charging conditions on in-situ coating.

(1) The first attempt to verify the feasibility of in-situ coating

Fig. 3.2-1 showed the surface SEM image and EDS analysis of pure V and V-4Cr-4Ti (oxidized for 8h at 700^{o}C and annealed for 16h at 700^{o}C) exposed in liquid lithium doped with erbium or yttrium for 100h at 600^{o}C. EDS data includes the contribution from the vanadium alloy substrates because of very thin surface layers.

In Fig. 3.2-1 (a) and (b) show no evidence indicating the formation of either Y_2O_3 or Er_2O_3 coatings on pure V exposed in liquid lithium doped with whether yttrium or erbium. The reason would be that the pre-charged oxygen in pure V substrate diffused into liquid lithium quickly prior to the formation of the oxide coating, since pure V lacks Ti element acting as strong oxygen trap.

Fig. 3.2-1 (c) shows that no Y_2O_3 coating can be formed by exposure in liquid lithium doped with yttrium powders. The reason was thought that metallic yttrium was quite insoluble in lithium [68].

In Fig. 3.2-1 (d), positive evidence appeared for the formation of Er_2O_3 coating on V-4Cr-4Ti, by exposure in liquid lithium doped with erbium powder at high temperature, although the solubility of erbium in liquid lithium is still low (0.15wt% at 600^{o}C). The SEM observation and EDS analysis of cross section need to be performed to prove a coating with required thickness.

Thus, the effort to make Y_2O_3 insulating coating on V-4Cr-4Ti by in-situ method was given up. Further investigation on Er_2O_3 in-situ insulating coating was performed in this study.

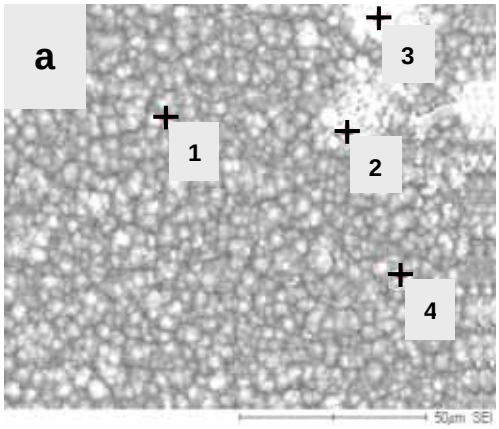

	+ 1	+ 2	+ 3	+ 4
O	15	42	17	57
Y	0.1	0.5	0.2	0.7

Pure V

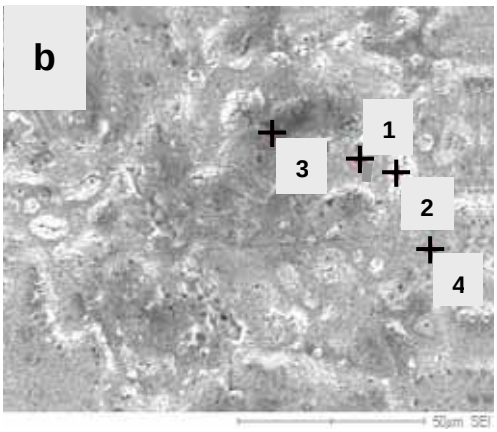

	+ 1	+ 2	+ 3	+ 4
O	–	3	25	–
Er	2	4	7	1

(wt%)

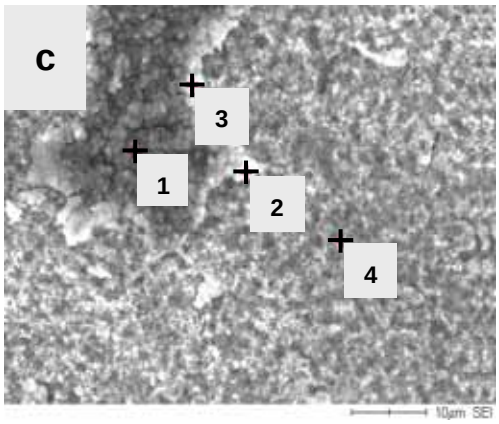

	+ 1	+ 2	+ 3	+ 4
O	31	26	35	–
Y	0.7	0.1	0.8	–

V-4Cr-4Ti

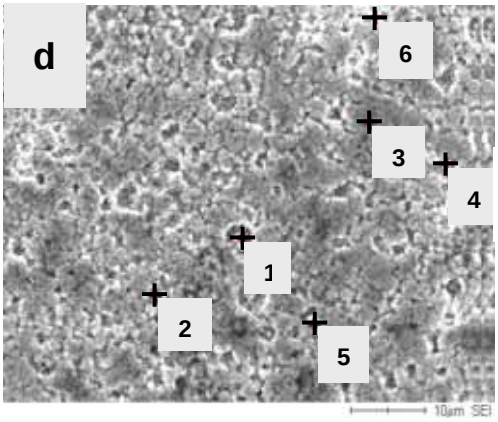

	+ 1	+ 2	+ 3	+ 4	+ 5	+ 6
O	11	7	–	–	9	1
Er	18	40	22	42	37	41

Fig. 3.2-1 Surface SEM image and EDS analysis of pure V and V-4Cr-4Ti (oxidized for 8h at 700°C and annealed for 16h at 700°C) exposed in liquid Li doped with Er or Y for 100h at 600°C.

(a) pure V in Li(Y) ; (b) pure V in Li(Er) ; (c) V-4Cr-4Ti in Li(Y) ; (d) V-4Cr-4Ti in Li(Er).

Fig. 3.2-2 showed a SEM image of the polished cross section of V-4Cr-4Ti specimen that was oxidized for 6h, annealed for 16h at 700^{o}C and exposed in liquid lithium doped with erbium for 300h at 600^{o}C. It is obvious that a layer with fairly uniform thickness of about 1.7μm formed on the surface of V-4Cr-4Ti. The figure also shows the EDS element line scans through the cross section, showing enrichment of erbium and shortage of vanadium near the surface. In that layer, the signal of vanadium or other elements was thought to originate from the contribution from the substrate because the surface layer was very thin.

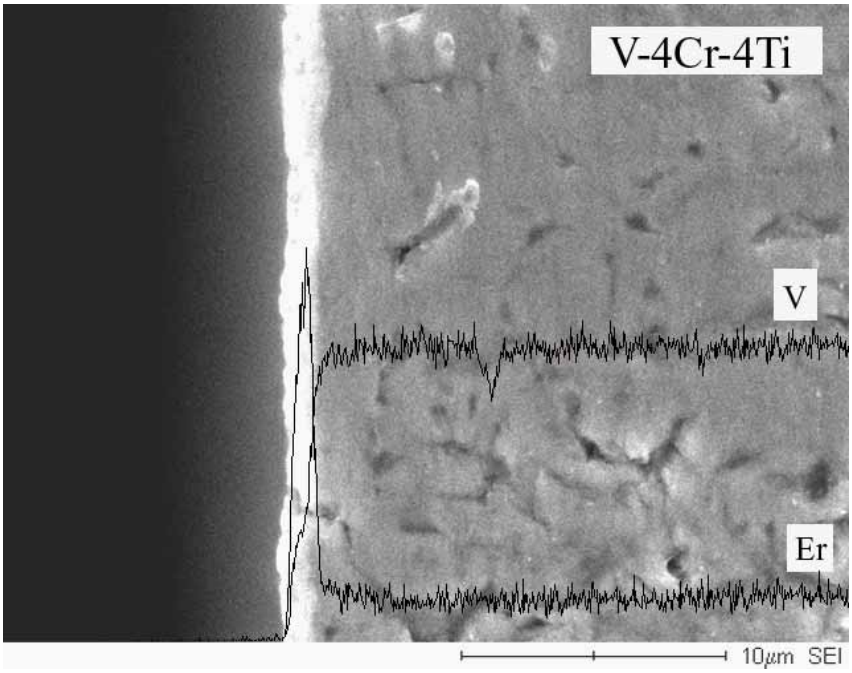

Fig. 3.2-2 SEM image and EDS line scan of cross section of V-4Cr-4Ti oxidized for 6h at 700^{o}C and annealed for 16h at 700^{o}C, exposed in Li doped with Er for 300h at 600^{o}C.

A surface layer enriched with Er and lacking of V was formed by in-situ method successfully. However mixture of V into Er-rich layer is necessary to be avoided, because all the known V-compounds have been conductive thus leading to a failure of insulating properties. In addition, EDS had low capability to detect light elements like oxygen and no ability to identify the phase.

Fig. 3.2-3 showed a relationship between depth profiles of the elements by XPS during Ar sputtering and resistivity measured at room temperature. The figure indicates that the V-free Er_2O_3 coating was formed on a V-4Cr-4Ti substrate that was oxidized plus annealed and finally exposed in liquid lithium doped with erbium. For an as-received V-4Cr-4Ti or V-4Cr-4Ti oxidized only followed by exposure in liquid lithium doped with erbium, Er-O-V mixture layer was formed including vanadium. The Er_2O_3 coated V-4Cr-4Ti have resistivity ~8 orders of magnitude higher than a minimum requirement (referred from [12]) for insulator of Li/V blanket. The resistivities of the other V-4Cr-4Ti with the mixture layers were just around or below the minimum requirement.

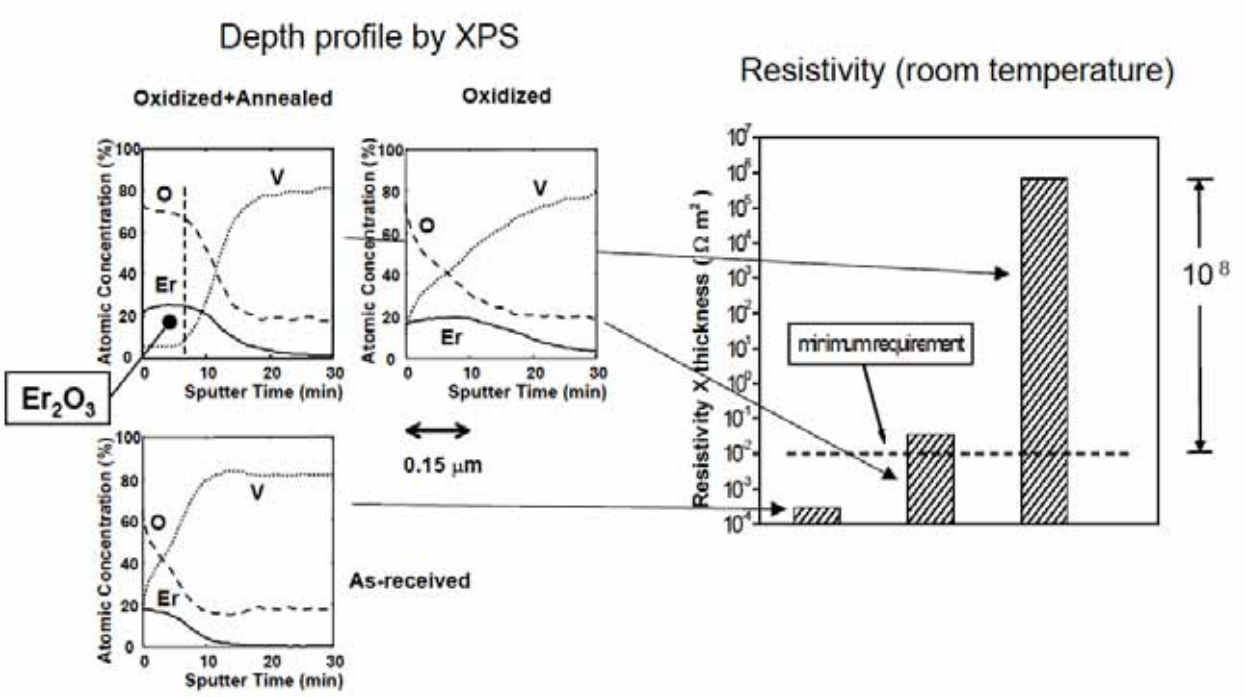

Fig. 3.2-3 Relationship between depth profiles of the elements by XPS during Ar sputtering and resistivity measured at room temperature

These results indicate that the oxygen source to form Er_2O_3 layer is from the pre-charging oxygen in the V-4Cr-4Ti, and the annealing after oxidation is a necessary process.

3.3 Summary

For formation of oxide insulating coating by so-called in-situ method, the enough oxygen storage in limited depth of vanadium alloys without influencing the bulk mechanical properties of the substrate is essential. To obtain the optimized condition for oxygen charging, a V-4Cr-4Ti alloy and pure V were oxidized in flowing high purity argon for 0.5-8h at 600-1000^{o}C and subsequently annealed in vacuum for 4-32h at 700^{o}C. The summary of the oxygen charging into vanadium alloys is as follows,

1) The initial level of oxygen or nitrogen has a small effect to weight gain in the further oxidation process. The difference is thought to be from the alloying elements.
2) For the purpose of keeping mechanical property of vanadium alloys and avoiding nitrogen introduction into the substrate, a temperature of 700^{o}C for oxidation or annealing is thought to be suitable.
3) From the standpoint of oxygen distribution, the times of 6h for oxidation and 16h for annealing were selected.
4) By the oxidation in argon, the charged oxygen was concentrated in the surface layer with large gradient to depth of substrate in addition to V-O compounds formed on surface. By the subsequent annealing, oxygen was homogeneously diffused into certain depth of the substrate where Ti-O net precipitates were formed. No Cr-O compounds were observed.
5) By oxidation and annealing at 700^{o}C, the contents of oxygen increased from original ~100ppm to ~10000ppm, while the contents of nitrogen did not increase significantly for both pure V and V-4Cr-4Ti.
6) By annealing, the oxygen did not diffuse into a depth exceeding ~150μm for V-4Cr-4Ti, because Ti-O precipitates acts as a strong trap to keep oxygen. In contrast diffusion depth of oxygen is much larger for pure V than that in V-4Cr-4Ti.
7) By exposure in Li doped with Er, no coating was formed on pure V because of quick loss of pre-charged oxygen. Er_2O_3 coating with high resistivity was formed on V-4Cr-4Ti oxidized plus annealed, because Ti-O acts as oxygen source for forming coating during the exposure. The annealing after oxidation is a necessary process.
8) It is feasible to control oxygen level and distribution in the surface region of V-4Cr-4Ti, by controlled oxidation and annealing.

CHAPTER 4

Formation, Growth and Characteristic of In-situ Erbium Oxide Insulating Coating

4.1 Experimental parameters

This chapter describes parametric dependence of the formation, growth and characteristics of the Er_2O_3 coating.

1) The effects of pre-treatment conditions to charge oxygen into V-4Cr-4Ti were reported in Chapter 3. In this chapter the pre-treatment condition is fixed to be: oxidation in argon flow with high purity for 6h at 700°C, subsequent annealing in vacuum for 16h at 700°C.
2) For examining the effects of doping level for Er on the formation of in-situ oxide coating, the exposures in liquid lithium under Er/Li doping level of 0.15, 1, 2.5 and 16wt% were performed.
3) To understand the effects of exposing temperature on the formation and growth of Er_2O_3 coating, tests with the exposing temperature of 500, 550, 600, 650 and 700°C were carried out.
4) To verify the stability of Er_2O_3 coating in liquid lithium doped erbium, the exposures with time of 100h at 500 and 550°C; 20, 100, 300 and 750h at 600°C; 20, 100, 300h at 650 and 700°C were performed.
5) To verify the stability of the coating once formed in Li doped with Er, in pure Li, the samples exposed in liquid Li doped with Er for 100h at 700°C was re-exposed in pure Li for 100h at 700°C.
6) To verify self-healing property of the coating, the samples with intentional cracks were re-exposed in liquid Li doped with Er for 100h at 700°C.
7) To understand the reasons of cracking observed, the samples with various thickness (0.5 and 4 mm) were exposed in liquid Li doped with Er for 100h at 700°C, and were washed by weak lotion (NH_3) at low temperature (-33.5°C) or strong lotion (H_2O) at room temperature to remove Li.
8) To understand the temperature dependence of resistivity of the coating, the resistance measurements were performed in vacuum from room temperature to 600°C.

4.2 Formation and growth of Er_2O_3 coating

Fig. 4.2-1 showed EDS element analysis and SEM image of surface (a) and cross section (b) for the same sample (V-4Cr-4Ti oxidized for 6h at 700°C plus annealed for 16h at 700°C, finally exposed in Li doped with Er for 300h at 600°C). EDS data included the contribution from vanadium alloy substrate. The data clearly indicate that a surface layer was enriched with erbium and oxygen. Comparing with Fig. 3.2-1 (d), the contents of erbium and oxygen were higher, implying that the exposing temperature is one of definitive factors to growth of the coating.

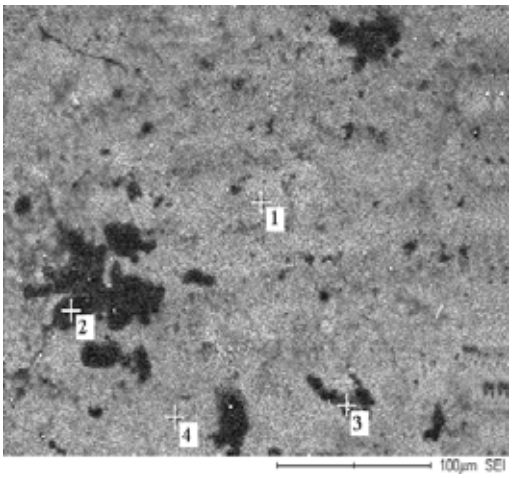

	+1	+2	+3	+4
O (wt%)	11.26	12.47	2.56	10.14
Er (wt%)	47.31	54.12	54.84	50.96

(a)

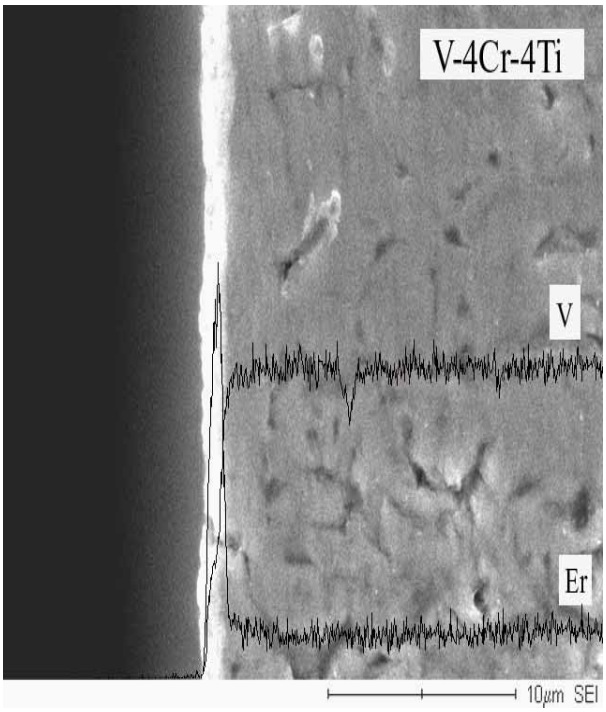

(b)

Fig. 4.2-1 EDS element analysis and SEM image of surface (a) and cross section (b) for the same sample (V-4Cr-4Ti oxidized for 6h at 700°C plus annealed for 16h at 700°C, finally exposed in Li doped with Er for 300h at 600°C).

Fig.4.2-2 shows the Er4d spectrum of XPS on the surface of various test specimens. The peak (a) corresponds to the layer containing Er and O made by exposing V-4Cr-4Ti in liquid lithium doped with erbium in the present experiment. The peak (b) is from a coating

fabricated by radio frequency (RF) sputtering which was identified to be Er_2O_3 by X-ray diffraction (XRD) [69]. The figure shows that the peak position of Er4d for the two specimens is almost the same. For further confirmation, a specimen of as-received unalloyed Er was examined and shown in (c). The (d) spectra are from the same Er specimen after sputtering with Ar ions for 20 min. The as-received Er specimen has a native Er_2O_3 film on the surface but the film is deleted after sputtering. The Er4d peak positions of (a), (b), and (c) were similar confirming the Er_2O_3 was formed. The peak in (d) shows metallic Er.

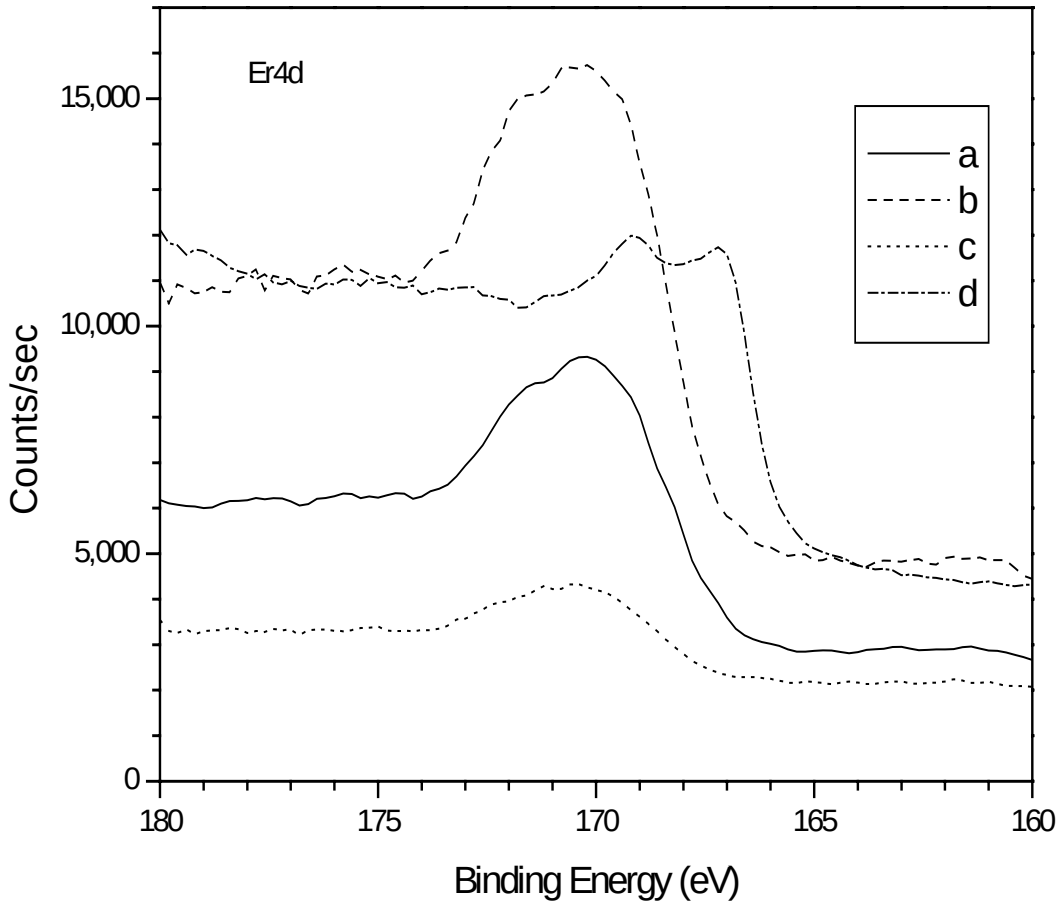

Fig. 4.2-2 Er4d spectrum of XPS on the surface

(a) Layer containing Er and O by exposing in Li (Er) (see Fig. 4.2-1); (b) Er_2O_3 coating by RF sputtering; (c) As-received Er plate (native oxide film); (d) Er plate after sputtering by Ar ions for 20 min (metallic).

Fig. 4.2-3 shows the resistivity of various samples measured by the two-electrode method at room temperature. For comparison, the data for unalloyed Er plate as-received and mechanically polished are also shown. The figure indicates that as-received, oxidized only, oxidized plus annealed V-4Cr-4Ti and polished Er plate are all highly conductive. The high resistivity of V-4Cr-4Ti appears only after exposure in liquid lithium doped with erbium. The resistivity of V-4Cr-4Ti after exposure in liquid lithium doped with erbium is higher than the native oxide formed or unalloyed Er. The resistivity of ~10^6 Ωm^2 of coated V-4Cr-4Ti is several orders of magnitude larger than the minimum requirement of $10^{-2}\Omega m^2$ for the MHD insulating layer [12]. The resistivity at high temperature will be investigated later. The result for oxidized vanadium alloys indicates that insulating layer is not formed by oxidation only.

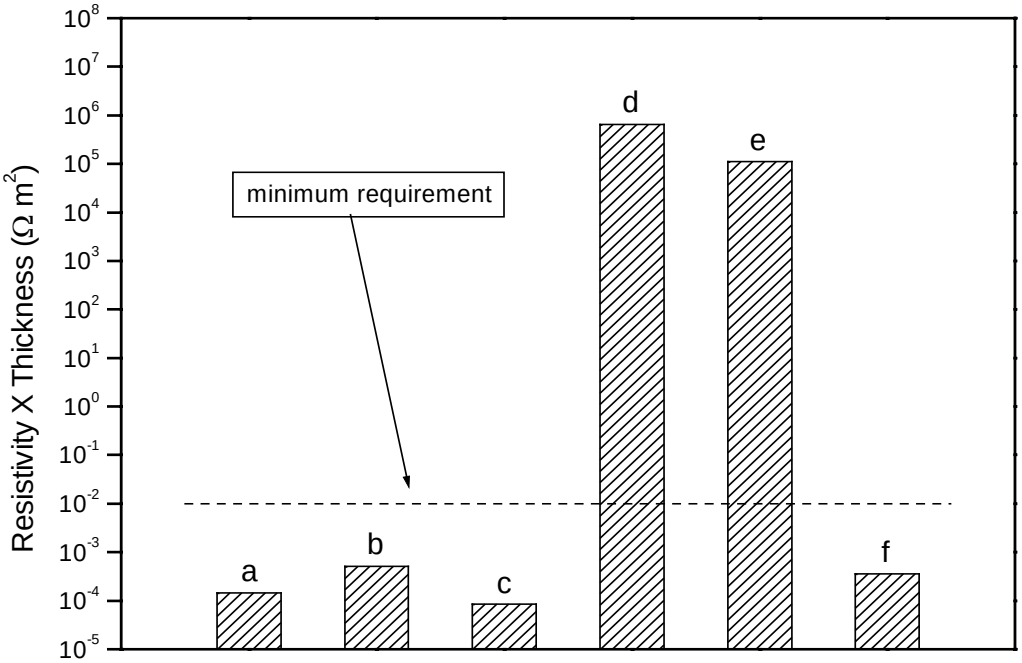

Fig. 4.2-3 Resistivity of various materials at room temperature

(a) V-4Cr-4Ti as received; (b) V-4Cr-4Ti, oxidized only; (c) V-4Cr-4Ti, oxidized + annealed; (d) V-4Cr-4Ti, oxidized + annealed + exposed in Li doped with Er (coating); (e) Er plate exposed in air (native oxide film); (f) Er plate polished with sand paper (metallic); The dotted line shows the minimum requirement for MHD insulator [12].

Fig. 4.2-4 shows the thickness of the Er_2O_3 coating after exposure to Li doped with Er for 100h as a function of the doping level for Er powder in Li. It appears that the lower limit of the doping level to form an Er_2O_3 coating is around 1wt% (0.04at%) at exposing temperature above 500^oC. It seems that the thickness of the coating is independent of the doping level above 2.5wt% (0.1at%). It should be noted that the chemical analysis of Er concentration in Li after exposure at 600^oC showed only 0.15wt% (0.006at%) as mentioned in Section 2.2. Presumably, since the oxygen impurity in liquid Li introduced from the cover gas in glove box is more active than that charged in V-alloy, the oxygen impurity in Li has a prior claim to react with dissolved Er in Li to form deposition in Li. After the oxygen impurity is exhausted by the superfluous Er, the charged oxygen begins to react with the remaining Er. Thus, once oxygen level in Li is reduced, the necessary doping level of Er powder will also be reduced and approach 0.15wt% at 600^oC. The level of impurity oxygen in reactor-grade Li is expected to be much lower than that in Li used in this study, because in the reactor cold trap system will be introduced for reducing oxygen impurity prior to doping Er.

Another consideration is the influence of Er doping level in Li on the nuclear performance or blanket neutronics. For a Li/V blanket concept for force free helical reactor (FFHR), the Er concentration of ~5-10wt% (0.2-0.4at%) perhaps could be accepted, from the standpoint to achieve an accepted local tritium breeding rate (TBR) [70]. For a Li/V blanket concept for demo-type reactor ARIES-RS, Er doping causes far more degradation to the TBR. ARIES-RS cannot tolerate morn than ~12wt% (0.5at%) Er without major design changes [71]. For the Er doping level in this study, it is far lower than the above estimated upper limit.

From the above results and discussion, a positive prediction can be raised, in which the influence of Er doping level in this study will not be an issue for the neutronics designing of the blanket.

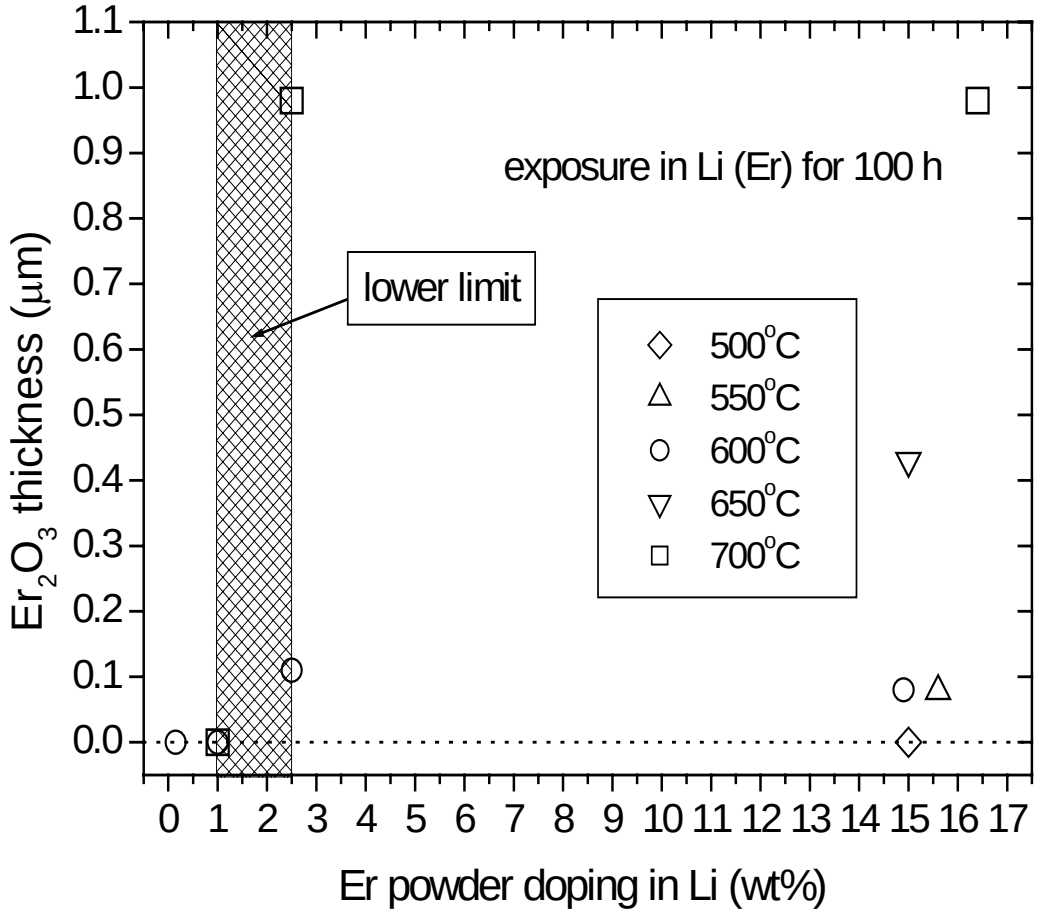

Fig. 4.2-4 Thickness of the Er_2O_3 coating as a function of the Er powder doping level in Li for an exposure of 100h at various temperature.

Note that the lower limit of Er powder doping level for the coating formation is expected to be much lower with reduced oxygen level in Li.

Fig. 4.2-5 shows the thickness of the Er_2O_3 coating with exposure time at temperature of 500-700°C. The Er_2O_3 coating was not formed at 500°C, perhaps owing to slow diffusion of Er and O, or weak reaction between Er and O at 500°C. The thickness of the Er_2O_3 coating is a function of the exposure time. The figure shows that coatings were already formed after exposure for 20h at 600°C, 650°C and 700°C, indicating that the incubation for the formation of coating is quite short. The exposing duration to the apparent saturation of thickness is about 100h at 600°C, 300h at 650°C and more than 300h at 700°C.

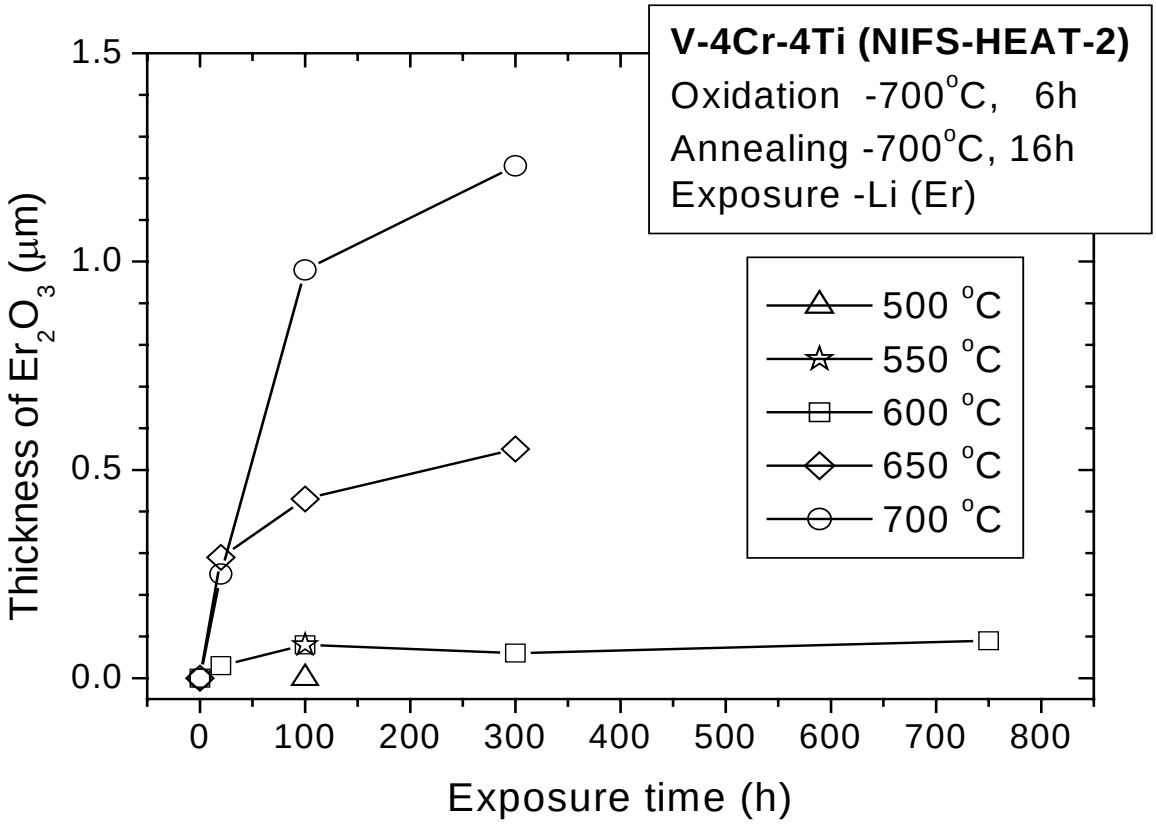

Fig. 4.2-5 Thickness of the Er_2O_3 coating on V-4Cr-4Ti as a function of the exposure time in Li doped with Er

4.3 Characterizations of Er_2O_3 coating

(1) The structures and phases of surface layer formed by in-situ method

Fig. 4.3-1 shows a SEM image of a cross-sectioned sample of coated V-4Cr-4Ti oxidized for 6h, annealed for 16h at 700°C and exposed to liquid Li doped with Er for 100h at 700°C. The image shows the region defeated by mechanical cutting. The coating near the cutting edge was partially peeled off by the external cutting force. It is very clear that the surface layer with a thickness of ~2μm consists of two sub-layers, namely a coating and an intermediate layer. Although the contribution from substrate was included, the analysis of EDS facing to each sub-layers showed that the coating was enriched with Er, O and few V or N, and intermediate layer appeared to be mixture of Er, N, O, and V.

However, the cracks appear in the coating. The reasons will be discussed later.

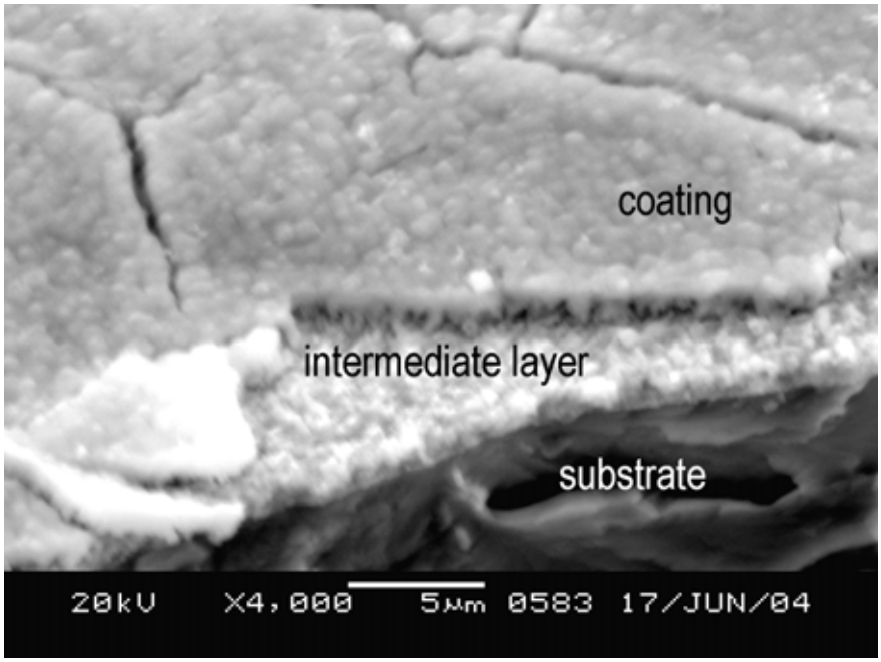

Fig. 4.3-1 SEM image at 45° of a cross-sectioned sample of coated V-4Cr-4Ti.

The sample was oxidized for 6h, annealed for 16h and exposed to Li (Er) for 100h at 700°C. Note that cracks are observed in this thick coating, while no cracks were observed in the previous thin coating.

To identify the phase of the coating, XRD is the most effective method. Fig.4.3-2 shows both low angle (0.2 ^{o}) and normal incidence XRD spectrum of same sample for V-4Cr-4Ti (oxidized for 6h at 700^{o}C, annealed for 16h at 700^{o}C and exposed to Li doped with Er for 300h at 600^{o}C).

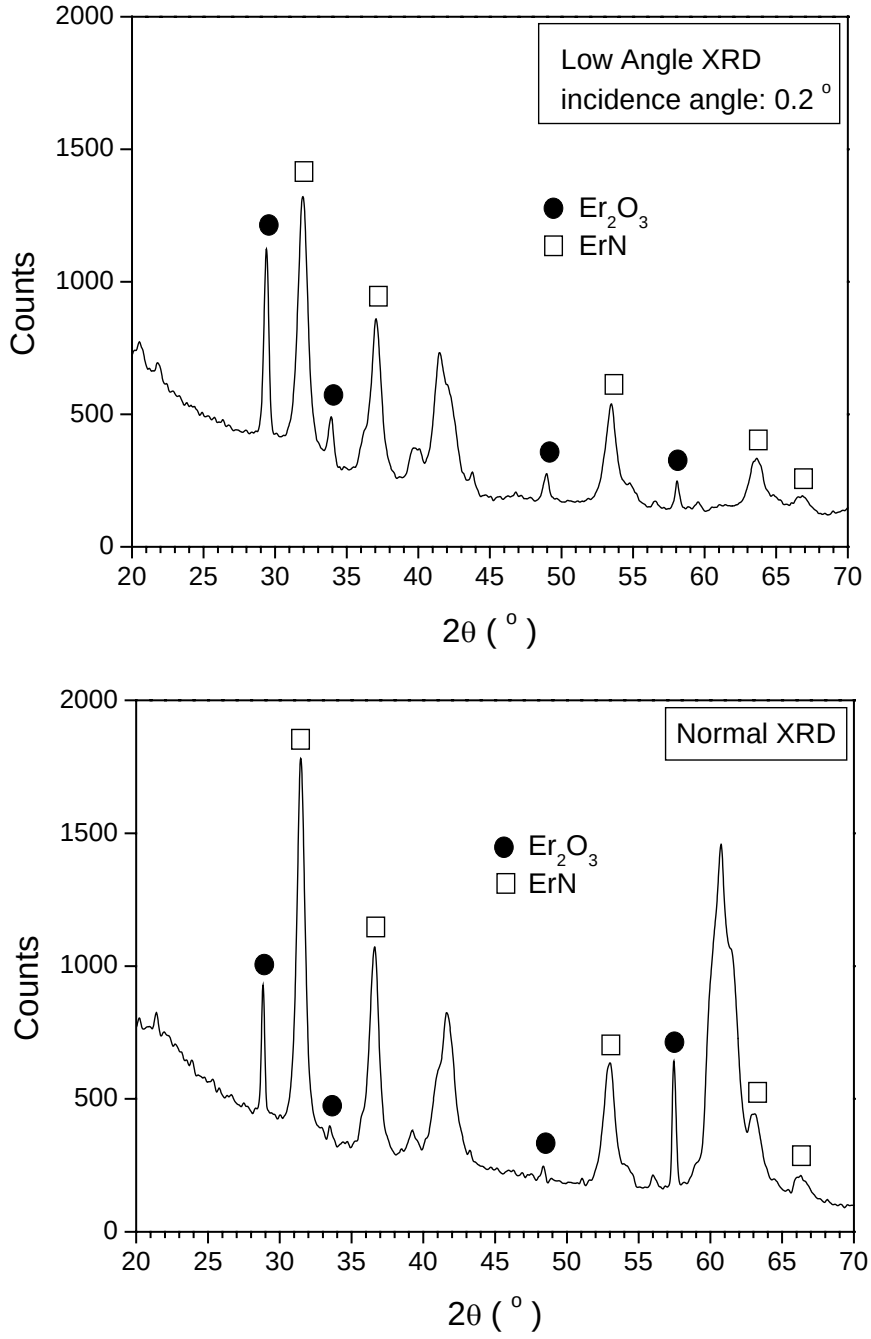

Fig. 4.3-2 Low angle and normal incidence XRD of V-4Cr-4Ti oxidized for 6h at 700^{o}C, annealed for 16h at 700^{o}C and exposed to Li doped with Er for 300h at 600^{o}C

The surface layer is very thin, especially for the top coating. By analysis of normal XRD, the signals for the coating were very weak because the spectrum includes those from the intermediate layer and the substrate. XRD with 0.2° incidence angle allows enhancing the contribution from the surface layer by suppressing the disturbance from the substrate. The results clearly show that the surface layer consists of Er_2O_3, ErN and unidentified phases.

Fig. 4.3.3 shows the depth profiles of elements by XPS during Ar sputtering for V-4Cr-4Ti oxidized for 6h, annealed for 16h at 700°C and finally exposed to liquid Li doped with Er for 100h at 600°C. It indicates that the region near surface is enriched with Er and O but free of V. Then a region mixed by elements as Er, N, V, O follows the top V-free region. The content of N increases with V in mixed region, perhaps it is absorbed into V-alloy substrate from liquid Li because no nitrogen is charged by oxidation and annealing. Just in the top region, Ti is a little enriched, perhaps owing to undissolved Ti-O. The content of Cr does not change, and Cr has not play a role to formation of surface layer, perhaps Cr has weak activity with oxygen compared with Ti.

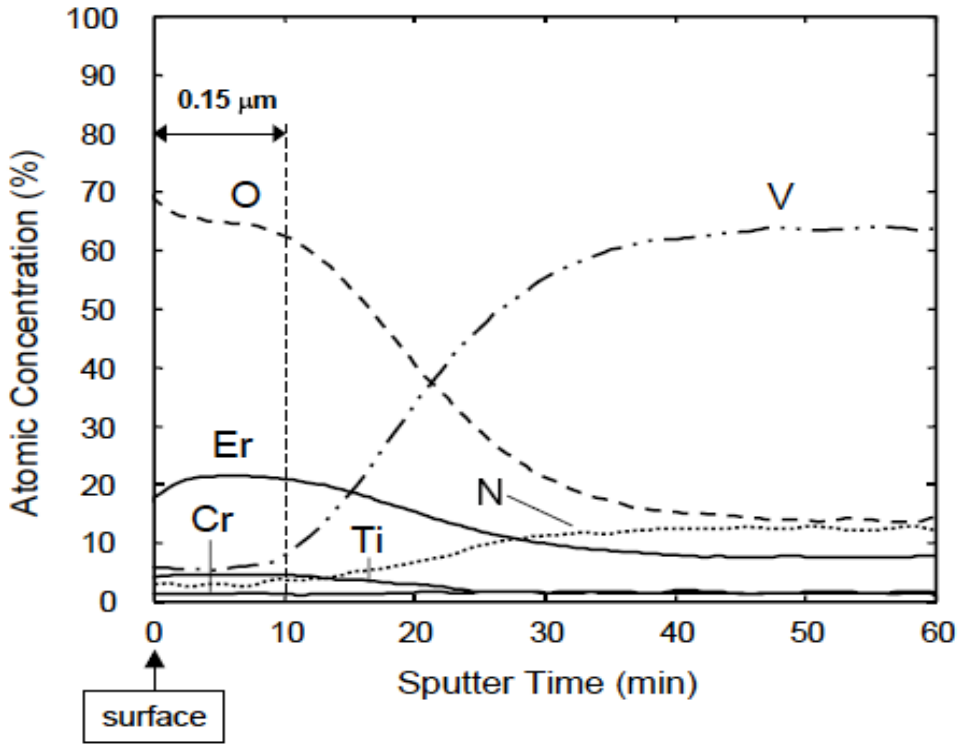

Fig. 4.3.3 Depth profiles of elements by XPS during Ar sputtering for V-4Cr-4Ti (oxidized for 6h, annealed for 16h at 700°C and finally exposed to liquid Li doped with Er for 100h at 600°C).

By combining Fig. 4.3-1, 4.3-2 and Fig. 4.3.3-3, the information indicated that the top layer is dominated by Er_2O_3, and that the intermediate layer consists of a mixture of ErN and V-compounds (or solid solution O in V substrate). The two layers can also be seen clearly at Fig. 4.3-4 by SEM of the cross section. The cracks were observed which only appeared in the top coating without relationship to grain boundary of V-4Cr-4Ti substrate. The reasons for the cracking will be examined later.

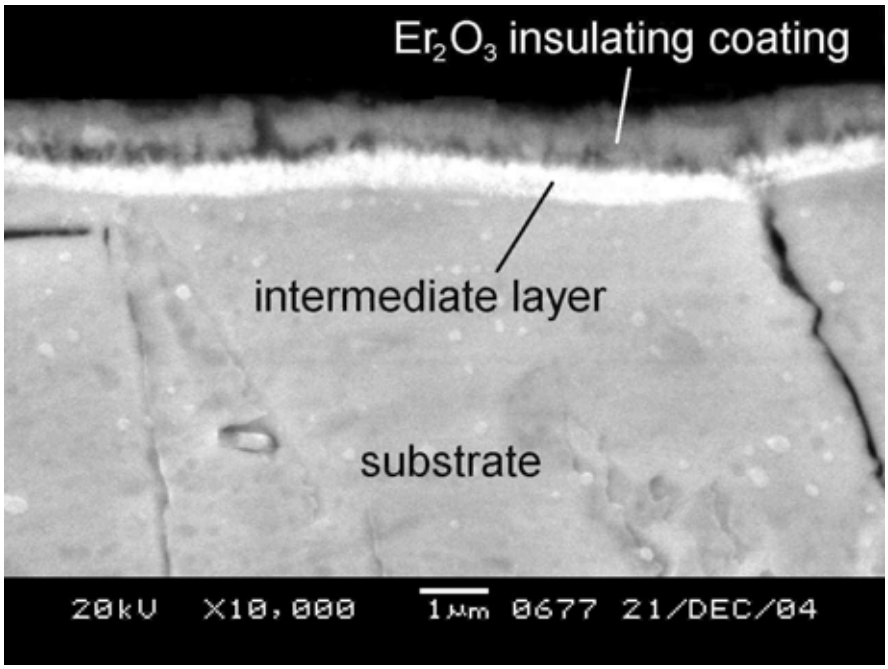

Fig.4.3-4 SEM image at cross section of V-4Cr-4Ti with coating.
The sample was oxidized for 6h, annealed for 16h and exposed in Li (Er) for 100h at 700^{o}C.

(2) The microstructure change of surface region of V-4Cr-4Ti charged by oxygen

Fig. 4.3-5 shows the TEM images of microstructure in region near the surface corresponding with Vickers hardness profile for V-4Cr-4Ti at various test conditions (as-received, oxidized, oxidized+annealed and oxidized+annealed+exposed in liquid Li doped with Er, respectively). The as-received V-4Cr-4Ti contained blocky precipitates of Ti-N-O-C. The oxidized V-4Cr-4Ti showed complex image of V-O compounds. The oxidized plus annealed V-4Cr-4Ti contained high density of <200> oriented Ti-O precipitates. After exposure in liquid lithium doped with erbium, the Ti-O net structure in near surface region of the vanadium alloy

disappeared completely. This supports the supposed process of Ti-O dissolution to release oxygen with solid solution followed by the oxygen diffusing toward the surface, to form the oxide coating [49]. The Ti-O formed during oxidation plus annealing acts as a necessary oxygen source.

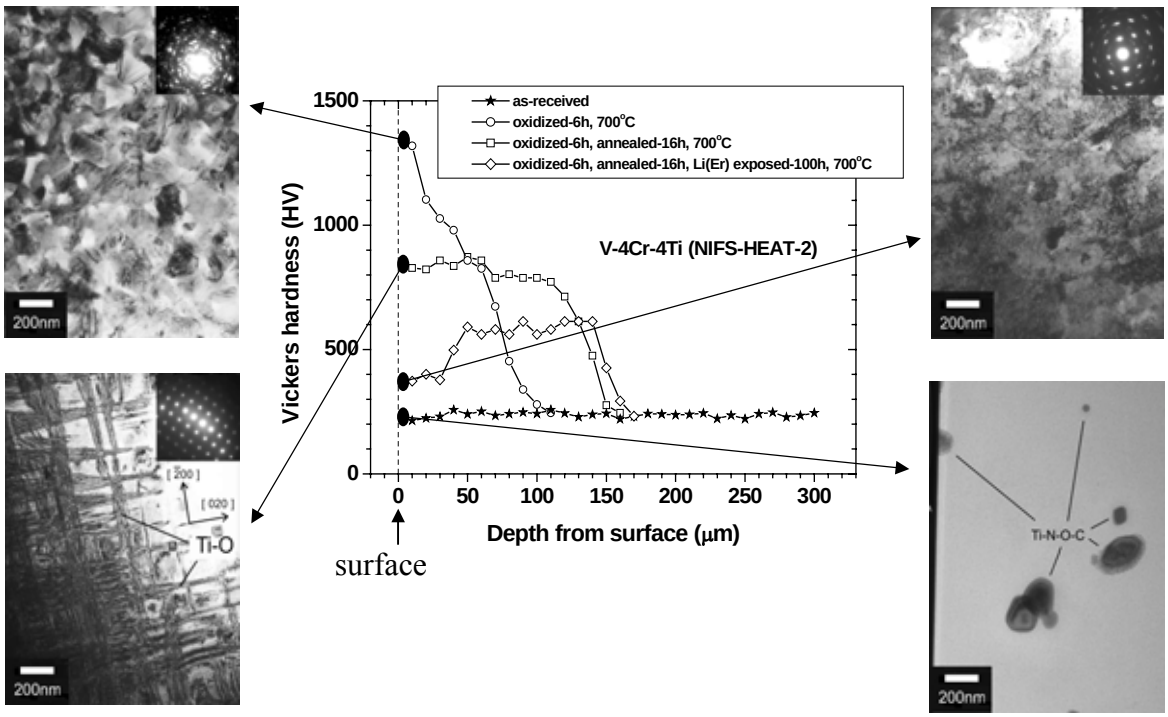

Fig. 4.3-5 TEM images of microstructure in region near the surface of V-4Cr-4Ti corresponding with Vickers hardness profile at various test conditions

Fig. 4.3-6 showed the SEM image of chemically etched cross section of V-4Cr-4Ti with coating, which was oxidized for 6h at 700°C, annealed for 16h at 700°C and exposed to Li doped with Er for 100h at 700°C (the same sample in Fig. 4.3-4). The very thin top layer is the coating. The region in which the grain boundary is shown clearly, is thought to correspond to the oxygen-rich region with thickness of ~150μm as is shown in Fig. 4.3-4. In the O-rich region, the sub-region of columnar grain is thought to correspond to region with thickness of ~30μm where oxygen was quite lost to form oxide coating (Fig. 4.3-4). The sub-region of equiaxial grain is thought to be region remaining enough oxygen (Fig. 4.3-4). The grain boundary is remarkable in O-rich region. The reason would be selective depletion of oxygen

at grain boundary. The grain boundary with reduced oxygen may be etched selectively. The grain boundary in original region is not clear because of lack of any selective oxygen depletion. The mechanism of transformation from equiaxial to column grain needs to be investigated further.

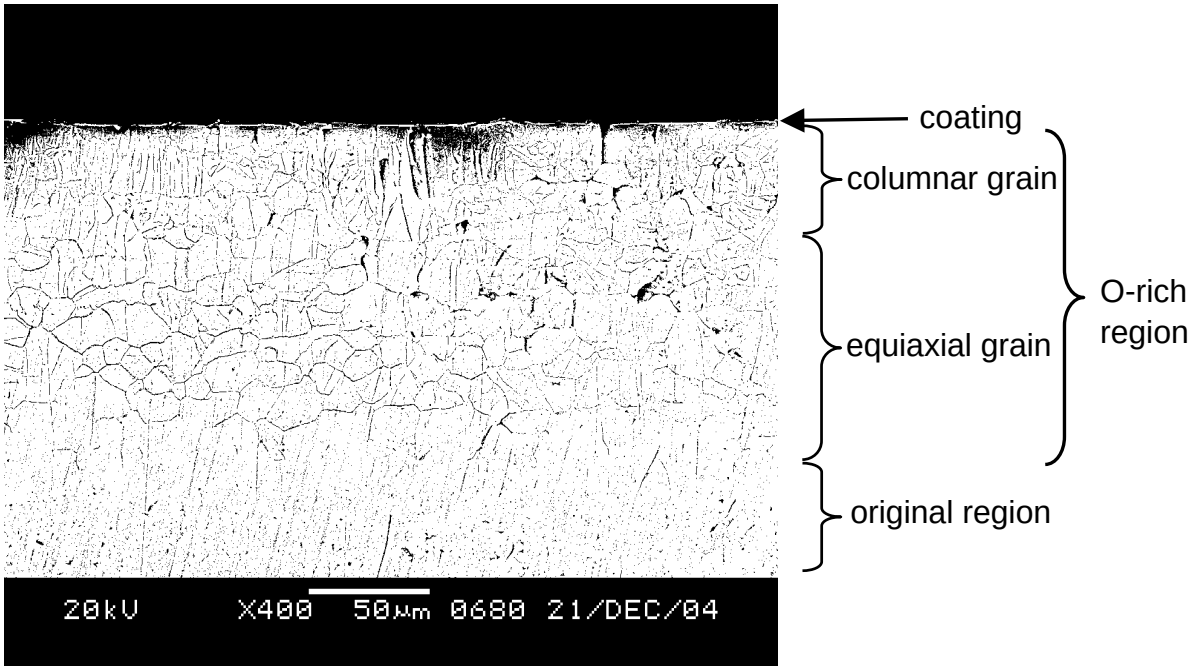

Fig. 4.3-6 SEM image of etched cross section of V-4Cr-4Ti with coating (oxidized for 6h at 700°C, annealed for 16h at 700°C and exposed to Li doped with Er for 100h at 700°C)

Fig. 4.3-7 shows the comparison of SEM at cross section for V-4Cr-Ti in two test conditions: (oxidized for 6h at 700°C, annealed for 16h at 700°C and exposed to Li doped with Er for 100h at 700°C) and (oxidized for 6h at 700°C, annealed for 16h at 700°C). The difference between the two photos is with/without exposure in liquid Li (i.e. with/without formation of oxide coating). The figure indicates that the columnar grains were formed only after the exposure in Li. Some change or re-orientation of phase may take place in the surface region where oxygen was lost during exposure. However the mechanism needs to be investigated further.

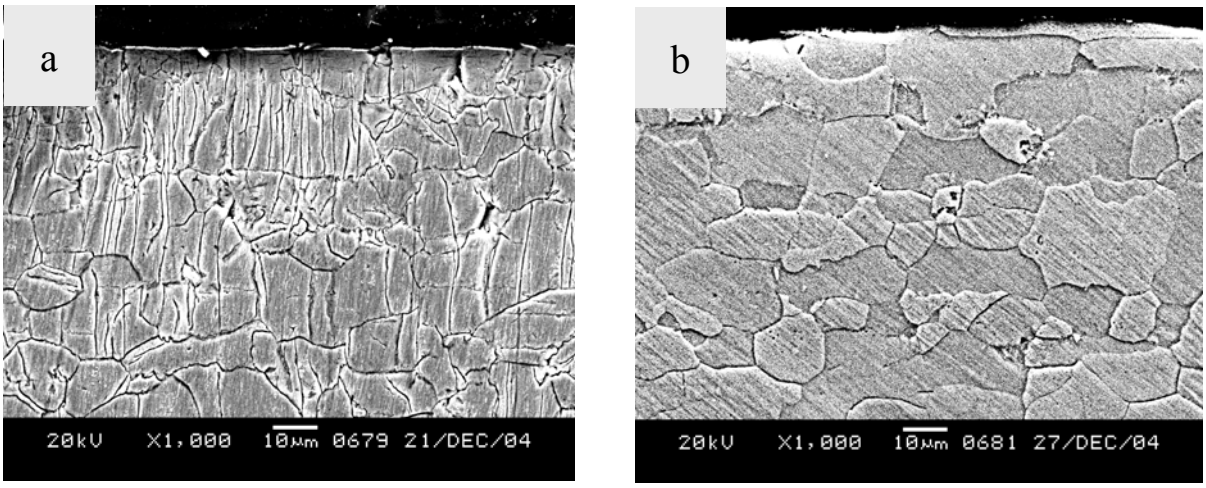

Fig. 4.3-7 Comparison of SEM at cross section for V-4Cr-Ti at two test conditions: (a) oxidized for 6h at 700°C, annealed for 16h at 700°C and exposed to Li doped with Er for 100h at 700°C ; (b) oxidized for 6h at 700°C, annealed for 16h at 700°C.

(3) The change of oxygen contents in the surface region of V-4Cr-4Ti charged with oxygen

Fig. 4.3-7 shows the Vickers hardness depth profile of V-4Cr-4Ti with various processing conditions. It is known that the Vickers hardness is a positive function of the oxygen level for V-4Cr-4Ti. Since the hardening resulted from oxygen diffusion, the hardness profiles correspond to oxygen diffusion profiles into vanadium alloy [72]. After the exposure for 100h at 600°C or 700°C, only limited amount of oxygen was lost to form the coating and little oxygen diffused into substrate deeper. However, the loss of the charged oxygen was enhanced significantly after exposure for 300h. Even after exposure at 600°C for 750h, the oxygen storage was maintained in certain depth of the substrate. It is thought that the enough oxygen can be supplied to support the stability of coating at 600°C. But at 700°C for 300h, it seems that all charged oxygen in surface region was lost, and at the same time the original oxygen in solid solution was partially lost as well. The result shows necessity for considering how to keep effectively oxygen in vanadium alloy at 700°C to avoid the exhaustion of oxygen source probably necessary for maintaining oxide coating and certainly necessary for healing cracks.

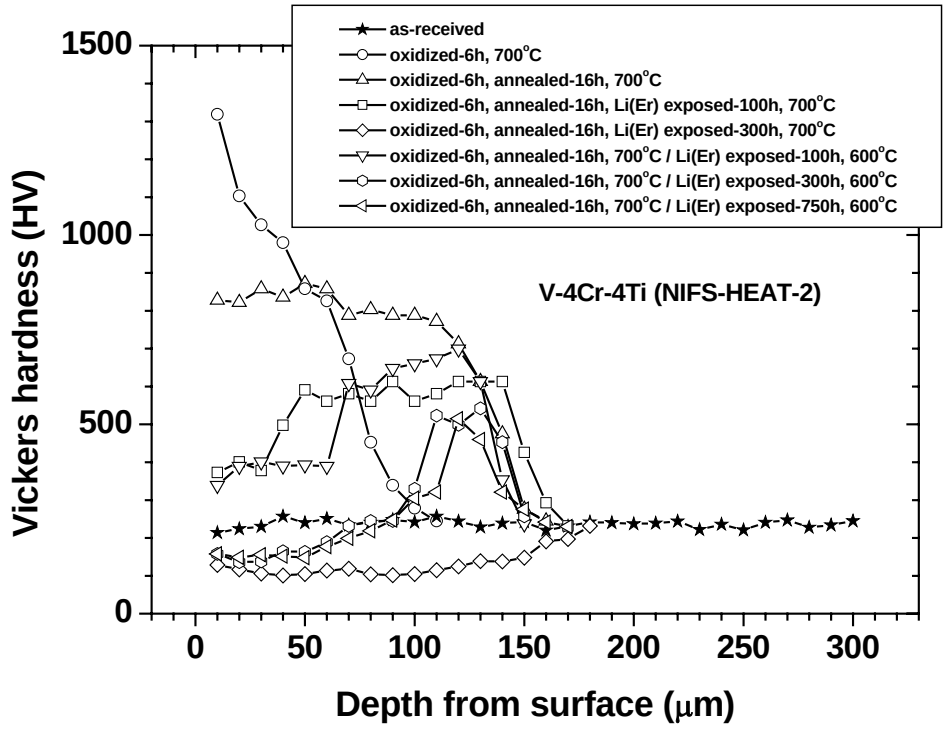

Fig. 4.3-7 Vickers hardness depth profile of V-4Cr-4Ti with various test conditions.

(4) Evaluation for insulating property of Er_2O_3 coating

The criterion to a successful or failed coating acting as insulator is the resistivity exceeding the minimum requirement of fusion blanket.

As the moisture in air could enhance the electric conductivity and the temperature is a negative factor for the resistivity of coating, a measurement of coating in vacuum during temperature elevation is essential. Fig. 4.3-9 showed the resistivity×thickness of V-4Cr-4Ti coated by Er_2O_3 in vacuum (~10^{-3}Pa) during heating comparing with a minimum requirement [12] for design of fusion blanket. Up to ~550°C, the in-situ measured resistivity was over the minimum requirement. However over 550°C, resistivity suddenly starts to drop below the minimum requirement. Perhaps this phenomenon are from the partial short-circuit, by the electrode degradation owing to melting or vaporization of Ag paste as a linker, or adhesion degradation between coating and substrate. However, the detailed reason and evaluation need to be investigated.

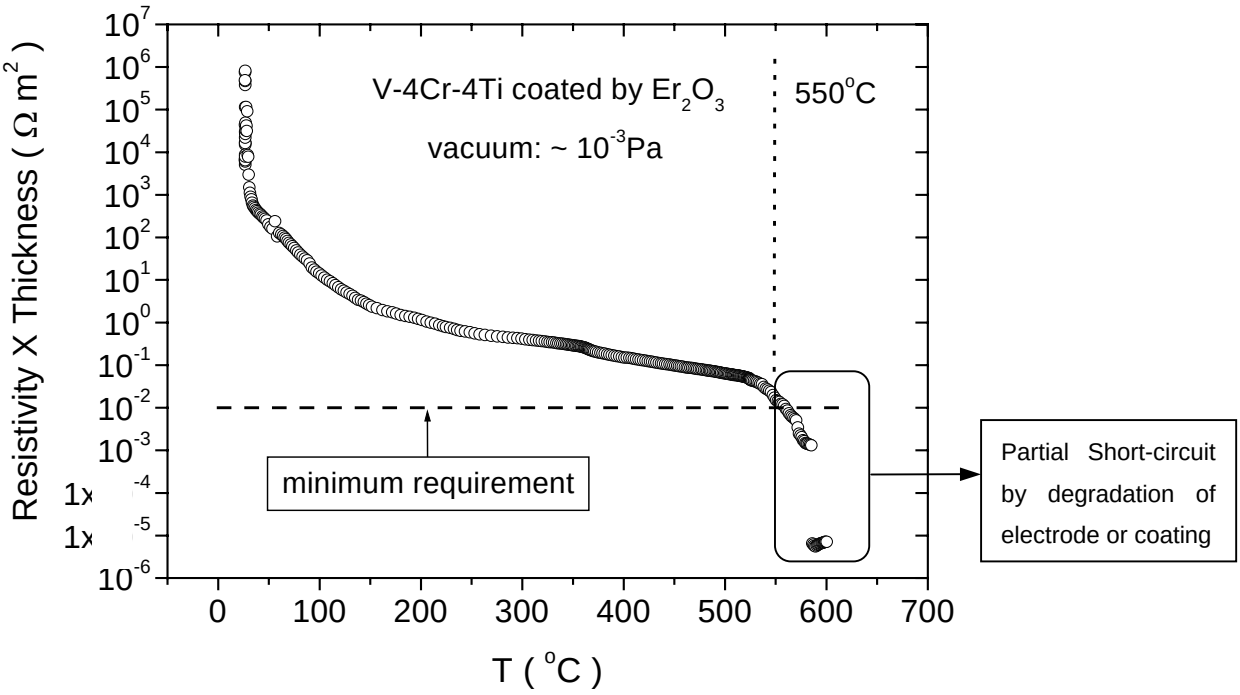

Fig. 4.3-9 Temperature dependences of resistivity of V-4Cr-4Ti coated by Er_2O_3 in vacuum during heating.

(5) Stability of the coating once formed in Li (Er) in pure Li

One of the optional methods to make the in-situ coating is to form the coating in Li doped with Er in factory after assembling of parts or in reactor site before operation. After formation of coating, Er dissolved or deposited in Li could be deleted, which could avoid the influence of Er to Li purity, heat-transfer and tritium breeding during the operation. In this case, Er_2O_3 coating will face a pure Li environment. For verification of this process, the stability of coating once formed in Li (Er) should be tested in pure Li. Fig. 4.3-10 showed the SEM and EDS analyses of V-4Cr-4Ti (with coating once formed by exposure in Li (Er) for 100h at 700°C) re-exposed in pure Li for 300h at 700°C. The coating (point, +1) includes high contents of Er and O as it did before the re-exposure. The results indicated that Er_2O_3 coating was stable in pure Li.

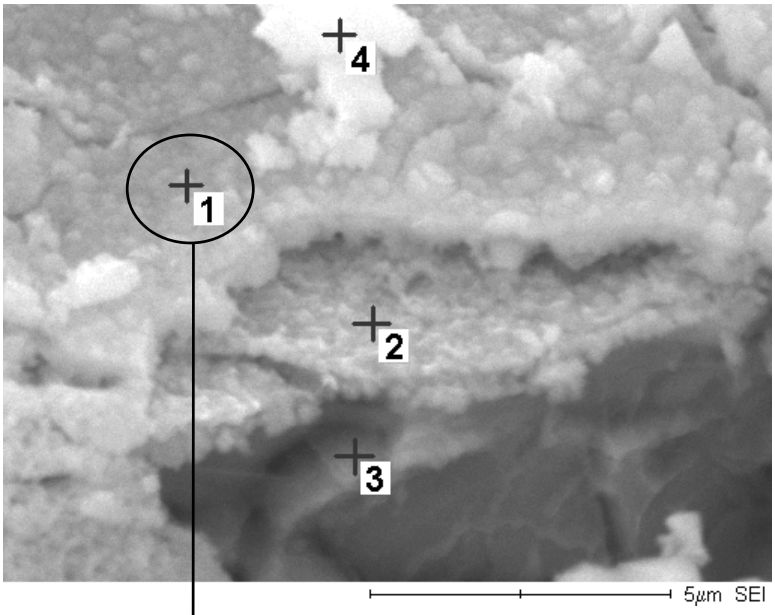

	+ 1	+ 2	+ 3	+ 4
Er	66	49	2	76
O	20	7	12	14
V	12	37	73	5

EDS(wt%)

Fig. 4.3-10 SEM and EDS analyses of V-4Cr-4Ti (with coating once formed by exposure in Li(Er) for 100h at 700^{o}C) re-exposed in pure Li for 300h at 700^{o}C.

(6) Cracking issue for in-situ coating

For an insulating coating, one of the issues is cracking which can lead to the leakage of current, thus could cause a large increase of MHD pump drop. Since a coating without cracks is a basic requirement, the reason of cracking needs to be explored.

As shown in above chapters, most coatings were with cracks after necessary Li cleanout for observations or analyses. It is important to know whether the cracking occurred during the exposure or the cleanout. The cracking during the Li cleanout could be avoided by choosing a better cleanout method.

Fig. 4.3-11 showed the surface view by SEM of the coating formed by exposure in Li (Er) for 100h at 700^{o}C, on which Li was cleaned by a strong lotion (H_2O) at room temperature and then dehydrated by ethanol. The thickness of the samples was 0.5mm (in this study) and 4mm (real size of blanket wall).

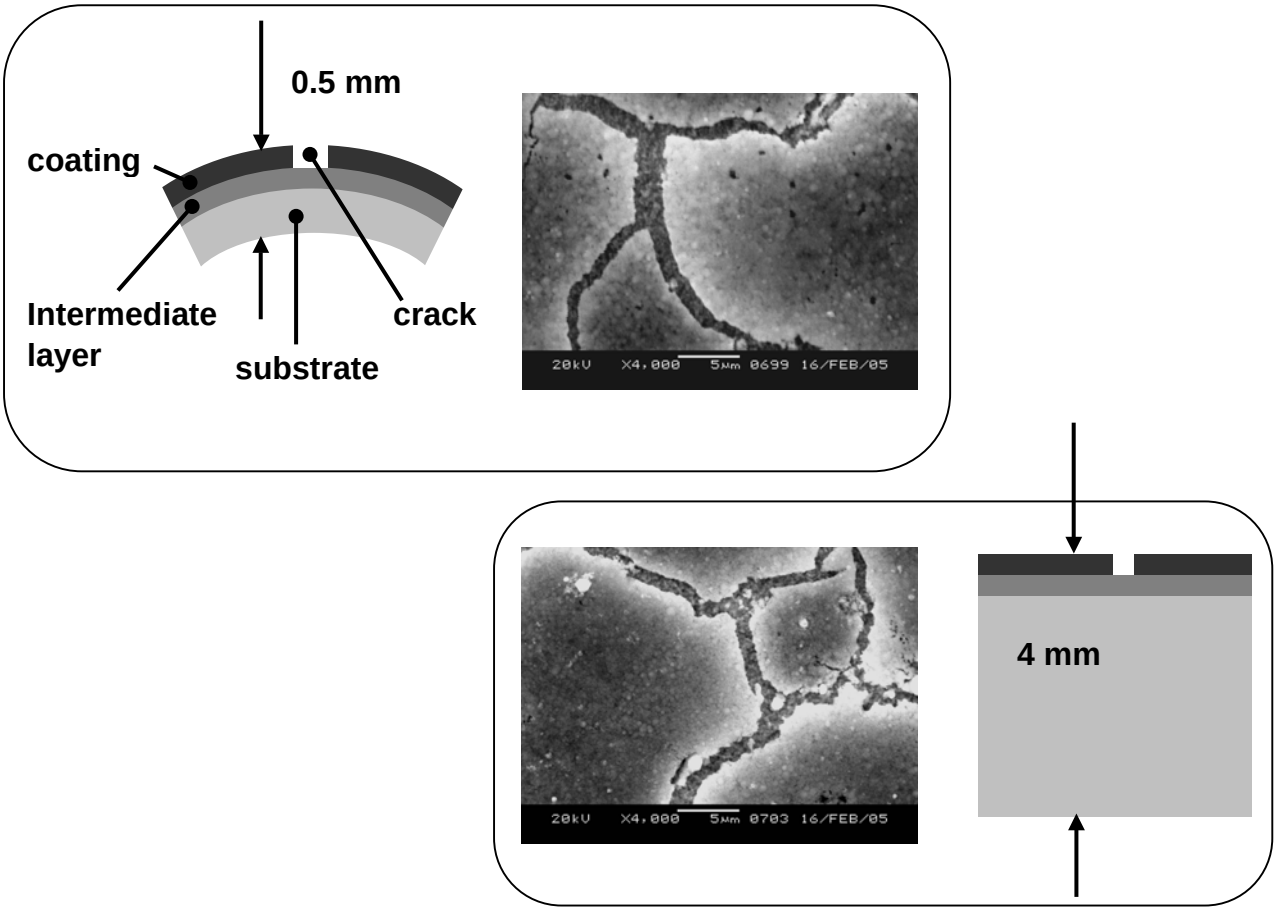

Fig. 4.3-11 Surface view by SEM of coating formed by exposure in Li(Er) for 100h at 700°C (Li was cleaned by a strong lotion (H_2O) at room temperature)

The figure shows that in either thin or thick sample, the cracking occurred after Li cleanout. The bending was observed on the thin sample but not on the thick sample. However the bending was not only reason of the cracking. The thin sample bended during exposure in Li(Er), but not during oxidation and annealing. The reason for the bending was presumed by stress from oxygen loss occurring on back of sample (there oxygen charging and coating formation were not uniform owing to reasons from test device). However no bending occurred in thick sample during exposure.

Fig. 4.3-12 shows the surface view by SEM of coating formed by exposure in Li(Er) for 100h at 700°C, on which Li was cleaned by a weak lotion (NH_3) at low temperature (-33.5°C) and then dehydrated by acetone.

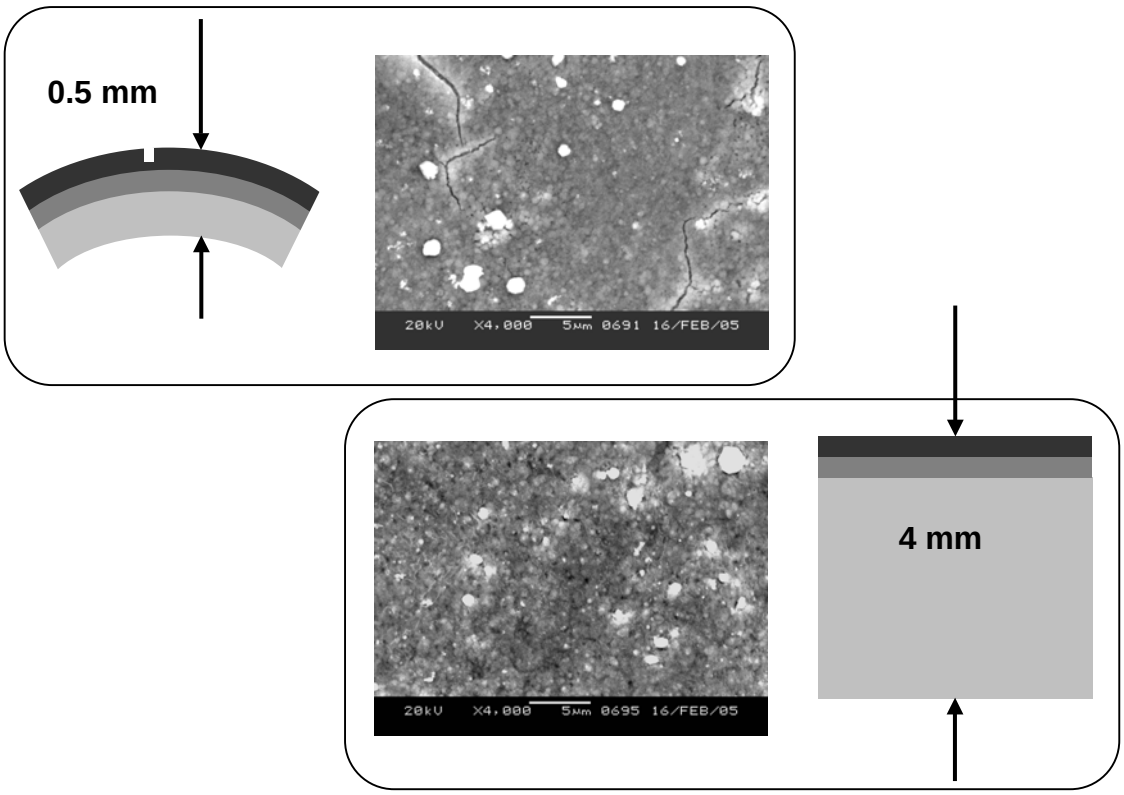

Fig. 4.3-12 Surface view by SEM of coating formed by exposure in Li(Er) for 100h at 700°C (Li was cleaned by a weak lotion (NH_3) at -33.5°C)

In the figure, the light cracking occurred in coating on the thin samples. However no cracking occurred in coating on the thick samples.

The difference between the two cleaning methods is just selection of the lotion and temperature. The cleaning process using H_2O at room temperature is much stronger than that using NH_3 at low temperature. The strong chemical reaction between H_2O and Li could cause overheat and stress locally on the coating.

Thus it is concluded that the cracking could be avoided in a real blanket wall with typical thickness of 4mm, where complete Li cleanout as the present experiment is unnecessary. Thus cracking observed in the experiment is not thought as a practical issue.

(7) Potential of self-healing property of in-situ coating in Li (Er)

During operation, a very complex environment including thermal or mechanical stress could lead to unavoidable cracking of the coating. Thus self-healing capability of in-situ coatings that is thought to be one of the advantages needs to be verified.

Fig. 4.3-13 showed concentrations of Er, O and V by EDS analysis at cracking place of coating after exposure for 100h at 700°C and after re-exposure for 100h at 700°C, in Li doped with Er.

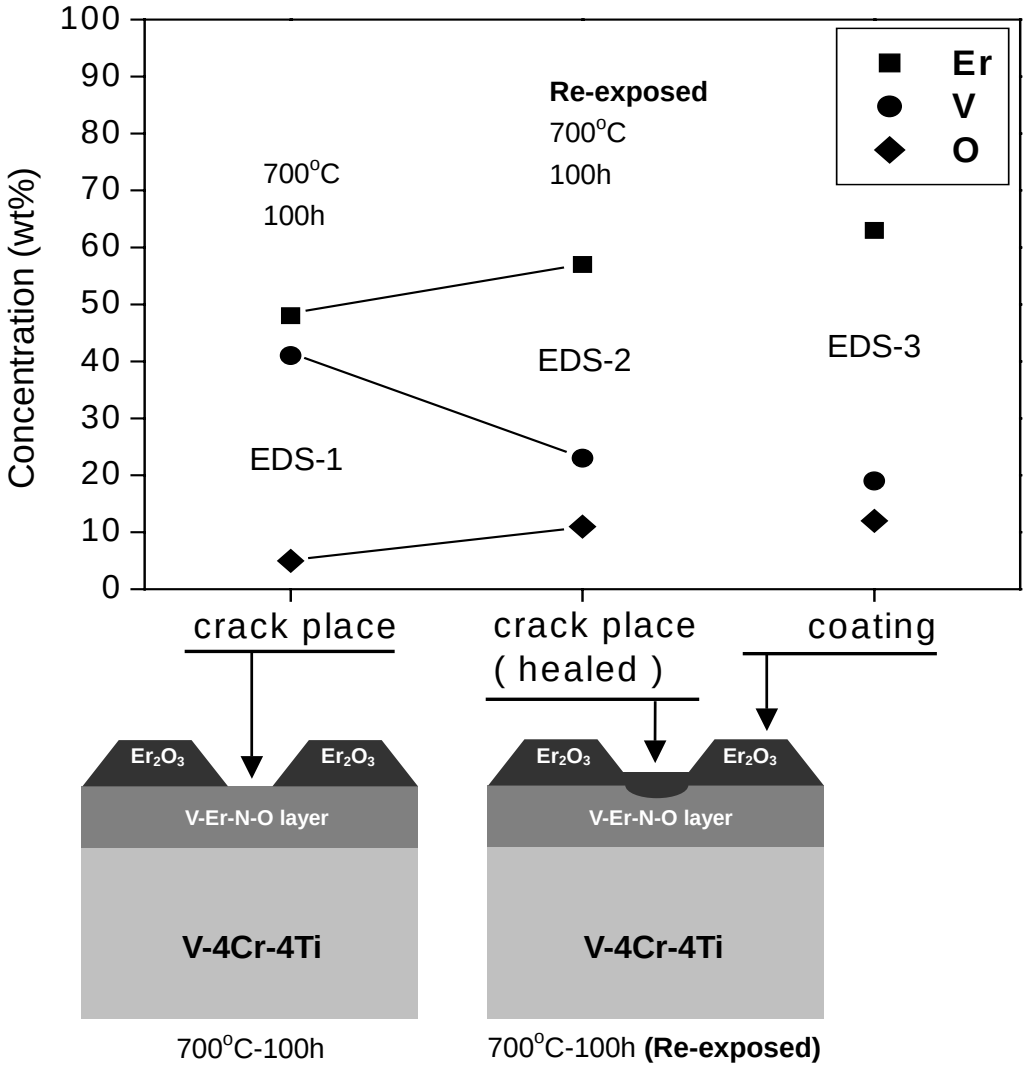

Fig. 4.3-13 Concentrations of Er, O and V by EDS analysis at the cracking place of coating after exposure and after re-exposure

After exposure in liquid Li doped with Er, the intentional cracking to the coating was applied by cleaning Li using hard lotion (H_2O) at room temperature. The EDS analysis was carried out at a complete and cracked place on coating locally, which included the contribution from intermediate layer and substrate. The EDS showed about 63wt% of Er, 19wt% of V and 12wt% of O as composition at the complete place on coating, and 48wt% of Er, 41wt% of V and 5wt% of O at the cracked place. The cracked place shorting of Er and O, seems to correspond to the intermediate layer. However, the cracked place showed 57wt% of Er, 23wt% of V and 11wt% of O by EDS-3 after re-exposure in Li doped with Er, which is close to that of complete coating. The results indicate that the in-situ Er_2O_3 coating has the potentiality of self-healing of cracks in liquid Li doped with Er. To verify the self-healing property of in-situ coating, an in-situ measurement of resistivity of coating in liquid Li doped with Er at high temperature is required as the next step.

4.4 Summary

To verify the feasibility and to characterize the property of Er_2O_3 coating on V-4Cr-4Ti by in-situ method, the exposures in liquid Li doped with/without Er were performed for 20-750h in a temperature range of 500-700^oC followed by a series of exanimations. The summaries of formation and characterization of Er_2O_3 are as follows,

1) A surface layer enriched with erbium and oxygen was formed successfully on V-4Cr-4Ti.
2) The surface layer consisted of two sub-layers, namely a top coating and an intermediate layer, by observation with SEM.
3) The top coating was dominated by Er_2O_3, and the intermediate layer consisted of a mixture of ErN and V-compounds, by verification of EDS, XPS and XRD.
4) The lower limit for the doping level of Er powder in Li to form oxide coating was far below the level that could influence the TBR of blanket.
5) The exposing temperature had a large effect on the formation and thickness of the coating. A lower limit of exposing temperature to form the coating is between 500 and 550^oC. The Er_2O_3 coating was stable at 600^oC up to 750h of exposure to liquid Li, and stable at 650^oC or 700^oC up to 300h.
6) The oxygen charged into V-alloy was lost accompanied by growth of coating. It is necessary to consider a method to keep effectively the oxygen storage in V-alloy during the exposure especially at such high temperature as 700^oC.
7) The resistivity of V-4Cr-4Ti coated by Er_2O_3 in vacuum exceeded minimum requirement up to 550^oC, perhaps owing to the partial short-circuit, by the electrode degradation, or adhesion degradation between coating and substrate.
8) Er_2O_3 coating once formed in Li (Er) was stable in pure Li.
9) The cracking in the coating would be avoided in a real size of blanket wall by avoiding Li cleanout with hard lotion.
10) In-situ Er_2O_3 coating shows potentiality of self-healing to cracks in liquid Li (Er)

CHAPTER 5

Modeling of In-situ Erbium Oxide Coating

In Chapter 3 and 4, the experimental characterizations to the oxygen charging into V-alloy bulk and the formation and growth of coating were performed. In this chapter, some phenomenological modelings are proposed to explain the mechanisms on the oxygen charging into bulk and the formation and growth of coating.

5.1 Phenomenological modeling for oxygen charging into V-alloys

The oxidation kinetics on V-4Cr-4Ti and pure V is shown in Fig. 5.1-1. The oxidation kinetics of V-4Cr-4Ti obeys a parabolic law, while pure V obeys a combination of parabolic and linear law. The parabolic kinetics indicates that the oxidation process is controlled by the rate of thermo-diffusion and that the V-O surface layer formed on V-alloys acts as a protective barrier for oxygen diffusion [57, 73]. The linear kinetics for pure V after oxidation for 4h indicates that the protective layer lost and more oxygen came into the substrate [74].

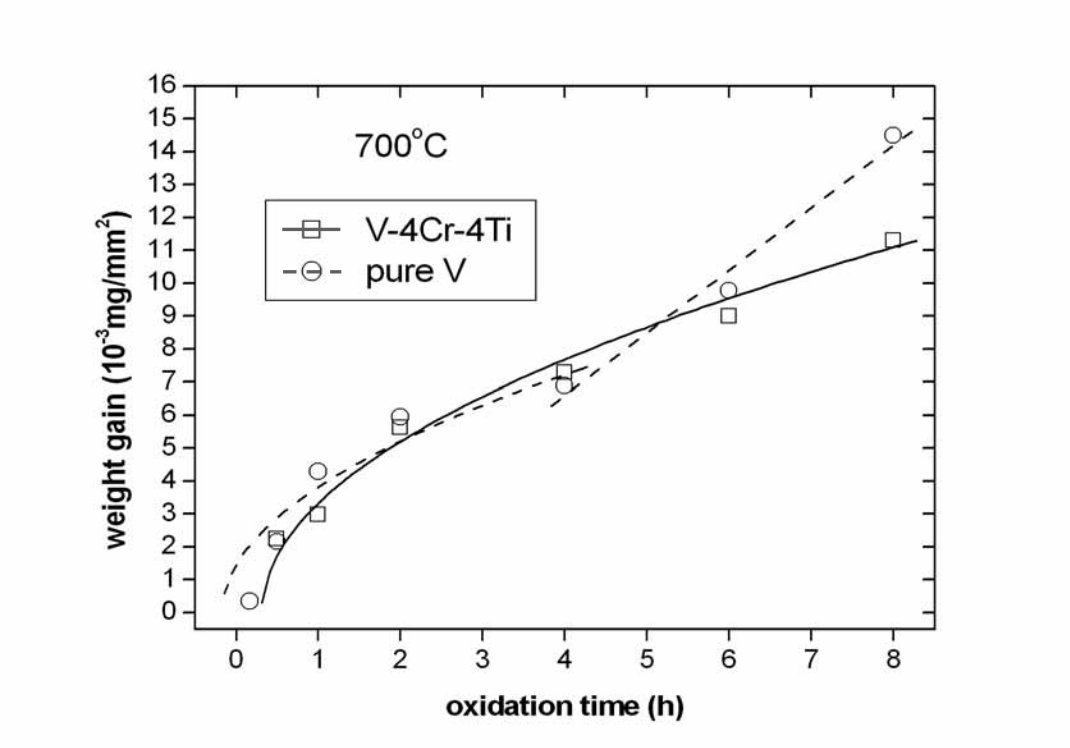

Fig. 5.1-1 Dependence of oxidation time on weight gain of V-alloys at 700°C

Based on the oxidation kinetics, the explanations of the mechanism on oxygen charging into V-alloys could be given. It is known that the addition of Ti may significantly lower the

solubility of oxygen in V-alloys and leads to an internal oxidation of Ti element [66]. In this case, the stable phases in V-alloys are Ti-based interstitial phases (Ti-O). Thus in a V-Cr-Ti alloy, the initial V_xO_y oxides are always metastable and should transform into a stable oxides with high Ti content (Ti-O) during heat treatment.

There are two possible mechanisms of phase transformation on the processes: initial $V_xO_y \rightarrow$ transition Ti-V-O $\rightarrow$ finally stable Ti-O, which depend on the mobility of components (Ti and O) and the rate of dissolution of initial V_xO_y phase during the heat treatments. Fig. 5.1-2 schematically shows the two mechanisms of the phase transformations.

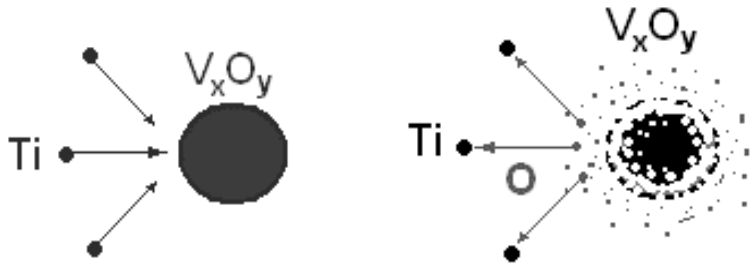

(a) (b)

Fig. 5.1-2 Scheme of two mechanisms to various phase transformations in V-alloys during heat treatment, (a) on site replacement and (b) dissolution-precipitation.

(a) If the mobility of Ti is high enough, an *on site transformation* mechanism of the type $V_xO_y \rightarrow$ Ti-O is possible. In this process, the Ti as active oxide-forming element replaces V atoms in the metastable phase without dissolution of the initial phase (V_xO_y). This mechanism of phase transformation could be realized at high temperature (about 1000° C for V-alloys), when the mobility of Ti atoms is high. In this case, Ti-V-O is a transition phase whose lifetime could be very short. The new created oxide (Ti-O) just follows the morphology of initial phase (V_xO_y). This on site mechanism could be used to explain formation of large Ti-rich precipitates in V-Ti-Cr alloys at high temperature [75].

However, since the oxidation and annealing temperature of 700^{o}C was used for oxygen charging in this study, this mechanism is not applied in the present study.

(b) If the rate of dissolution of the metastable phase precipitates (V_xO_y) exceeds the rate of supplying of Ti atoms to a reaction region, the oxide particle (V_xO_y) turns to be an internal

sources of oxygen. Oxygen migrates in a state of solid solution and new stable oxide phase (Ti-O) appears in region where the solid solution is saturated. The morphology of new particle (Ti-O) is completely different from initial phase (V_xO_y). This mechanism is so-called *dissolution-precipitation* mechanism and has the features typical for the internal oxidation process and could be realized at moderate temperate (600-700°C), while Ti atom is only slightly mobile. The necessary condition for realization of this mechanism is $C_O D_O >> C_{Ti} D_{Ti}$, here C and D are the concentrations and diffusion coefficients respectively of O and Ti in solid solution at reaction region.

Considering that the oxidation process at 700°C just causes a formation of V_xO_y phase on the surface of V-alloys, the mechanism (b) can be realized for annealing in vacuum at 700°C without outer oxygen source. The Ti-O structure formed after the annealing is responsible for the interaction between O charged V-alloy and Er doped liquid Li to form the Er_2O_3 coating.

The oxygen charging process and oxygen trap effect of Ti could be described by the following generic equation:

$$\begin{cases} \partial C(x,t)/\partial t = D(t)\partial^2 C(x,t)/\partial x^2 - \alpha(t)[C(x,t) - C_0] \\ \textbf{boundary condition:} \\ D(t)\partial C(x,t)/\partial x = \beta(t)[C(x,t) - C_m] \ , \ \textit{at surface} \end{cases}$$

C : oxygen concentration in V-4Cr-4Ti
t : oxygen charging time
C_0 : initial oxygen concentration
D : diffusion coefficient in V-4Cr-4Ti
C_m : surface oxygen concentration
α : coefficient –chemical reaction between Ti and O
x : diffusion depth
β : coefficient –boundary response at surface of sample

In equation, item $D(t)\partial^2 C(x,t)/\partial x^2$ could describe the process of oxygen diffusion in pure V in which no oxygen trap, item $\alpha(t)[C(x,t) - C_0]$ could describe the O trap effect by Ti in V-alloy that results a limited oxygen distribution into more depth of substrate.

Fig. 5.1-3 shows scheme on modeling of microstructure changes of pre-oxidized V-4Cr-4Ti during various annealing time in vacuum. After pre-oxidation, just V_xO_y phase appeared in surface region of V-4Cr-4Ti (Chapter 3). After vacuum annealing of pre-oxidized specimen at 700°C, the various structures changed with annealing time are formed in substrate.

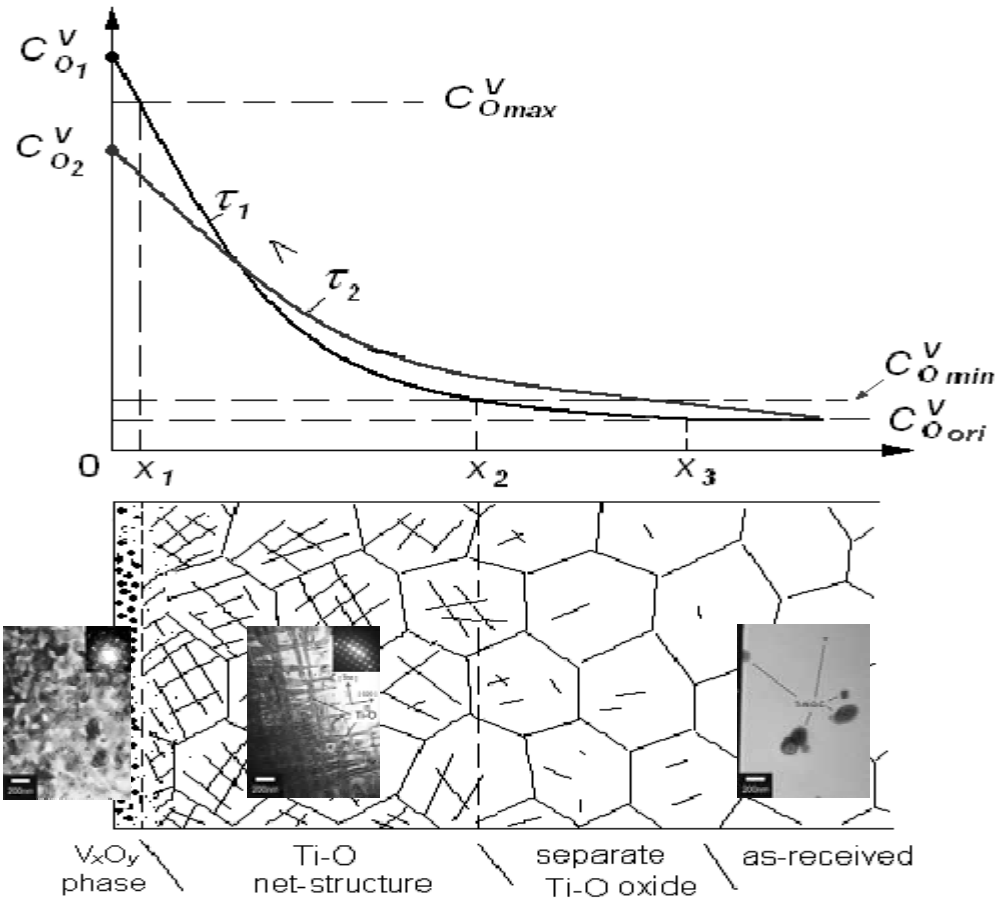

Fig. 5.1-3 Structure in pre-oxidized V-4Cr-4Ti during vacuum annealing at 700°C

τ_1, τ_2 — annealing time
$C_{O1}{}^V$, $C_{O2}{}^V$ — surface concentration of oxygen
$C_{Omax}{}^V$ — solubility limit of oxygen in V-alloy at 700°C
$C_{Omin}{}^V$ — minimal oxygen concentration to provide Ti-O net structure in V-alloy at 700°C
$C_{Oori}{}^V$ — original oxygen concentration in as-received V-alloy
0-x_1 — region with undissolved V_xO_y
x_1-x_2 — region with Ti-O net structures
x_2-x_3 — transitional region (with separate Ti-O) between oxygen enriched and as-received
$x>x_3$ — region with initial precipitates (as-received)

(a) Annealing with shorter time of τ_1

A narrow region (0-x_1) near surface shows the residuary undissolved V_xO_y, which indicates that the exposure time τ_1 is not enough for the complete dissolution of V_xO_y and the surface oxygen concentration (C_{O1}^{V}) still exceeds the solubility limit of O in V-alloys (C_{Omax}^{V}) at 700°C. However this region with undissolved V_xO_y is not expected as a good oxygen storage.

Due to the major dissolution of initial V_xO_y, the oxygen diffuses into substrate and forms oriented needle-shaped Ti-O net structure in region of x_1-x_2. In this region, the concentration of oxygen is over the minimal oxygen concentration to provide Ti-O net structure in V-alloy at 700°C (C_{Omin}^{V}). The creation of net-structure in substrate is extremely important for delivering the oxygen to the interface for formation of the oxide coating.

The transitional region (x_2-x_3) between Ti-O structure and as-received could be very narrow. Perhaps this region is with separate Ti-O phase, in which the concentration of oxygen is over the original oxygen concentration in as-received V-alloy (C_{Oori}^{V}).

The region ($x>x_3$), with initial precipitates showing as-received structure, is free from the effect of the oxygen charging.

The total oxygen-rich region (0-x_3) that corresponds to a Vickers hardness profile described in the former chapters, could act as oxygen storage.

(b) Annealing with longer time of τ_2

The annealing with longer time of τ_2 enhances the oxygen reduction (C_{O2}^{V}) at surface and complete dissolution of V_xO_y. The net structure is connected with surface ($x=0$) while V_xO_y region (0-x_1) disappeared. The depth (x_2) of Ti-O net region and also depth (x_3) of transitional region could be extended.

5.2 Phenomenological modeling for formation and growth of Er_2O_3 coating

Fig. 5.2-1 shows the thickness (*T)* of Er_2O_3 coating formed on the V-4Cr-4Ti substrate (oxidized for 6h at 700°C, annealed for 16h at 700°C and finally exposed in liquid Li doped with Er) at 600°C, 650°C and 700°C as a function of the exposure time (*t*), $T^n = k \cdot t + a$. Here *a=0* was assumed, corresponding to a negligible nucleation duration observed. The figure shows the growth kinetics of Er_2O_3 coating obey a logarithmic law with high exponent (n≈3 or 4) at 600°C, and 650°C, suggesting that the rate of growth to Er_2O_3 coating should be significantly low. As was shown in Chapter 2, the solubility of erbium is very low (0.15 wt%) in liquid lithium at 600°C. Thus slow delivery of either oxygen from substrate or erbium from Li to the interface is thought to be responsible for the slow growth of the coating. The growth process was expedited suddenly at 700°C exhibiting a low exponent (n≈2) that almost obeys a parabolic law resulting in the quick growth of the coating.

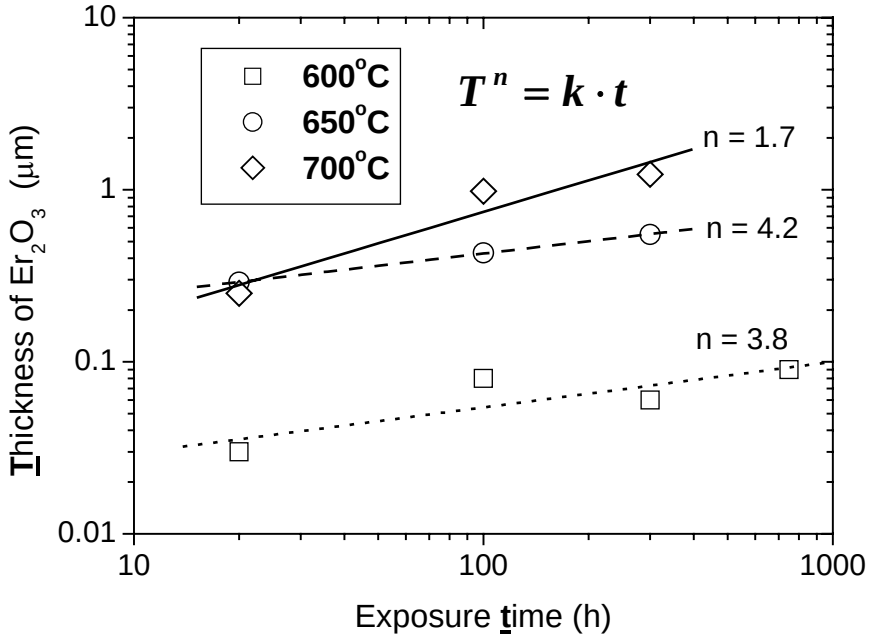

Fig.5.2-1 Thickness of Er_2O_3 coating on V-4Cr-4Ti substrate as a function of the time of exposure to liquid Li doped with Er. Here *T* is thickness of Er_2O_3 coating, *t* is exposure time in Li (Er), *n* is exponent and *k* is constant.

Fig. 5.2-2 shows a sketch on reasons to various growth kinetics of coating at 600, 650 and 700^0C. It could explain the parabolic kinetic or logarithmic kinetic shown at Fig. 5.2-1. The oxygen supplied for the growth of coating is mainly from the oxygen released by decomposition of Ti-O net phase. At 700^oC, the growth of coating obeys a parabolic law. From generic theory for the growth of surface layer, it could be explained that the growth process is controlled by oxygen diffusion under a quick decomposition of Ti-O in substrate. That perhaps due to insufficient supply of oxygen, because of slow decompositions of Ti-O net phase. No linear law is shown at all, thus coating growth is not controlled by surface reaction of oxygen and erbium.

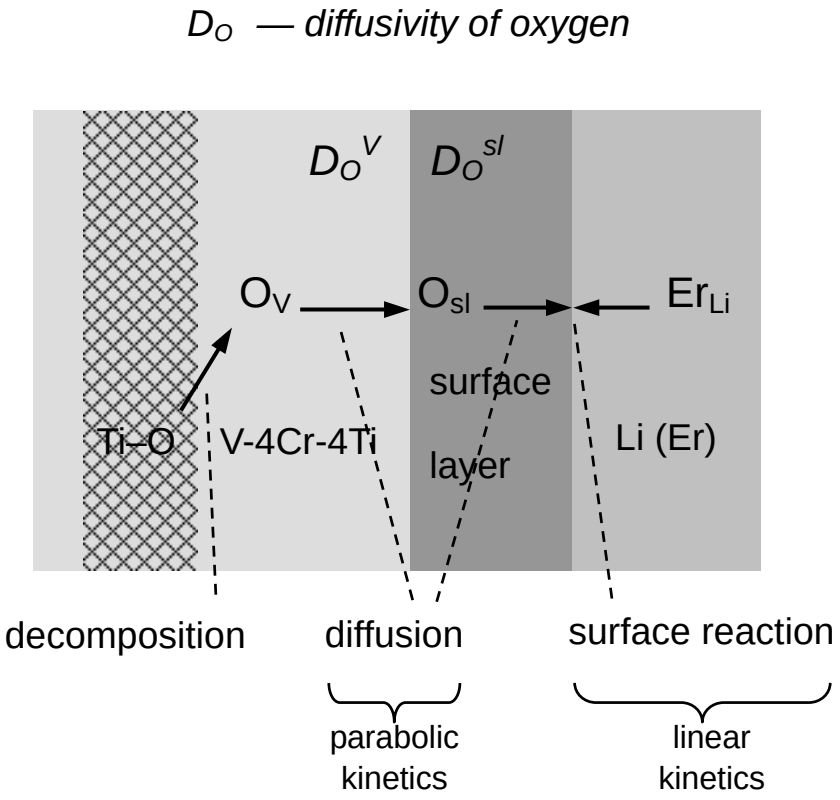

Fig. 5.2-2 Sketch on various growth kinetics of coating at 600, 650 and 700^0C.

Fig. 5.2.3 shows a model on the coating growth. Here it is assumed that oxygen storage C_{sub}^{0} is sufficient to keep the level, and oxygen supply $C_{sub}(x)$ keeps a linear relationship with O-depleted depth in substrate $T_d(t)$, and coating grow uniformly with thickness.

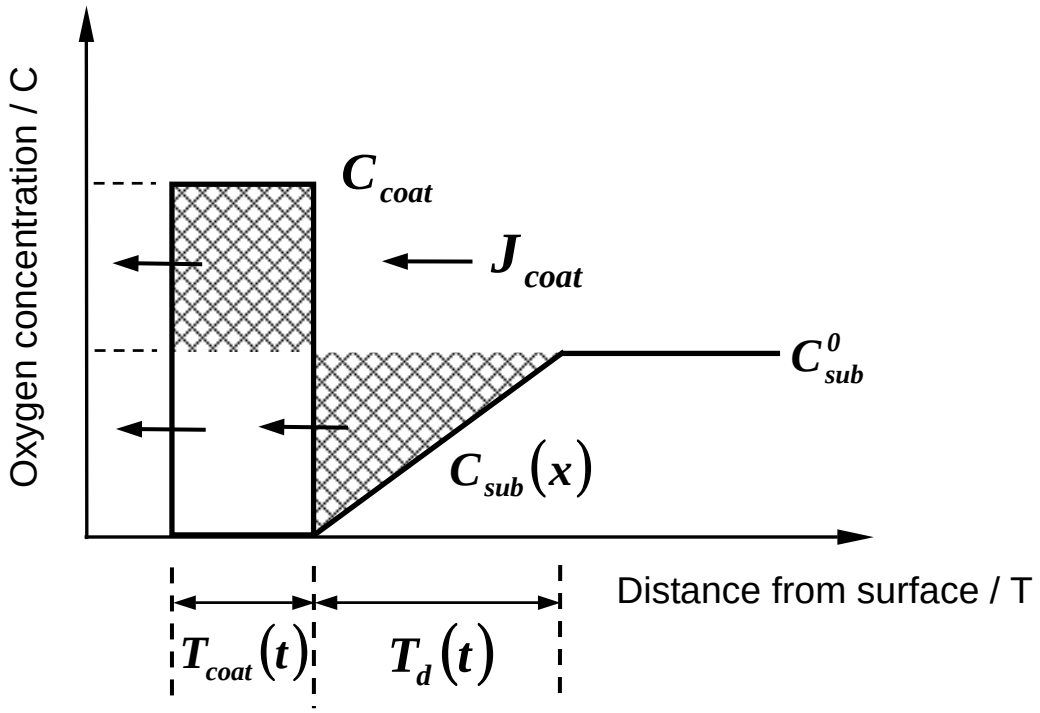

J_{coat} : oxygen flow to form coating
C_{coat} : oxygen concentration in coating
C_{sub}^{0} : oxygen concentration in substrate
$C_{sub}(x)$: oxygen concentration in O-depleted zone
$T_{coat}(t)$: thickness of coating
$T_d(t)$: thickness of O-depleted zone
D_{sub} : oxygen diffusion in substrate

Fig. 5.2.3 Model on the coating growth.

$$\begin{cases} J_{coat} = C_{coat} \cdot \dfrac{d\left[T_{coat}(t)\right]}{dt} & \text{Coating growth by oxygen flow} \\ J_{coat} = D_{sub} \cdot \dfrac{d\left[C_{sub}(x)\right]}{dx} = D_{sub} \cdot \dfrac{C_{sub}^{0}}{T_d(t)} & \text{Oxygen supply by diffusion} \end{cases}$$

$$\left(C_{coat} - C_{sub}^{0}\right) \cdot T_{coat}(t) = \frac{1}{2} \cdot C_{sub}^{0} \cdot T_d(t) \qquad \text{Oxygen conservation}$$

$$\frac{d\left[T_{coat}(t)\right]}{dt} = \frac{D_{sun}}{C_{coat}} \cdot \frac{C_{sub}^{0}}{T_d(t)} = \frac{D_{sun}}{C_{coat}} \cdot C_{sub}^{0} \cdot \frac{C_{sub}^{0}}{2} \cdot \frac{1}{\left(C_{coat} - C_{sub}^{0}\right) \cdot T_{coat}(t)}$$

$$= \frac{D_{sub} \cdot {C_{sub}^{0}}^{2}}{2 \cdot C_{coat} \cdot \left(C_{coat} - C_{sub}^{0}\right)} \cdot \frac{1}{T_{coat}(t)}$$ growth rate of coating

The kinetics of coating growth is as follows,

$$T_{coat}(t) = \left[\frac{D_{sub} {C_{sub}^{0}}^{2}}{2C_{coat}\left(C_{coat} - C_{sub}^{0}\right)} \right]^{1/2} \cdot t^{1/2} = A^{1/2} \cdot t^{1/2}$$

$$T^2 = k \cdot t$$ (parabolic law)

With extending exposure time *t*, the oxygen storage C_{sub}^{0} continue to decrease. Then *k* could decrease resulting in the apparent increased exponent (*n*).

In general, the expression for parabolic or logarithmic law is $T^n = k \cdot t$. As the above, *n=2* for parabolic law, and *n=3 or 4* for logarithmic law in this study.

In the case of logarithmic kinetics (*n=3 or 4*), the mathematic expression for explanation of growth process would be complex. The only assumption for reason is non-linear $C_{sub}(x)$ for oxygen flow, owing to insufficient oxygen supply.

Fig. 5.2-4 schematically shows a general phenomenological model on nucleation and growth processes of the surface layer on V-4Cr-4Ti in liquid lithium doped with erbium. Here V[O]+(Ti-O) is the vanadium alloy charged by oxygen, which includes both solid solution oxygen and titanium oxide, and Li[Er][N,O] is lithium doped with erbium and containing impurities of nitrogen and oxygen. The ordinate *d=0* is the initial interface between the substrate and the liquid lithium.

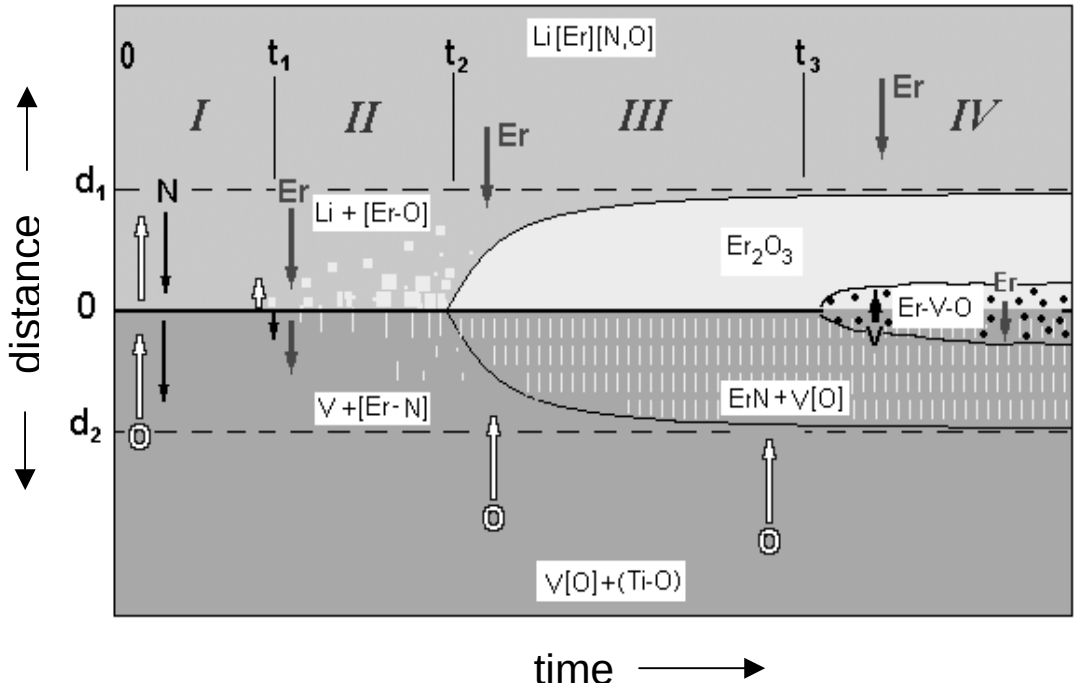

Fig.5.2-4 Scheme on nucleation and growth process of surface layers on V-4Cr-4Ti in liquid Li doped with Er.

The process could be divided into four stages that corresponds to Fig. 5.2-5 (a)-(d):

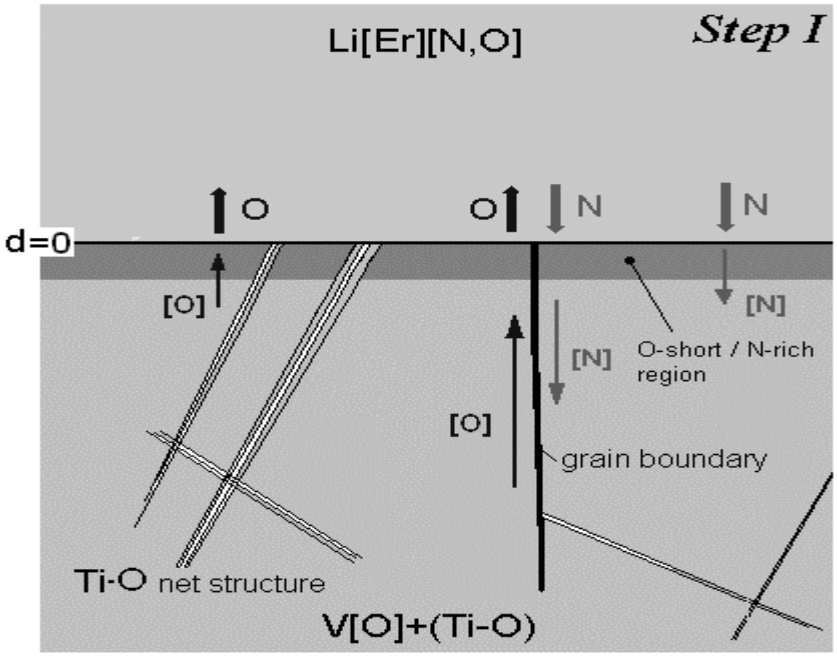

Fig. 5.2-5 (a) *Step I* of formation and growth of coating

S*tage I* (*0-t_1*) [Fig. 5.2-5 (a)]. The vanadium alloy substrate donates oxygen to and absorbs nitrogen from the liquid lithium. Interdependent redistribution of nonmetallic elements (O and N) is dominant during the first stage, because the erbium solubility in Li and thus the erbium delivery to the interface (*d=0*) is very slow. At this stage only liquid and solid solutions of oxygen and nitrogen occur in the reactive region in depth d_1 and d_2. Because of quick movement of oxygen and nitrogen at liquid or solid solution states, the duration of *Stage I* is thought to be negligibly short.

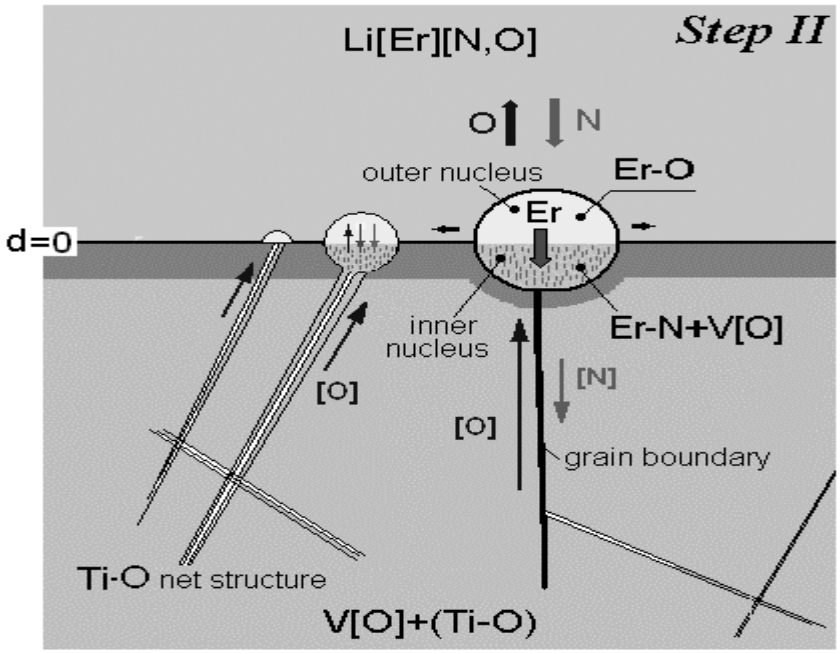

Fig. 5.2-5 (b) *Step II* of formation and growth of coating

S*tage II* (*t_1-t_2*) [Fig. 5.2-5 (b)]. In condition of low oxygen delivery rate, the erbium concentration increases in the reaction region. The nucleation of oxide and nitride starts above and below the interface respectively. The solid metal surface facilitates the deposition, nucleation and growth in the both directions. First of all, stable nucleuses appear and grow in oxygen- and nitrogen-rich regions (grain boundaries, Ti-O precipitates, dislocation clusters and other surface defects containing O and N). At the end of the second stage the islands of erbium compound cover almost all surfaces. Previous (during first stage) exchange of nonmetallic elements (O and N) between vanadium alloy and lithium causes the formation of

erbium nitride into solid metal and that of erbium oxide as outer layer. Since the rates for both diffusion of oxygen and migration of erbium to interface at 700°C are similar to that at 650°C and 600°C, the difference of starting time and duration for nucleation at three temperatures cannot be seen. In reality, because the nucleation is so quick that duration of *Stage II* also is thought to be short.

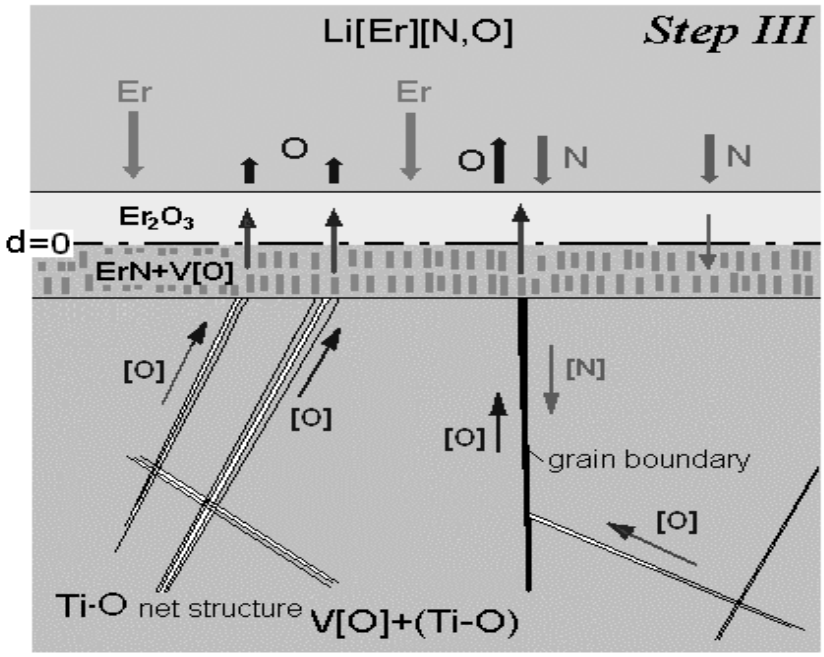

Fig. 5.2-5 (c) *Step III* of formation and growth of coating

S*tage III* (t_2-t_3) [Fig. 5.2-5 (c)]. To provide the subsequent growth of Er_2O_3 coating, the Ti-O net phases in alloy decompose deeper in the bulk of the substrate. Since the oxygen diffusion through the two layers becomes difficult in comparison with the previous stages, the thickness of oxide coating is saturated at the end of this stage. Since migration rate of erbium from lithium to the oxide layer does not change, the growth and state of the coating is controlled by oxygen diffusion through the surface two layers. The third stage could be characterized as a quasi-stable state of coating due to timely supply of oxygen and erbium to interface from vanadium substrate and lithium, respectively. Since the nitrogen absorbed in the substrate is limited, the thickness of the intermediate layer is also saturated. It was showed in Chapter 4 that coatings were already formed after exposure for 20h at 600, 650 and 700°C. The exposing duration (*0*-t_3) from starting to almost saturation for coating thickness is about 100h at 600°C,

300h at 650°C and more than 300h at 700°C. The reasons for the increased exposure time to apparent saturation of coating thickness with exposure temperature may be either thermal decomposition of Ti-O net phase, diffusion of oxygen through two surface sub-layers or solution level of erbium in liquid Li.

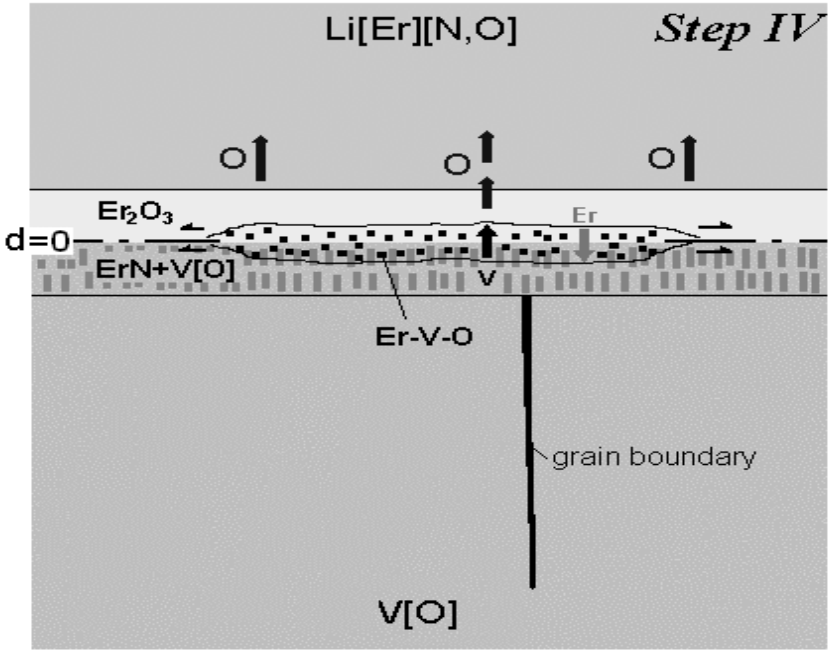

Fig. 5.2-5 (d) *Step IV* of formation and growth of coating

S*tage IV* (> t_3) [Fig. 5.2-5 (d)]. The oxygen stored in the surface region is almost exhausted. The outer oxide coating could donates oxygen to lithium but vanadium substrate cannot maintain a balanceable oxygen concentration in the coating. The solid phase reaction could occur between the outer and the intermediate layers at the interface (*d=0*). As a result, complex Er-V-O compound appears which could be negative to insulating property, accompanying diffusion of Er and V oppositely in the two layers.

The evaluation for coating lifetime needs to be base on examination experimentally by long-term exposure in liquid lithium with or without erbium.

The model on the pre-charging of oxygen in V-alloys described the observed microstructure corresponding to the oxygen level, especially the region of Ti-O net structure whose thickness needed to be maintained for keeping an oxygen source to form the oxide coating.

The model on formation of coating on V-alloys described that the growth of Er_2O_3 coating after quick nucleation is controlled by delivery of either oxygen from substrate or erbium from Li to the interface. The model also showed the formation mechanism of the observed intermediate layer.

CHAPTER 6

Conclusions

The objective of this study is to investigate the feasibility and characteristic of an Er_2O_3 insulating coating on V-alloys by in-situ method in liquid Li doped with Er, for the purpose of reducing MHD pressure drop to an acceptable level for a self-cooled Li/V blanket.

This study aims to demonstrate the feasibility of coating, to perform the characterization of coating and to understand the mechanism of oxygen pre-charging in V-4Cr-4Ti, and the nucleation and growth kinetics of the coating in Li. The research steps are to pre-charge oxygen in V-4Cr-4Ti by oxidation and annealing, and to obtain in-situ insulating Er_2O_3 coating by exposing O-charged V-4Cr-4Ti in liquid Li doped with Er.

To form an oxide insulating coating by in-situ method, the enough oxygen storage in limited depth of V-alloys is essential. For oxygen charging, V-4Cr-4Ti alloy was oxidized in flowing high purity Ar and subsequently annealed in vacuum.

1) By the oxidation in Ar at 700^{o}C, the charged oxygen was concentrated in the surface layer with V-O compounds. By the subsequent annealing in vacuum at 700^{o}C, oxygen was homogeneously distributed to a certain depth where Ti-O net precipitates were formed.
2) By oxidation and annealing, the contents of oxygen increased to ~10000ppm with little charge in nitrogen.
3) By annealing at 700^{o}C, oxygen diffused into a limited depth of ~150μm because of formation of Ti-O precipitates as strong trap of oxygen.
4) Annealing after oxidation is a necessary process to form Er_2O_3 coating, because Ti-O precipitates act as oxygen source during exposure.
5) It is feasible to control oxygen level and distribution in the surface region of V-4Cr-4Ti, by controlled oxidation and annealing.

To verify the feasibility and to characterize the property of Er_2O_3 in-situ coatings on V-4Cr-4Ti, the exposures in Li doped with Er were performed followed by examinations.

1) A surface layer composed of two sub-layers (top coating and intermediate layer) was formed on V-4Cr-4Ti successfully. The top coating was dominated by Er_2O_3, and the intermediate layer consisted of a mixture of ErN and V-compounds.

2) The lower limit for the doping level of Er powder in Li to form oxide coating was far below the level that could influence the TBR of the blanket.
3) The exposing temperature had a large effect on the formation and growth of the coating. A lower limit of exposing temperature to form the coating was between 500 and 550^{o}C. The Er_2O_3 coating was stable at 600^{o}C up to 750h of exposure to liquid Li, and stable at 650^{o}C or 700^{o}C up to 300h. The thickness was almost saturated to ~0.1μm at 600^{o}C, ~0.6μm at 650^{o}C and ~1.3μm at 700^{o}C.
4) The oxygen charged into V-alloy was exhausted accompanied by growth of coating. It is necessary to consider a method to keep effectively the oxygen storage in V-alloy during the exposure especially at such high temperature as 700^{o}C.
5) The resistivity of V-4Cr-4Ti coated by Er_2O_3 in vacuum exceeded minimum requirement up to 550^{o}C. The resistivity seems to satisfy the requirement to ~700^{o}C by the extrapolation of the data obtained.
6) Er_2O_3 coating once formed in Li (Er) was stable in pure Li.
7) The cracking in the coating could be avoided in a real size of blanket wall by avoiding Li cleanout with hard lotion.
8) In-situ Er_2O_3 coating shows potentiality of self-healing to cracks in liquid Li (Er)

Some phenomenological modelings were proposed to explain the mechanisms on the oxygen charging of substrate or the formation and growth of coating.

1) The model on the pre-charging of oxygen in V-alloys described depth-dependent microstructures corresponding to oxygen levels. The modeling also showed that control of the thickness of the region with Ti-O precipitate is a necessary process for maintaining the oxygen source to form the oxide coating.
2) The model on formation of the coating on V-alloys described that the growth of Er_2O_3 coating after quick nucleation is controlled by delivery of either oxygen from substrate or erbium from lithium to the interface. The modeling also showed formation mechanism of the observed intermediate layer.

Remaining issue to coating is considered as follows,

1) Oxygen keeping in V-alloy during long-term exposure in Li. Because pre-charged oxygen source could be exhausted so that it would be difficult to supply for self-healing of coating.
2) Coating stability at interface between coating and intermediate layer. E-V-O compound occurred around interface, which perhaps is conductive, could play a negative role to insulating property of coating.
3) Adhesion of coating with substrate. Because the expansion of coating is different from that of substrate, keeping the adhesion may become seriously difficult under large thermal-impact or thermal-cycle during operating the blanket.

Throughout the present study, the demonstration was made that in-situ formation of Er_2O_3 insulating coating on V-4Cr-4Ti in liquid Li doped with Er is a feasible coating technology.

REFERENCES

[1] ITER homepage http://www.iter.org

[2] F. Najimabadi and The ARIES Team, Fusion Eng. Des. 38 (1997) 3-25.

[3] D. L. Smith, C. C. Baker, D. K. Sze, et al, Fusion. Technol., 8 (1985) 10-44.

[4] G. Kalinin, V. Barabash, S. Fabritsiev, et al, Fusion Eng. Des., 55(2001) 231-246.

[5] G. Kalinin, W. Gauster, R. Matera, A-A.F. Tavassoli, et al, J. Nucl. Mater., 233-237 (1996) 9- 16.

[6] M. I. Solonin, J, Nucl. Mater., 258-263 (1998) 30-46.

[7] T. Muroga, M. Gasparotto, S.J. Zinkle, Fusion Eng. Des., 61-62 (2002) 13-25.

[8] R. H. Jones, C. H. Henager, Jr.G. W. Hollenberg, J. Nucl. Mater., 191-194 (1992) 75-83.

[9] T. Muroga, T. Nagasaka, K. Abe, et al, J. Nucl. Mater., 307-311 (2002) 547-554.

[10] T. Muroga, Materials Transactions, 46 (2005) 405-411.

[11] S. Malang, K. Arheidt, L. Barleon, et al, Fusion Technol., 14 (1988) 1343-1356.

[12] R. F. Mattas, D. L. Smith, C. B. Reed, et al, Fusion Eng. Des., 39-40 (1998) 659-668.

[13] Y. A. Sokolov, I. V. Altovskij, A. A. Borisov, et al, Fusion Eng. Des., 41 (1998) 525-533.

[14] T. Tanaka, T. Muroga, A. Sagara, Fusion Sci. Technol., 47 (2005) 530-534.

[15] T. Muroga, T. Tanaka, Fusion Sci. Technol., 47 (2005) 540-543.

[16] T. Q. Hua, J. S. Walker, B. F. Picologlou, et al, Fusion Technol., 14 (1988) 1389-1398.

[17] T. Q. Hua, B. F. Picologlou, Fusion Technol., 19 (1991) 102-112

[18] Y. S. Cha, Y. Gohar, A. M. Hassanein, et al, Fusion Technol., 8 (1985) 90-113.

[19] T. Q. Hua, Y. Gohar, Fusion Eng. Des., 27 (1995) 696-702.

[20] S. Malang, H. U. Borgstedt, . H. Farnum, et al, Fusion Eng. Des., 27 (1995) 570-586.

[21] D. K. Sze, R. F. Mattas, A. B. Bull, et al, Fusion Technol., 21 (1992) 2099-2106.

[22] Y. Yamada-Takamura, F. Koch, H. Maier, et al, Surf. Coat. Technol., 142-144 (2001) 260-264.

[23] P. J. Martin, R. P. Netterfield, A. Bendavid, et al, Surf. Coat. Technol., 54-55 (1992) 136-142.

[24] G. Wang, B. Wang, A. Huang, et al, Mater. Letter, 58 (2004) 2486-2488.

[25] T. Terai, T. Mitsuyama, T. Yoneoka, Fusion Eng. Des., 51-52 (2000) 207-212.

[26] D. L. Smith, J. H. Park, K. Natesan, J. Nucl. Mater., 307-311 (2002) 1405-1410.

[27] MALT2 (MAterials oriented Little Thermodynamic database), Version 1.06, The Japan Society of Calorimetry and Thermal Analysis.
[28] T. Mitsuyama, T. Terai, T. Yoneoka, et al, Fusion Eng. Des., 39-40 (1998) 811-817.
[29] D. L. Smith, J. Konys, T. Muroga, et al, J. Nucl. Mater., 307-311 (2002) 1314-1322.
[30] K. Natesan, C. B. Reed, D. L. Rink, et al, J. Nucl. Mater., 258-263 (1998) 488-494.
[31] D. L. Smith, J. H. Park, I. Lyublinski, et al, Fusion Eng. Des., 61-62 (2002) 629-641.
[32] A. Suzuki, T. Tanaka, , private communication, unpublished.
[33] T. Tanaka, A. Suzuki, T. Muroga, et al, J. Nucl. Mater., 329-333 (2004) 1434-1437.
[34] J. H. Park, T. Domenico, G. Dragel, et al, Fusion Eng. Des., 27 (1995) 682-695.
[35] A. Suzuki, T, Muroga, B.A. Pint, et al, Fusion Eng. Des., 69 (2003) 397-401.
[36] B. A. Pint, L. D. Chitwood, J. R. Di Stefano, J. Nucl. Mater., 289 (2001) 52-56.
[37] T. Terai, A. Suzuki, T. Yoneoka, et al, J. Nucl. Mater., 283-287 (2000) 1322-1325.
[38] B. A. Pint, J. H. DeVan, J. R. DiStefano, J. Nucl. Mater., 307-311 (2002) 1344-1350.
[39] B. A. Pint, P. F. Tortorelli, A. Jankowski, et al, J. Nucl. Mater., 329-333 (2004) 119-124.
[40] T. Terai, T. Kobayashi, T. Mitsuyama, et al, Surf. Coat. Technol., 106 (1998) 18-22.
[41] A. Sawada, A. Suzuki, T. Terai, et al, J. Nucl. Mater., 329-333 (2004) 1411-1413.
[42] K. Natesan, J. Nucl. Mater., 233-237 (1996) 1403-1410.
[43] A. V. Vertkov, V. A. Evtikhin, I. E. Lyublinski, Fusion Eng. Des. 58-59 (2001) 731-735.
[44] I. V. Vitkovsky, A. V. Gorunov, V. I. Engelko, et al, Fusion Eng. Des., 61-62 (2002) 739-743.
[45] Z. Zeng, K. Natesan, Fusion Eng. Des., 70 (2004) 87-93.
[46] K Natesan, M. Uz, S. Wieder, J. Nucl. Mater., 283-287 (2000) 1277-1281.
[47] K Natesan, M. Uz, D. L. Smith, J. Nucl. Mater., 307-311 (2002) 1323-1328.
[48] O. I. Yeliseyeva, V. M. Chernov, T. V. Tsaran, Fusion Eng. Des., 61-62 (2002) 745-748.
[49] O. I. Yeliseyeva, V. M. Chernov, M. M. Potapenko, et al, J. Nucl. Mater., 329-333 (2004) 1424-1428.
[50] B. A. Pint, K. L. More, J. L. Moser, Fusion Materials Semi-Annual Progress Reports, ORNL, USA, DOE/ER-0313/37, Dec. 31, 2004, 101-106.
[51] F. Koch, R. Brill, H. Maier, et al, J. Nucl. Mater., 329-333 (2004) 1403-1406.
[52] A. Suzuki, T. Muroga, H. Maier, et al, Annual Report of National Institute for Fusion Science, Japan, Apr. 2003- Mar. 2004, 433.

[53] T. Terai, A. Sawada, A. Suzuki, et al, Annual Report of National Institute for Fusion Science, Japan, Apr. 2002- Mar. 2003, 235.

[54] T. Terai, A. Suzuki, A. Sawada, et al, Annual Report of National Institute for Fusion Science, Japan, Apr. 2003- Mar. 2004, 235.

[55] T. Muroga, T. Nagasaka, K. Abe, et al, J. Nucl. Mater., Vol. 307-311 (2002) 547-554.

[56] T. Nagasaka, T. Muroga, Y. Wu, et al, J. Plasma Fusion Res. SERIES, 5 (2002) 545-550.

[57] M. Uz, K. Natesan, V. B. Hang, J. Nucl. Mater., 245 (1997) 191-200.

[58] N. J. Heo, T. Nagasaka, T. Muroga, et al, J. Nucl. Mater., 307-311 (2002) 620-624.

[59] T. Nagasaka, H. Takahashi, T. Muroga, et al, J. Nucl. Mater., 283-287 (2000) 816-821.

[60] H. Matsui, et al, Fusion Technol., 30 (1996) 1293.

[61] D. L. Smith, M. C. Billone, S. Majumdar, et al, J. Nucl. Mater., 258-263 (1998) 65.

[62] T. Muroga, T. Nagasaka, Int. J. Refr. Metals & Hard Mater., 18 (2000) 225-230.

[63] J. F. Moulder, W. F. Stickle, P. E. Scbol, et al, Handbook of X-ray Photoelectron Spectroscopy (Physical Electronics, Inc. United States of America 1995).

[64] R. Hayakawa, Y. Hatano, K. Fujii, et al, J. Nucl. Mater., 307-311 (2002) 580-584.

[65] K. Natesan, M. Uz, Fusion Eng. Des. 51-52 (2000) 145-152.

[66] J. R. DiStefano, B. A. Pint, J. H. DeVan, Int. J. Refr. Metals & Hard Mater., 18 (2000) 237-243.

[67] H. Nakajima, S. Nagata, H. Matsui, Philosophical Magazine A, 67 (1993) 557-571.

[68] R. E. Buxbaum, E. F. Johnson, Nucl. Technol., 49 (1980) 307-314.

[69] A. Sawada, Master Thesis, Department of Quantum Engineering and Systems Science, School of Engineering, the University of Tokyo, March, 2003, pp. 74.

[70] T. Muroga, T. Tanaka, A. Sagara, Proceeding of ISFNT-7 Conference, Tokyo, Japan, 22-27 May 2005 (to be published in Fusion Eng. Des.).

[71] L. A. El-Guebaly, Proceeding of ISFNT-7 Conference, Tokyo, Japan, 22-27 May 2005 (to be published in Fusion Eng. Des.).

[72] M. Fujiwara, M. Satou, A. Hasegawa, et al, J. Nucl. Mater. 283-287 (2000) 1311-1315.

[73] P. Kofstad, High-temperature Oxidation of Metals, John Wiley & Sons, Inc., New York, 1996, pp.11-19.

[74] B. A. Pint, J. R. DiStefano, J. Nucl. Mater., 307-311 (2002) 560-565.

[75] N. J. Heo, T. Nagasaka, T. Muroga, J. Nucl. Mater., 325 (2004) 53-60.

LIST OF PAPERS

1. Z. Yao, A. Suzuki, T. Muroga, K. Katahira, Chemical Formation of Erbium Oxide Layer on V-4Cr-4Ti during Exposure to Liquid Lithium Doped with Erbium, Journal of Nuclear Materials, 329-333 (2004) 1414-1418.

2. Z. Yao, A. Suzuki, T. Nagasaka, T. Muroga, Behavior of Oxygen in Fusion Candidate Vanadium Alloys during Oxidation and Annealing, Materials Science Forum, 475-479 (2005) 1445-1448.

3. Z. Yao, A. Suzuki, T. Muroga, K. Katahira, In-situ Formation and Chemical Stability of Er_2O_3 Coating on V-4Cr-4Ti in Liquid Lithium, Fusion Engineering and Design, in press, 2005.

4. Z. Yao, A. Suzuki, T. Muroga, O. Yeliseyeva, T. Nagasaka, The In-situ Growth of Er_2O_3 Coatings on V-4Cr-4Ti in Liquid Lithium, Fusion Engineering and Design, to be published.

LIST OF PRESENTATIONS

1. Z. Yao, A. Suzuki, T. Muroga, K. Katahira, Chemical Formation of Erbium Oxide Layer on V-4Cr-4Ti during Exposure to Liquid Lithium Doped with Erbium, 11th International Conference on Fusion Reactor Materials (ICFRM-11), December 7-12, 2003, Kyoto, Japan.

2. Z. Yao, A. Suzuki, T. Muroga, In-situ Formation of Erbium Oxide Insulating Layer in Liquid Lithium, Atomic Energy Society of Japan (AESJ) Spring Meeting, March 29-31, 2004, Okayama, Japan.

3. Z. Yao, A. Suzuki, T. Muroga, K. Katahira, In-situ Formation and Chemical Stability of Er_2O_3 Coating on V-4Cr-4Ti in Liquid Lithium, 23rd Symposium on Fusion Technology (SOFT-23), September 20-24 2004, Venice, Italy.

4. Z. Yao, A. Suzuki, T. Muroga, Formation and Stability of Er_2O_3 In-situ Coating in Liquid Li, 8th Japan-China Symposium on Materials for Advanced Energy Systems and Fission & Fusion Engineering (JCS-8), October 4-8, 2004, Sendai, Japan.

5. Z. Yao, A. Suzuki, T. Nagasaka, T. Muroga, O. Yeliseyeva, Behavior of Oxygen in Fusion Candidate Vanadium Alloys during Oxidation and Annealing, 5th Pacific Rim International Conference on Advanced Materials and Processing (PRICM-5), November 2-5, 2004, Beijing, China.

6. Z. Yao, A. Suzuki, T. Muroga, O. Yeliseyeva, T. Nagasaka, The Growth of Er_2O_3 In-situ Coating on V-4Cr-4Ti in Liquid Lithium, 7th International Symposium on Fusion Nuclear Technology (ISFNT-7), May 22-27, 2005, Tokyo, Japan.

ACKNOWLEDGEMENTS

At first, I would like to express the appreciation to my supervisor – Prof. Takeo MUROGA of National Institute for Fusion Science (NIFS) in Japan and The Graduate University of Advanced Studies (Sokendai) in Japan, for his aborative guidances and elaborate discussions on my study, and kind helps on my living in Japan.

I am thankful to Associate Prof. A. Suzuki of University of Tokyo (the former researcher of NIFS) for his guided advices and powerful helps on this study.
I am also thankful Dr. O. Yeliseyeva of Karpenko Physico-Mechanical Institute in Ukraine for her guidances and collaborations on the modeling.
I wish to thank Prof. N. Noda, Prof. A. Nishimura and Prof. A. Sagara of NIFS for their guided comments, and Associate Prof. T. Nagasaka and Dr. T. Tanaka of NIFS for their great helps and collaborations on this study. I also extend thanks to other members of Fusion Engineering Research Center (FERC) of NIFS for their kind helps.
The financial support by Fusion Science Association is gratefully acknowledged.
The thanks should go to Dr. K. Katahira and his group of R&D Center of TYK Corporation, and Mr. A. Sawada of University of Tokyo for their collaborations and helps.
The thanks also should go to Mr. K. Matsuura, Ms. S. Urushihara and Ms. M. Ohmori of NIFS for their studious work to Sokendai affairs.
I am also thankful to Mr. LI Baiwen, Mr. LI Huailin and Mr. LI Zaixin as classmates of Sokendai for their helps and friendships.

Finally, I would like to express the best appreciations to my parents (father-YAO Shibin and mother-TAO Yanbin), wife (LU Xiaozhou) and daughter (YAO Xiaoyue), younger brother (YAO Zhenhui) for their support with endless love during my PhD study for three years.

YAO Zhenyu

August 22, 2005